Epeirogenic transients related to mantle lithosphere removal in the southern Sierra Nevada region, California: Part II. Implications of rock uplift and basin subsidence relations

J. Saleeby[1], Z. Saleeby[1], and L. Le Pourhiet[2]
[1]*Caltech Tectonics Observatory, California Institute of Technology, Pasadena, California 91125, USA*
[2]*Université Pierre et Marie Curie Paris 6, Institut des Sciences de la Terre de Paris, F-75005, Paris, France, and Centre National de la Recherche Scientifique, UMR 7193, F-75005, Paris, France*

ABSTRACT

We investigate the putative Pliocene–Quaternary removal of mantle lithosphere from beneath the southern Sierra Nevada region using a synthesis of subsidence data from the Great Valley, and geomorphic relations across the Sierra Nevada. These findings are used to test the results and predictions of thermomechanical modeling of the lithosphere removal process that is specific to the Sierra Nevada, as presented in an accompanying paper referenced here as Part I. Our most successful thermomechanical model and the observational data that it explains are further bundled into an integrated physiographic evolution–geodynamic model for the three-dimensional epeirogenic deformation field that has affected mainly the southern Sierra Nevada–San Joaquin Basin region as a result of underlying mantle lithosphere removal.

The coupled Sierra Nevada mountain range and Great Valley basin are recognized as a relatively rigid block (Sierra Nevada microplate) moving within the San Andreas–Walker Lane dextral plate juncture system. Our analysis recognizes that the Sierra Nevada possessed kilometer-scale local and regional paleotopographic relief, and that the Great Valley forearc basin possessed comparable structural relief on its principal stratigraphic horizons, both dating back to the end of Cretaceous time. Such ancient paleorelief must be accounted for in considering late Cenozoic components of uplift and subsidence across the microplate. We further recognize that Cenozoic rock and surface uplift must be considered from the perspectives of both local epeirogeny driven by mantle lithosphere removal, and regional far-field–forced epeirogeny driven by plate tectonics and regional upper-mantle buoyancy structure. Stratigraphic relations of Upper Cretaceous and lower Cenozoic marine strata lying on northern and southern Sierra Nevada basement provide evidence for near kilometer-scale rock uplift in the Cenozoic. Such uplift is likely to have possessed positive, and then superposed negative (subsidence) stages of relief generation, rendering net regional rock and surface uplift. Accounting for ancient paleorelief and far-field–driven regional uplift leaves a residual pattern whereby ~1200 m of southeastern Sierra crest rock and similar surface uplift, and ~700 m of spatially and temporally linked tectonic subsidence in the southern Great Valley were required in the late Cenozoic by mantle lithosphere removal. These values are close to the predictions of our modeling, but application of the model results to the observed geology is complicated by spatial and temporal variations in the regional tectonics that probably instigated mantle lithosphere removal, as well as spatial and temporal variations in the observed uplift and subsidence patterns. Considerable focus is given to these spatial-temporal variation patterns, which are interpreted to reflect a complex three-dimensional pattern resulting from the progressive removal of mantle lithosphere from beneath the region, as well as its epeirogenic expressions. The most significant factor is strong evidence that mantle lithosphere removal was first driven by an east-to-west pattern of delamination in late Miocene–Pliocene time, and then rapidly transitioned to a south-to-north pattern of delamination in the Quaternary.

INTRODUCTION

The late Cenozoic removal of mantle lithosphere from beneath the southern Sierra Nevada region has gained attention by virtue of its extraordinary geophysical documentation (cf. Jones et al., 1994, 2004; Ruppert et al., 1998; Zandt et al., 2004; Reeg, 2008; Frassetto et al., 2011; Gilbert et al., 2012), and its diversity of geologic expression (cf. Ducea and Saleeby, 1996, 1998a; Manley et al., 2000; Saleeby and Foster, 2004; Farmer et al., 2002). Geophysical imaging of large-scale structures resulting from this process, and data on its geologic expressions provide valuable constraints for formulation and iteration of thermomechanical models that explore the underlying dynamics. One class of such models was presented in Le Pourhiet et al. (2006) and is refined in the accompanying paper (Saleeby et al., 2012, this themed issue, referred to below as Part I). In these models, arrays of geological and geophysical data are formulated into initial and boundary conditions, and input parameters, and a number of testable geological predictions emerge. With this in mind, the primary aim of this paper is to present new and to integrate existing constraints for late Cenozoic uplift and subsidence of the Sierra Nevada and Great Valley that appear to be related to this mantle lithosphere removal event, and to test the results of the Part I modeling against these observables.

We pose the concept of both anomalous rock uplift and tectonic subsidence applied to vertical displacements that are specific to the southern Sierra region of mantle lithosphere removal. In order to pursue the results of these displacements, it is necessary to develop a working model for the physiographic development of the entire Sierra Nevada and Great Valley. This coupled system is widely recognized as a semicoherent crustal block named the Sierra Nevada microplate, which moves semi-independently within the San Andreas–Walker Lane transform system (Fig. 1) (Argus and Gordon, 1991, 2001; Unruh et al., 2003). As such, the topographic evolution of the Sierra Nevada, and the

Geosphere; June 2013; v. 9; no. 3; p. 394–425; doi:10.1130/GES00816.1; 13 figures; 3 tables; 8 supplemental files.
Received 2 May 2012 ♦ Revision received 23 January 2013 ♦ Accepted 19 February 2013 ♦ Published online 17 April 2013

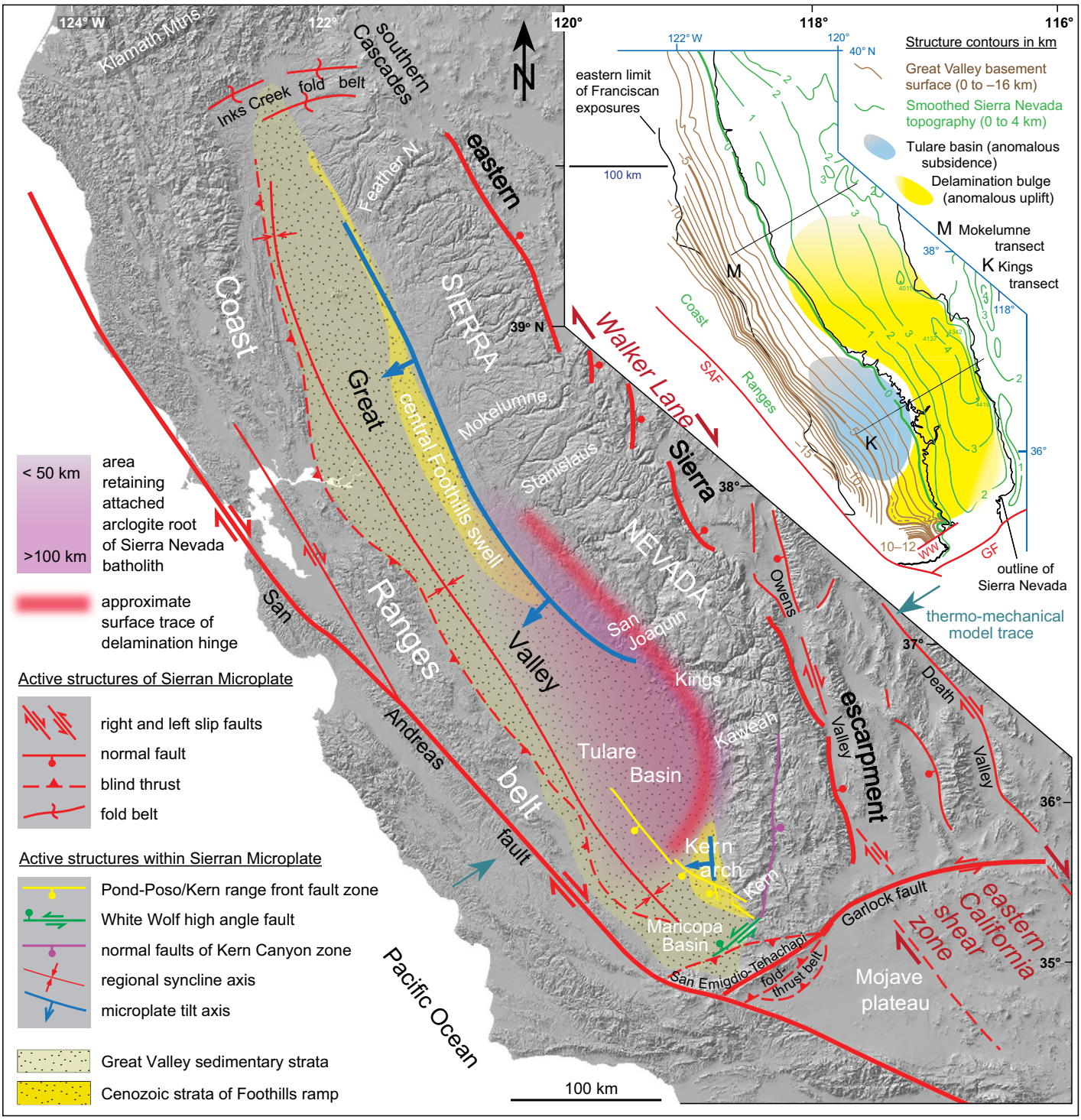

Figure 1. Map showing principal bounding and active internal structures of the Sierra Nevada microplate and selected geomorphic and tectonic features discussed in text (after Wentworth and Zoback, 1989; Unruh, 1991; Unruh et al., 2003; Saleeby et al., 2009a). Delamination hinge trace is taken from Part I, and depicts the locus of east-to-west and south-to-north separation of arclogite root (eclogitic cumulates) from lower felsic crust of Sierra Nevada batholith. Inset shows regional averaged topography of Sierra Nevada smoothed across major interfluves (modified after Wakabayashi and Sawyer, 2001) mated to structure contours on the Great Valley basement surface (after Wentworth and Zoback, 1989; Wentworth et al., 1995; Figs. 5 and 8 herein). Also shown on inset is area interpreted as undergoing rock uplift resulting from Pliocene–Quaternary delamination (delamination bulge), and the dynamically linked subsidence area (Tulare Basin), as well as traces of Figure 11 transects.

subsidence history of the Great Valley are commonly assumed to be uniform across the microplate. We depart from this convention and assert that the southern Sierra Nevada and San Joaquin Basin of the southern Great Valley both underwent profound Pliocene–Quaternary rock uplift and tectonic subsidence phases that are missing from the northern reaches of the microplate, and that these phases were genetically related to underlying mantle lithosphere removal. The elucidation of these anomalous vertical displacement components is confounded, however, by paleorelief variations along the Sierra Nevada (House et al., 2001; Wakabayashi and Sawyer, 2001; Stock et al., 2004, 2005; Chapman et al., 2012), and ancient segmentation patterns of the Great Valley inherited from its Cretaceous forearc setting (Repenning, 1960; Harwood and Helley, 1987; Reid, 1988; Imperato, 1995). For this reason, the subject of anomalous uplift and subsidence must be considered from the perspective of the uplift-subsidence history of the entire microplate.

The goals of this paper and of Part I are to address the observed vertical displacements in Earth's surface resulting from mantle lithosphere removal in the southern Sierra region, and to relate these displacements to the mechanisms governing the removal process. We refer to these displacements as epeirogenic in that they reflect relatively long wavelength to amplitude vertical displacements that arise primarily from radial force components. We posit that the physiographic expression of these displacements has been superposed over paleorelief patterns of the Sierran Nevada microplate that are inherited from the Late Cretaceous convergent margin history of the region, as well as the effects of far-field–driven vertical displacements that operated over Cenozoic time at a regional scale. We further posit that these factors considered together with the flexural-isostatic responses to late Cenozoic drainage basin erosion and related sediment loading of the Great Valley can explain the first-order physiography of the microplate. Here, we pose a working model for the late Cenozoic physiographic evolution of the Sierra Nevada microplate, and link it to a geodynamic analysis of the underlying governing processes as approximated in the thermomechanical models of Le Pourhiet et al. (2006) and Part I. We further iterate between physiographic and dynamic aspects of our integrated model, along with insights derived from volcanism and heat flow patterns, in the derivation of a three-dimensional kinematic model for mantle lithosphere removal. We focus on uplift and subsidence, which we interpret as the imprints of the epeirogenic deformation field resulting from mantle lithosphere removal in the southern Sierra Nevada region. We recognize that this process is most clearly documented in the southern Sierra region, and that it is likely to be concentrated in, or restricted to, this region (Jones et al., 1994; Ruppert et al., 1998; Zandt et al., 2004; Reeg, 2008; Frassetto et al., 2011; Schmandt and Humphreys, 2010; Gilbert et al., 2012). We further note that modern debate on Sierran landscape evolution rarely recognizes the physiographic variation between the southern and northern Sierra Nevada, as was clearly noted in early literature on the subject (Matthes, 1965; Christensen, 1966). Our integrated physiographic evolution–geodynamic model suggests that a significant component of this variation has arisen over the past ~5 m.y. as a direct result of mantle lithosphere removal that was restricted to, or concentrated in the southern half of the microplate.

TECTONOMORPHOLOGY OF THE SIERRA NEVADA MICROPLATE

At first order, the Sierran Nevada microplate behaves as a W-tilted fault block, the tilt and erosion of which are roughly balanced by westward-increasing subsidence and sedimentation in the Great Valley (Fig. 1). The bounding structures of the microplate are all diffuse zones. To the east, there is the eastern Sierra escarpment system and the Walker Lane–Eastern California shear zone, which, in the current kinematic regime, is a system of dextral and en echelon normal fault segments along which ~10 mm/yr movement of the Pacific–North American plate motion is partitioned (Unruh et al., 2003). The west margin of the microplate is defined by the San Andreas fault system and Coast Range fold belt (Argus and Gordon, 1991, 2001). The northern end is bounded by the Inks Creek fold belt, which accommodates modest convergence between the microplate and the Klamath Mountains (Harwood and Helley, 1987; Unruh et al., 2003; Fay and Humphreys, 2008). The southern end is bounded by the Garlock fault and the Tehachapi–San Emigdio fold-and-thrust belt (Davis and Burchfiel, 1973; Davis and Lagoe, 1988; Chapman and Saleeby, 2012). The southern ~100 km segment of the microplate is deforming internally by normal motion on the Kern Canyon fault system and Kern range front–Pond-Poso zone, and along sinistral breaks of the White Wolf zone (Guacci and Purcell, 1978; Clinton et al., 2006; Mahéo et al., 2009; Nadin and Saleeby, 2010; Amos et al., 2010).

Figure 1 also shows the axial trace of the Great Valley syncline, a regional fold in Upper Cretaceous through Cenozoic strata exhibiting a low-dipping broad east limb and a steeper-dipping west limb. Maximum subsidence in the Great Valley is linked to west tilt of the microplate along an axis that runs along the western Foothills ramp (Fig. 1). The tilt axis runs continuously for ~350 km along the ramp, where, between ~37°N and ~36°N, it is deformed and obscured by anomalous subsidence along the eastern margin of the Tulare (sub-) Basin. South of Tulare Basin, the tilt axis is deflected into a more northerly trend along the eastern margin of the Kern arch. Upper Cretaceous and Cenozoic strata with low west dips are exhuming adjacent to the western Foothills tilt axis. The across-strike dimension of the exhuming strata increases significantly along the Kern arch and a zone to the north of Tulare Basin that we designate as the central Foothills swell (Fig. 1).

Regional patterns in topographic relief across the Sierra Nevada are exhibited in the Figure 1 inset by smoothed contours that have been constructed by mechanical contouring across major interfluve surfaces (after Wakabayashi and Sawyer, 2001). The contour pattern removes the topographic effects of major west-flowing rivers and displays the regional geometry of a slowly denuding low-relief landscape surface that was inherited from the western shoulder of the Nevadaplano, a regional orogenic plateau that characterized the U.S. Cordillera in Late Cretaceous through mid-Cenozoic time (De Celles, 2004). The Figure 1 inset mates the smoothed topographic profiles of the Sierran uplands to structure contours on the basement surface beneath the Great Valley (Wentworth et al., 1995; see structure sections later herein). The inset also includes color tones that denote the regions undergoing both anomalous rock uplift (delamination bulge) and tectonic subsidence (Tulare Basin) in Pliocene–Quaternary time (explained further later herein).

The Figure 1 inset shows that, in addition to the regional west tilt of the basement surface, Sierran uplands have more subtle longitudinal regional topographic gradients, which slope to the NW and SE off an ~175-km-long range crest culmination that is in excess of 4000 m elevation. Geomorphic and isotopic data resolve paleorelief dating back to the end of the Cretaceous (House et al., 2001; Wakabayashi and Sawyer, 2001; Stock et al., 2004, 2005; Sousa et al., 2013). Figure 2 is the same digital elevation model base as in Figure 1, but with ancient relief and tectonic features displayed for the region that was to become the Sierra Nevada microplate. On this figure, the regions of the Sierran uplands that retain evidence for local paleorelief are shaded in tones denoting greater paleorelief southward, culminating in the Mount Whitney region. The areas of paleorelief possessed major canyons that drained off the west flank of the Nevadaplano, prior to the calving

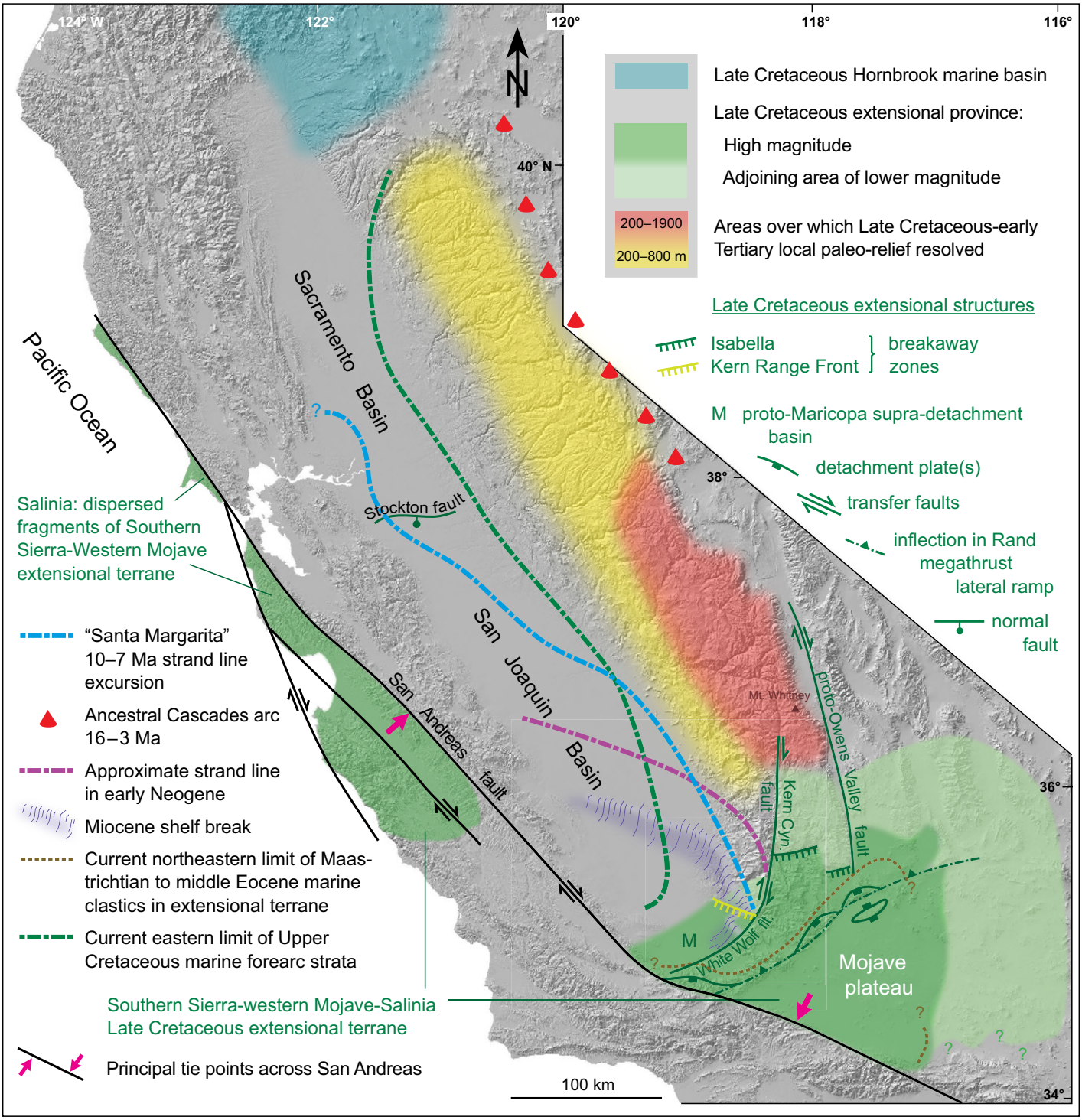

Figure 2. Map showing major features of the Sierran Nevada microplate inherited from the Late Cretaceous convergent margin and Neogene transitional tectonic regimes. Local paleorelief is after House et al. (1998, 2001), Wakabayashi and Sawyer (2001), Stock et al., (2004, 2005), and Sousa et al. (2013). Hornbrook basin is after Nilsen (1984), southern Sierra–Mojave–Salinia Late Cretaceous extensional province is after Miller et al. (1996), Wood and Saleeby (1998), Saleeby (2003), Bartley et al. (2007), Saleeby et al. (2009b), and Chapman et al. (2010, 2012). Facies relations are after Repenning (1960), Bandy and Arnal (1969), Harwood et al. (1981), Cox (1987), Harwood and Helley (1987), Reid (1988), Lucas and Reynolds (1991), Williams, (1997), Monastero et al. (2002), and Figures 5 and 8. Ancestral Cascades arc of northeastern Sierra Nevada is after Busby and Putirka (2009).

off of the Sierra Nevada microplate from the plateau margin at 10 ± 2 Ma (Busby and Putirka, 2009; Saleeby et al., 2009a; Henry, 2012).

The longitudinal topographic gradients of the Sierran uplands also reflect regional paleorelief patterns, as indicated by structural and stratigraphic relations along the northern and southern ends of the microplate. To the north, there is the Late Cretaceous marine Hornbrook Basin, which sits in the subsurface immediately north of the Sierra Nevada (Fig. 2), with its transition into the northern Great Valley marked by the Upper Cretaceous shoreline environment that extended across northern Sierra basement (Nilsen, 1984; Harwood et al., 1981; Harwood and Helley, 1987; Batt et al., 2010). The steeper longitudinal gradient that slopes SE off the range crest culmination represents a paleogradient that developed in response to Late Cretaceous large-magnitude extension of the southern Sierra Nevada–western Mojave region (Wood and Saleeby, 1998; Bartley et al., 2007; Saleeby et al., 2007; Chapman et al., 2010, 2012). Large-magnitude extension of this region was controlled by segmentation patterns in the Late Cretaceous convergent margin (Malin et al., 1995; Saleeby, 2003; Liu et al., 2010), denoted on Figure 2 by the inflection in the Rand (subduction) megathrust lateral ramp. Major crustal structures that developed during this regime are shown on Figure 2 as the Kern Canyon–White Wolf and proto–Owens Valley transfer zones, the Isabella and Kern range front breakaway zones, the Maricopa supradetachment basin, and the southern Sierra detachment system. Figure 2 also shows the presently known extent of the Late Cretaceous southern Sierra–western Mojave extensional terrane and its southwest extension into the displaced Salinia batholithic terrane (after Grove, 1993; Saleeby, 2003; Bartley et al., 2007; Ducea et al., 2009; Saleeby et al., 2009b; Chapman et al., 2010, 2012). The principal tie point between the Salinian basement exposures and those of the western Mojave, across the San Andreas fault, is shown after Huffman (1972). Basement rock exposures of the Late Cretaceous extended terrane are characterized by widespread depositional remnants of Maastrichtian to middle Eocene clastic marine strata (Cox, 1987; Lucas and Reynolds, 1991; Grove, 1993; Wood and Saleeby, 1998; Monastero et al., 2002; Lofgren et al., 2008; Chapman et al., 2012). These depositional remnants sit in structural positions suggestive of formation in supradetachment basins, and/or active graben-horst systems, and they further indicate the development of a continental borderland across the southernmost Sierra Nevada, western Mojave, and restored Salinia in conjunction with extensional tectonism.

Figure 3 is a map of the southern Sierra Nevada region showing selected features that are referred to throughout the text, and Table 1 is an explanation and supporting references for these features. Remnants of Eocene strata interpreted as filling supradetachment basins (Wood and Saleeby, 1998; Chapman et al. 2012) occur along the N-tilted footwall of the proto–Garlock (normal) fault (Fig. 3). These contain marine trace fossils and demonstrate that the low elevations that resulted from Late Cretaceous extension persisted in the southern Sierra region into Tertiary time. A comparison of the positions of the Late Cretaceous extensional terrane and the Hornbrook basin (Fig. 2), and the Upper Cretaceous and Eocene remnants of marine strata lying on northern and southern Sierra Nevada basement (Figs. 2 and 3) with the smoothed topographic contour map of the Figure 1 inset elucidates the importance of regional longitudinal paleorelief variation along the Sierra Nevada.

Regional subbasin domains of the Great Valley consist of the Sacramento and San Joaquin Basins, which are separated by the Stockton arch, a structural high located at ~38°N that is expressed as a transverse ridge in basement surface structure contours (Fig. 1, inset). The Stockton arch is controlled in the subsurface by fault-controlled relief that is buried by upper Cenozoic strata. It is a polyphase structure, with the (principal) Stockton fault (Fig. 2) originating in the Late Cretaceous as a S-down normal fault, which inverted to reverse motion in the early Cenozoic (Imperato, 1995).

Cenozoic strata of the San Joaquin Basin thicken and reflect progressively greater proportions of marine environments southward from ~36.5°N as they pass into a deep-marine basin of Neogene age. The approximate positions of the early and late Miocene shoreline environments and the Neogene shelf break are shown on Figure 2. Shallow-marine and adjacent terrestrial environments of the southeastern San Joaquin Basin extended for at least 10 km eastward across the current southern Sierra basement uplift (Fig. 3; Mahéo et al., 2009; Saleeby et al., 2009a, 2013; Saleeby and Saleeby, 2010). In Quaternary time, the eastern San Joaquin Basin was partitioned into the Tulare (sub-) Basin to the north, and the Maricopa (sub-) Basin to the south by uplift of the Kern arch. The southern end of the original San Joaquin Basin has been destroyed by Quaternary uplift driven by N-S shortening of the Tehachapi–San Emigdio fold-and-thrust belt, and the western margin is actively deforming along the Coast Range fold belt (Fig. 1).

A comparison of Figures 1 and 2 shows that active structures of the diffuse southern margin of the microplate developed in crust that had been highly extended in the Late Cretaceous. Major structures of this diffuse margin that appear to be direct precursors to active structures are the proto–Owens Valley and Kern Canyon–White Wolf transfer zones, and the hinge of the Rand megathrust lateral ramp, along which the Garlock fault formed. Seismic imaging, structural mapping, and petrologic studies indicate that the megathrust lateral ramp was responsible for the Late Cretaceous tectonic erosion of the mantle wedge from beneath the southernmost Sierra Nevada batholith and the adjacent western Mojave–Salinia region of the southern California batholith (Cheadle et al., 1986; Jacobson et al., 1988; Li et al., 1992; Malin et al., 1995; Saleeby et al., 2003; Yan et al., 2005; Luffi et al., 2009; Chapman et al., 2010, 2012). Synchronous with this profound tectonic erosion event, the residual mantle wedge that lay north of the lateral ramp was quenched to a lithospheric geotherm (Ducea and Saleeby, 1996, 1998b; Saleeby et al., 2003). It is the geologically recent and ongoing removal of this residual mantle wedge domain that presents the dynamic system for which we pursue the epeirogenic expression.

INTEGRATED PHYSIOGRAPHIC EVOLUTION–GEODYNAMIC MODEL OF MANTLE LITHOSPHERE REMOVAL AND ITS SURFACE EXPRESSIONS

We present an analysis that leverages observational data against thermomechanical modeling results as a means to pursue the underconstrained problem of the late Cenozoic rock and surface uplift history of the Sierra Nevada. The principal geologic imprint of such uplift is erosion, or removal of rock record. We assert that if our modeling is properly posed in terms of initial and boundary conditions (Part I), it follows that valuable insights into the likely uplift history may be gained from model predictions. We recognize that such modeling can only offer approximations compared to the complexity of the geodynamic system modeled. By linking subsidence data constraints for the adjacent Great Valley to our analysis, we can incorporate geologic imprints that produce rock record, subsidence, and sedimentation. This in turn provides model validation tests that help lend confidence to our treatment of the more poorly constrained (uplift) aspects of our analysis.

We hypothesize that resolvable epeirogenic displacements related to mantle lithosphere removal in the southern Sierra Nevada region are superposed over local and regional paleorelief patterns, and potential far-field–induced vertical displacements that may have affected much of,

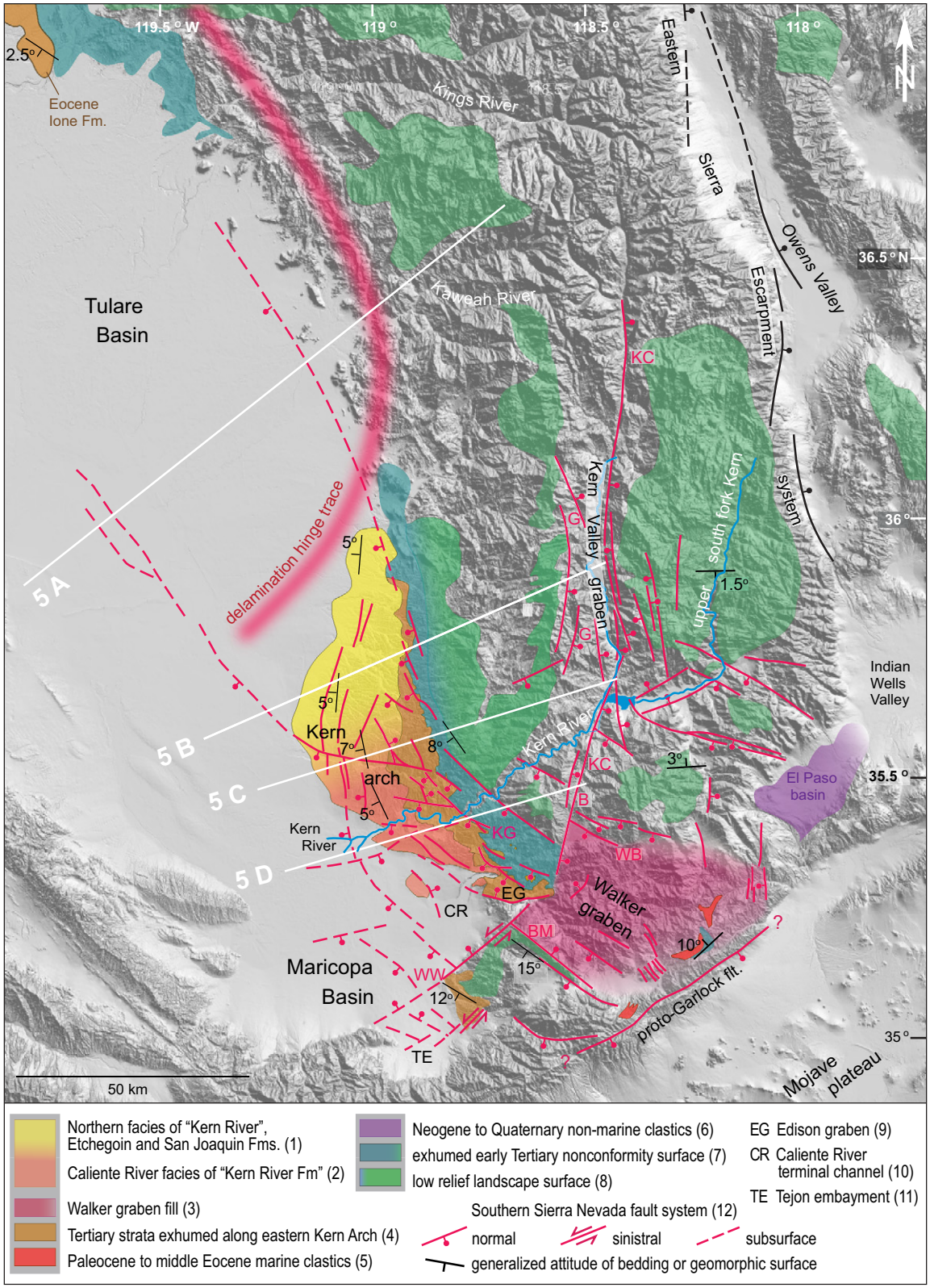

Figure 3. Map showing selected geologic features of southern Sierra Nevada and southeastern San Joaquin Basin, as well as locations of Figure 5 transverse structure sections. Brief descriptions of features as well as sources are given in Table 1, and numbers in parentheses in map explanation refer to entries in Table 1. Note that blind thrusts of Tehachapi–San Emigdio fold-and-thrust belt (Fig. 1) are not shown due to interference with high-angle faults of the southern Sierra fault system. Abbreviations for selected faults of this system are explained under entry 12, Table 1.

TABLE 1. EXPLANATION OF SELECTED GEOLOGIC FEATURES ON FIGURE 3 MAP AND SUPPORTING REFERENCES

Map feature and sources	Explanation
1. Northern facies of "Kern River Formation" that is transitional to San Joaquin and Etchegoin Formations	Pliocene gray-green sandstones and gritty green mudstones and widespread derivative colluvium of northern Kern arch that are transitional to at least upper Pliocene shallow-marine San Joaquin Formation. Transition into uppermost Miocene–lower Pliocene Etchegoin Formation is inferred from spatial and stratigraphic relations. Western Sierra and possible Kern River canyon basement provenance that is distinct from Caliente River facies (2) provenance.
2. Caliente facies of "Kern River Formation" (MacPherson, 1978; Saleeby and Saleeby, 2010; Saleeby et al., 2013)	Upper Miocene to lower Quaternary fluvial, deltaic, and alluvial sandstones and conglomerates deposited across area of southern Kern arch and adjacent western Sierra Nevada by Caliente River, which exhumed most of Walker graben fill, and the headwaters of which probably reached upper south Fork of the Kern River.
3. Walker graben fill (Buwalda, 1954; Michael, 1960; Dibblee and Louke, 1970; Coles et al., 1997; Mahéo et al., 2009; Saleeby and Saleeby, 2010; and unpub. data)	Lower to middle Miocene (21–16 Ma) silicic volcaniclastic and dome/plug complex deposits, andesitic to basaltic flows, hypabyssals and volcaniclastics, and interbedded and overlying fluvial, alluvial, and lacustrine strata as young as upper Miocene–Pliocene. Thickness totals ~2 km. Graben-bounding structures include Walker Basin, Breckenridge/Kern Canyon and Bear Mountains normal faults and proto–Garlock fault footwall tilt block.
4. Tertiary strata exhumed along eastern Kern arch (Addicott, 1965, 1970; Dibblee et al., 1965; Bartow, 1984; Bartow and McDougall, 1984; Olson, 1988; Saleeby and Saleeby, 2010; and unpub. data)	In sequence: Eocene–lower Oligocene and lower Miocene terrestrial Walker Formation, Oligocene shallow-marine Veddar Formation, lower Miocene deep-marine Freeman-Jewett Formation, lower to middle Miocene shallow-marine Olcese Formation, middle Miocene deep-marine Round Mountain Formation, and upper Miocene shallow-marine Santa Margarita Formation. Section is erosionally truncated along eastern margin of Kern Arch.
5. Lower Paleogene marine clastics (Michael, 1960; Dibblee and Louke, 1970; Wood and Saleeby, 1998; Monastaro et al., 2002; Saleeby and Saleeby, 2010; and unpub. data)	Nonconformable remnants of Paleocene to middle Eocene marine fauna bearing extensional clastic strata of the Whitnet Formation resting on Sierran basement. Subsurface data from adjacent Indian Wells Valley encounter widespread similar strata transitional to the Golar Formation exposed to east of Indian Wells Valley.
6. El Paso basin, nonmarine clastics (Loomis and Burbank, 1988)	Middle and upper Miocene Dove Springs Formation records initiation of Garlock fault sinistral slip at ca. 10 Ma, and initiation of southernmost eastern Sierra escarpment system at ca. 8 Ma.
7. Exhumed early Tertiary nonconformity surface (Saleeby and Saleeby, 2010; and unpub. data)	Low-relief, deeply weathered basement surface that maps into continuity with basal nonconformity of Kern arch Tertiary section along relay ramps in range front faults of southern Sierra fault system, and which continues upslope into low-relief end of Cretaceous apatite He isochrone surface. Similar surface emerges from basal Ione and Whitnet Formations at northern and southern ends of map area, respectively.
8. Low-relief landscape surface (Clark et al., 2005; Cecil et al., 2006; Mahéo et al., 2009; Phillips et al., 2011)	Low-relief landscape surface that characterizes large areas of Sierran uplands, and which regionally coincides with end of Cretaceous (ca. 70–65 Ma) apatite He isochrone surface that paralleled western margin of Nevadaplano landscape surface at termination of Cretaceous Sierran arc magmatism.
9. Edison graben (Dibblee and Warne, 1986; Mahéo et al., 2009; Saleeby et al., 2009b; Saleeby and Saleeby; 2010)	Structural trough defined by NE-side-down Edison normal fault and SW-side-down Kern range front normal fault system that is filled by lower to middle Miocene fluvial and rock avalanche and debris-flow strata, middle to upper Miocene shallow-marine strata, and upper Miocene to Pleistocene fluvial strata.
10. Caliente River channel (MacPherson, 1978; Saleeby and Saleeby, 2010; Saleeby et al., 2013)	Abandoned Pleistocene major river channel that currently hosts ephemeral creek is geomorphic remnant of major river drainage that redistributed Walker graben fill into southeastern San Joaquin Basin initiating in late Miocene time.
11. Tejon Embayment (Dibblee et al., 1965; Bartow, 1984; Hirst, 1986; Goodman and Malin, 1992; Mahéo et al., 2009)	Remnant of southernmost San Joaquin Basin that formed a faulted footwall platform in the Neogene controlled by normal displacements on White Wolf and Bear Mountains faults. Currently partly under deformation above blind thrusts of Tehachapi–San Emigdio fold-and-thrust belt (Fig. 1).
12. So. Sierra fault system (Nugent, 1942; Dibblee et al., 1965; Croft and Gordon, 1968; Guacci and Purcell, 1978; Castle et al., 1983; Bartow, 1984; Goodman and Malin, 1992; Mahéo et al., 2009; Saleeby et al., 2009a; Blyth et al., 2010; Blyth and Longinotti, 2013; Amos et al., 2010; Nadin and Saleeby, 2010; Saleeby and Saleeby, 2010; and Figs. 5 and 8)	System of early to middle Miocene graben and horst forming high-angle normal and linked transfer faults, including north-up proto–Garlock fault. Many are remobilized as Pliocene–Quaternary high-angle normal and oblique-slip normal faults. Also includes faults of the Kern arch, southeastern Tulare Basin and Maricopa Basin. Abbreviated faults on Figure 3: B—Breckenridge, BM—Bear Mountain, G—Greenhorn, KC—late Quaternary scarps of Kern Canyon system, KG—Kern gorge, WB—Walker Basin; and WW—White Wolf.

or the entire, Sierra Nevada microplate through Cenozoic time (Suppe et al., 1975; Murphy et al., 1998; Lowry et al., 2000; Pierce et al., 2002; Humphreys, 2008). The region hypothesized to have undergone net rock and surface uplift under the mantle lithosphere removal regime is shown as the delamination bulge on the Figure 1 inset. The bulge dissipates northward across ~38°N latitude and appears to be bounded to the east by the eastern Sierra escarpment system. South of ~36°N, it turns southwestward and runs across the Sierra Nevada and into the eastern San Joaquin Basin, where it is bounded by W-side-down normal faults that step down toward the basin along the Kern arch (Fig. 3). The principal zone of delamination, and hence the area of the resulting bulge, was controlled by the lithospheric structure inherited from Cretaceous high-magma-flux growth of the southern Sierra Nevada batholith (Part I, Fig. 4 therein). The delamination bulge is peripheral to the eastern and southern margins of Tulare Basin, which represents focused tectonic subsidence that is dynamically linked to the bulge. The principal area of the delamination bulge underwent anomalous rock uplift and accelerated river incision mainly in the Pliocene across the San Joaquin, Kings, and Kaweah drainages, and in the Quaternary along the lower Kern drainage (Wakabayashi and Sawyer, 2001; Stock et al., 2004, 2005; Saleeby et al., 2009a; Figueroa and Knott, 2010; Nadin and Saleeby, 2010). Stratigraphic, geomorphic, geodetic, and isotopic data (Stock et al., 2004, 2005; Mahéo et al., 2009; Figueroa and Knott, 2010; McPhillips and Brandon, 2010; Nadin and Saleeby, 2010; Hammond et al., 2012; Cecil et al., 2013) indicate that this phase of rock uplift is diminishing in the north (San Joaquin to Kings transition) and accelerating in the south (lower Kern drainage and Kern arch). Here, we interpret this as the mark of mantle lithosphere removal progressing in three dimensions from the northern to the southern region.

Pliocene–Quaternary rock uplift of the delamination bulge was contemporaneous with anomalous subsidence in Tulare Basin (Saleeby and Foster, 2004; see following). The subsidence is anomalous in that for any given longitudinal trace of the axial to eastern Great Valley, significantly more sediment of younger than 7 Ma age has accumulated in the Tulare Basin; also, the eastern margin of Tulare Basin is the only area of the western Sierra Foothills

that is embayed by Quaternary sediments that have aggraded up drainages, as opposed to either being actively incised or in regional offlap relationship downslope from the tilt axis (Figs. 1 and 3).

Based on geophysical data, petrogenetic data on volcanic-hosted mantle xenoliths, and patterns in Neogene–Quaternary volcanism, the region between the San Joaquin and Kern River drainages is where geologically recent removal of mantle lithosphere has most clearly occurred (Ducea and Saleeby, 1996, 1998a, 1998b; Ruppert et al., 1998; Farmer et al., 2002; Zandt et al., 2004; Reeg, 2008; Frassetto et al., 2011; Gilbert et al., 2012; C.H. Jones, 2012, written commun.; Part I). Thermomechanical modeling (Le Pourhiet et al., 2006; Part I) suggests that removal was initiated in middle Miocene time by Rayleigh-Taylor (RT) convective mobilization of the cooled mantle wedge that formed beneath the Sierra Nevada batholith. The instability progressed to the state of promoting the delamination of the eclogitic root (arclogite) of the batholith. Arclogite is defined as eclogitic arc cumulates and subordinate interlayered spinel ± garnet (wedge) peridotites (Anderson, 2005), which in this application refers to an ~40-km-thick cogenetic sequence that developed beneath the southern Sierra Nevada batholith (Ducea and Saleeby, 1996, 1998b; Saleeby et al., 2003; Fig. 4A). Much of the Sierran arclogite is of crustal origin, but its mechanical properties and vertical position place it in the upper level of the mantle lithosphere, where in primary state it sat above ~40 km of mantle wedge peridotite (Ducea and Saleeby, 1996, 1998b; Ducea, 2001; Saleeby et al., 2003).

The thermomechanical model developed in Le Pourhiet et al. (2006) and Part I used a finite-element code that modeled topography, visco-elasto-plastic temperature-dependent rheologies, and temperature- and composition-dependent densities (after Cundall and Board, 1988; Poliakov et al., 1993; Le Pourhiet et al., 2004). The better-constrained geological parameters such as initial geotherm, structural geometry, and elastic and brittle rheologies were fixed, and the most poorly constrained creep parameters were varied and evaluated in terms of their ability to simulate observed mantle structure and geological resultants. The model trace is along a transverse section centered along the Kings and Kaweah interfluves (Part I, Fig. 1 and Fig 1. herein), and it accounts for initial lithospheric structure, geotherm, and topography. The model does not account for motion across the model trace. Errors induced by not accounting for dextral shear of the San Andreas fault and Walker Lane shear zones (Unruh et al., 2003) are uncertain, but they are provisionally considered to be minimal considering the apparently low degree of coupling between normal and tangential stress and strain components observed along these strike-slip systems (Zoback et al., 1981, 1987; Mount and Suppe, 1987).

In Figure 4A, we present a summary of our preferred model, highlighting the initial state (0 m.y.) and two key steps in forward model time at 10 and 20 m.y. (after Part I; Figs. 5 and 6). The 10 m.y. step is critical because it shows the break-off of the Sierra Nevada microplate by the ascent of asthenosphere to the base of the crust east of the Sierra Nevada batholith. The sequence of events that arises in our preferred model suggests that arclogite root delamination began to progress slowly as microplate break-off occurred (Part I, Fig. 6, 10 m.y. and 14 m.y. steps), accelerated rapidly over ~5 m.y., and that it is still progressing (Fig. 4A, 20 m.y. step). The Tulare Basin coincides with much of the area where the partly delaminated root remains attached to the lower felsic crust (Zandt et al., 2004; Reeg, 2008; Frassetto et al., 2011; Gilbert et al., 2012; C.H. Jones, 2012, written commun.). Integration of all available seismic data for the region suggests that the partially delaminated root is suspended in the upper mantle steeply eastward and southward from its residual zone of attachment (Le Pourhiet et al., 2006; Part I). Accordingly, we constructed the vertically projected surface trace of the locus of root detachment and defined it as the delamination hinge trace on Figures 1 and 3. This trace approximates the transition between anomalous subsidence of Tulare Basin and the delamination bulge. The delaminated portion of the arclogite root that is suspended in the mantle and the associated thermal anomaly that extends to within the adjacent peridotitic mantle form the high-wavespeed "Isabella anomaly" (after Jones et al., 1994; Part I, Fig. 3 therein).

Model predictions (Part I) for the vertical displacements in Earth's surface along a transverse profile across the microplate arising from root delamination are plotted in Figure 4B. This shows displacement profiles initiating at ~10 m.y. (forward model time), the time at which lithospheric break-off is predicted, resulting in the inception of the Sierra Nevada microplate (Fig. 4A). Several lines of evidence indicate that microplate inception, as recorded by initiation of the eastern Sierra escarpment system, occurred at 10 ± 2 Ma (Loomis and Burbank, 1988; Henry and Perkins, 2001; Surpless et al., 2002; Mahéo et al., 2004; Busby and Putirka, 2009; Saleeby et al., 2009a). The initial conditions for our model simulate a basal thermal perturbation arising from the opening of the Pacific-Farallon slab window as instigating mantle lithosphere instability. Slab window opening occurred at ca. 23–20 Ma beneath the model trace, but was time transgressive over ~10 m.y. across the entire southern Sierra Nevada region (Atwater and Stock, 1998; Wilson et al., 2005). This leads to several million years of uncertainty in applying the model results to observed geologic history. The 10 m.y. model prediction for microplate inception and the 10 ± 2 Ma inception from observations are in very close agreement, considering the temporal and spatial relations of slab window opening. The vertical displacement profiles of Figure 4A correspond to minimum rock uplift in upland areas and tectonic subsidence in basinal areas. Added components of subsidence and uplift arising from sediment loading and exhumation are pursued later herein. We interpret the 20–22 m.y. period of model time (Fig. 4A) to correspond to modern geologic time, given the range of uncertainties outlined earlier, and to be applicable to an ~150-km-wide transverse corridor centered along the Kings and Kaweah drainages (Figs. 1 and 3). Vertical displacement values of Figure 4B are summarized for Tulare Basin and the eastern Sierra crest in Table 2. A comparison of these values to observations is complicated by the limited nature of the observational data, as well as the complexity in temporal and spatial relations. In terms of tectonic subsidence, the best data constraints are for stratigraphic markers in the ≤7 +1/–0 Ma age range (discussed later herein), and thus we adopt the 14–22 m.y. period of subsidence (~680 m) as most appropriate for comparison. An additional complexity for the rock uplift comparison is the model predictions for rapid eastern crest uplift from 20 m.y. to 22 m.y., followed by rapid crest subsidence. We discuss observational data that perhaps mimic such a pattern across space. For our main comparison with the observational data, we adopt ~800 m as the best nominal prediction for delamination-driven eastern crest rock uplift, and we discuss geographic variations that could reflect positive growth through the ~800 m phase (21–22 m.y.), as well as a possible transition into the post–22 m.y. eastern crest subsidence phase.

Model iterations presented in Part I suggest that vertical displacements in Earth's surface are driven primarily by arclogite root delamination, with RT-driven displacements being of second-order importance. We thus refer primarily to the delamination process here. Delamination-related epeirogenic transients are driven by a combination of flexure of the outer elastic crust related to the changing distributed load geometry of the arclogite root, and to isostatic changes related to upper-mantle–lower-crustal density redistributions. The relative contributions

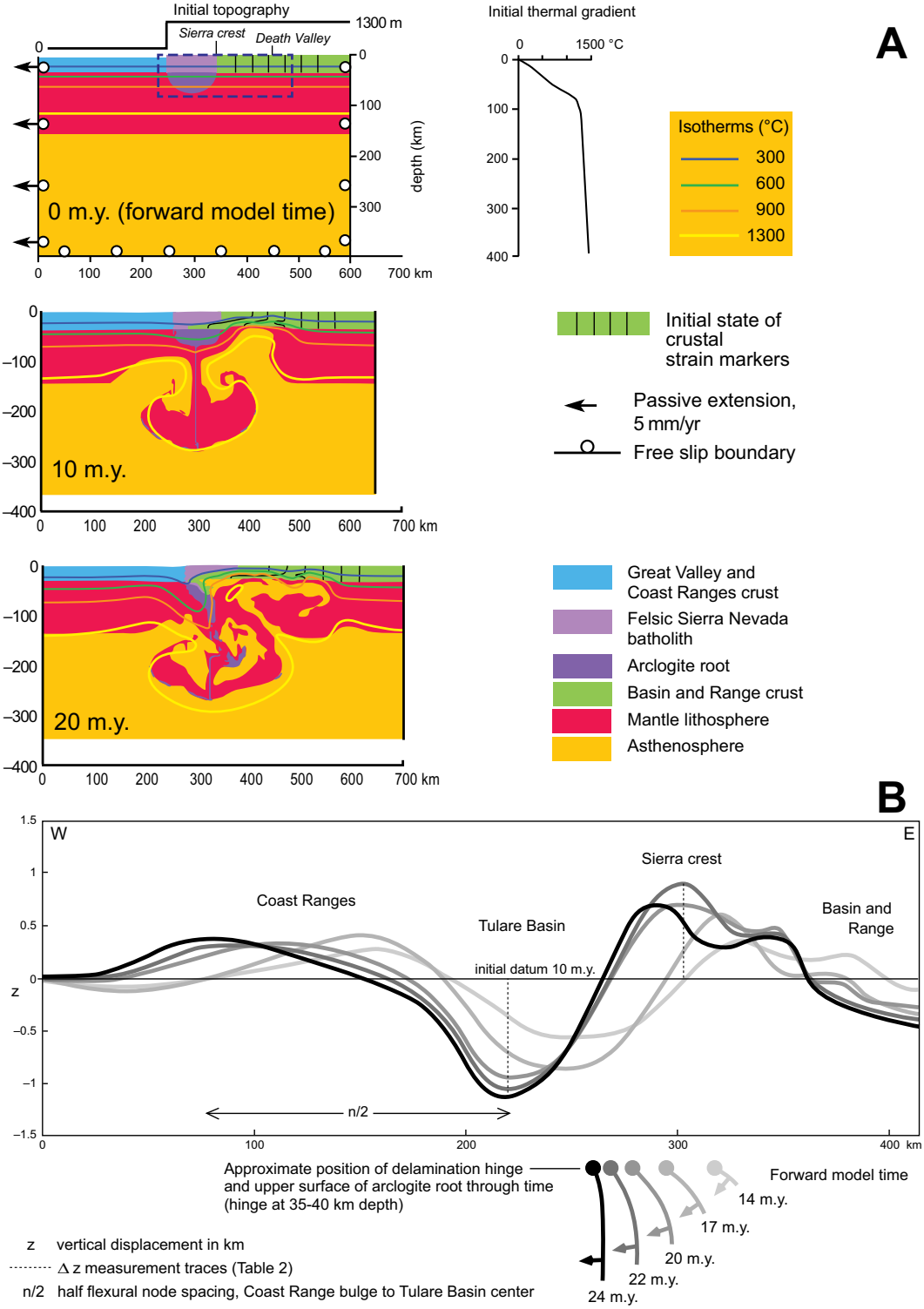

Figure 4. Selected results from preferred thermomechanical model of Part I. (A) Overview of results showing initial model state (0 m.y. model time) and two key time steps, at 10 m.y. (model time) showing lithospheric separation at time of Sierra Nevada microplate inception, and 20 m.y., which approximates contemporary state (after Part I, Figs. 5 and 6 therein). (B) Plot showing vertical displacement profiles in Earth's surface along transverse model trace for selected time steps after 10 m.y. (model time) inception of the Sierra Nevada microplate. Upland displacements equate to minimum rock uplift, and basinal displacements equate to tectonic subsidence. Model trace crosses eastern Sierra crest at ~36.8°N. The modeled migration path of the delamination hinge is registered to the profiles along the bottom of the plot. The rock uplift domain east of Tulare Basin is defined as the delamination bulge, with dynamically linked rock uplift of the Coast Ranges defined as the sympathetic bulge. Vertical displacement profiles for earlier model time are shown in Part I (their Fig. 13).

TABLE 2. THERMOMECHANICAL MODEL PREDICTIONS FOR TECTONIC SUBSIDENCE AND ROCK UPLIFT FOR 10 M.Y. TO 24 M.Y. PERIOD OF MODEL TIME (FIG. 4B) DERIVED FROM PREFERRED MODEL OF ARCLOGITE ROOT DELAMINATION (MODEL 4, PART I)

	Tulare Basin tectonic subsidence (m)		Eastern Sierra rock uplift (m)	
Time (m.y.)	Time increment	Running total	Time increment	Running total
10–14	360	360	–100	–100
14–17	340	700	365	265
17–20	245	945	450	715
20–22	95	1040	195	910
22–24	70	1110	–375 (–195)	535 (715)*
14–22 difference	–	*680*	–	*1010*

*For eastern Sierra crest rolling ~15 km to west from 20–22 m.y. position.

from flexure and isostasy in the production of the delamination bulge cannot be quantitatively extracted from the model, but they can be visualized at first order in Figure 4B, with the flexural component being comparable to the modeled flexural uplift of the Coast Ranges resulting from the root load, and the added isostatic component summing to the form of the delamination bulge. The double peaks for the delamination bulge result from the maximum flexural and isostatic components being slightly out of phase. We provisionally relate our model results quantitatively to observational data on subsidence and uplift, recognizing that the model system is highly idealized relative to the actual physical system that we are modeling. Pysklywec and Cruden (2004) performed analogue experiments investigating surface vertical displacement patterns arising from mantle lithosphere removal, and they found that structural flaws in the crust induce local-scale vertical displacements that are nontrivial with respect to the length scales of the epeirogenic zone. The crust of the southern Sierra Nevada and San Joaquin Basin possessed numerous tectonic structures that predated mantle lithosphere removal that could likewise induce vertical displacements and changes in horizontal length scales that are not accounted for in our numerical modeling approach. We discuss such limitations in our modeling as we proceed.

We now proceed to the observational data on uplift and subsidence, and we compare these data quantitatively to model results along transverse profiles, parallel to the model trace. We then use specific features predicted by the modeling to qualitatively pursue delamination in three dimensions.

LATE CENOZOIC ROCK UPLIFT OF THE SOUTHERN SIERRA NEVADA

Estimates for late Cenozoic rock uplift along the eastern Sierra crest are 2 ± 0.5 km (Huber, 1981; Unruh, 1991; Wakabayashi and Sawyer, 2001; Wakabayashi, 2013) to little or zero (Poage and Chamberlain, 2002; Mulch et al., 2006; Cassel et al., 2009, 2012). The former interpretation is based mainly on the updip projection of upper Cenozoic strata lying along the Foothills ramp, and basement incision beneath Neogene surfaces, both determined north of 37°N. The latter interpretation is based mainly on stable isotope paleo-altimetry. The accuracy of the former procedure is called into question by the modeling of geomorphic forcing (Small and Anderson, 1995; Pelletier, 2007), as well as thermomechanical modeling (Part I), both of which suggest flexure of the Sierra Nevada crust during rock uplift, drainage basin exhumation, and Great Valley sediment loading. Furthermore, the updip projections of some key upper Neogene units along the Foothills ramp yield crest elevations up to ~400 m too high (Wakabayashi and Sawyer, 2001), and the updip projections of apatite (U-Th)/He isochrone surfaces within the batholith of the Kings and San Joaquin drainages yield crest elevations that are ~1500 m too high (McPhillips and Brandon, 2010). These findings show that the microplate deformed internally during its west tilt, undermining the precision of the geometric analysis of tilt. Nevertheless, the tilt analysis based on differentially tilted strata of the Foothills ramp (Unruh, 1991) clearly shows that some component of west tilt operated over Pliocene–Quaternary time. Unfortunately, basement incision alone, even below given Neogene surfaces, offers little in terms of the timing of such incision and its application to eastern Sierra uplift. Paleo-altimetric constraints on Sierra Nevada elevation history based on stable isotopes are not robust at up to ~1000 m resolving power (Galewsky, 2009a, 2009b; Molnar, 2010). Thus, the contrary findings of both procedures for determining Sierra Nevada uplift, or lack thereof, carry comparable uncertainties.

Considering that direct evidence for both geologically recent (Pliocene–Quaternary) delamination, and the timing and amount of rock uplift is restricted to the Sierra Nevada south of 38°N, we focus primarily on Pliocene–Quaternary rock uplift constraints for the region south of 38°N.

Pliocene–Quaternary Rock Uplift Patterns in the Southern Sierra Nevada

Constraints for Pliocene–Quaternary rock uplift are direct for Kings River and lower Kern River drainages, and by inference relatively strong for the Kaweah, San Joaquin, and Stanislaus drainages. Kings River drainage rock uplift is directly constrained by cosmogenic dating of tiered cave sediments in a deeply incised vertical marble unit (Stock et al., 2004, 2005). These studies indicate a total of ~400 m of incision between 3.0 and 1.5 Ma, with an order of magnitude drop in rates between 1 and 1.5 Ma, interpreted by these workers as a result of protective mantling of the channel bottom by glacially derived debris. Alternatively, the drop in incision rates could result from the upstream migration of a knickpoint past the point where the incision rate was measured. We also note here, and return to under our discussion of Tulare Basin subsidence, that our modeling predicts phases of subsidence across the Sierran uplands, as well as phases of rock uplift (Fig. 4B). Such subsidence phases superposed on the regional tilt pattern could have temporarily dampened river gradients, thereby temporarily slowing incision. Cosmogenic age data for marble units in three forks of the Kaweah drainage (Fig. 1) fall on the Kings River array, suggesting a common incision history. One data point along the lower Stanislaus drainage (Fig. 1) lies at the lower end of the Kings and Kaweah data array, which could be argued to lie on the rapid incision trend, or a slower trend. Proximity of the San Joaquin drainage to the Kings drainage, its intermediate position relative to the Kings and Stanislaus drainages, and the commonly cited evidence for Pliocene west tilt and incision for the San Joaquin drainage (Huber, 1981; Unruh, 1991; Wakabayashi and Sawyer, 2001; Wakabayashi, 2013) indicate a common forcing and incision regime as that which is directly documented for the Kings drainage.

The ~400 m of late Pliocene incision documented in the Kings drainage was modeled by Stock et al. (2004) as a transient response to ~1500 m of eastern crest uplift initiating in the late Miocene. Such tectonic forcing is in line with 10 ± 2 Ma inception of the Sierra Nevada microplate, the development of the eastern Sierra escarpment system (Loomis and Burbank, 1988; Henry and Perkins, 2001; Surpless et al., 2002; Mahéo et al., 2004; Busby and Putirka, 2009; Saleeby et al., 2009a), and our model results, which predict the initial stages of delamination bulge growth between 10 and 14 m.y. model time (Fig. 4B).

Quaternary rock uplift along the lower Kern River area is constrained by stratigraphic relations

of the eastern San Joaquin Basin, low-temperature thermochronologic data, and geomorphic relations. Map and stratigraphic relations summarized in Figure 3 and in the Figures 5B–5D structure sections show that the upper Pliocene shallow-marine San Joaquin Formation is erosionally truncated updip along the Kern arch. The Kern arch differs from the Foothills ramp north of 37°N in being intensely broken by high-angle normal faults, i.e., far too many to show on Figure 3 (Nugent, 1942; Bartow, 1984; Mahéo et al., 2009; Saleeby et al., 2009a). Normal faulting of the Kern arch extends northwards into Tulare Basin (Figs. 3 and 5; Croft and Gordon, 1968; Saleeby and Foster, 2004, Data Repository map). Regardless of late Cenozoic normal faulting in Tulare Basin and the Kern arch, bedding is regionally homoclinal like that of the main Foothills ramp and eastern Great Valley to the north. Stratal thickness and erosional truncation patterns suggest that in excess of ~1000 m of Kern arch strata were stripped off the basement along the eastern margin of the arch in the Quaternary (Figs. 5C and 5D). The lower Kern River basement gorge (Fig. 3) was cut subsequent to erosional stripping of the eastern Kern arch strata off the basement, and it represents a superimposed drainage with its large meanders resembling in wavelength and amplitude the meanders that are cut into the Tertiary section downslope on the arch. The lower gorge of the Kern River has incised ~700 m into basement below the exhumed Tertiary nonconformity surface. Integration of stratigraphic, geomorphic, and apatite He thermochronometric data presented later herein under "Quaternary cryptic subsidence and rock uplift of the Kern Arc" indicate ~1–1.8 km of Quaternary exhumation and rock uplift for the lower Kern Gorge area, in addition to the ~700 m of lower gorge basement incision. In terms of local relief variation, the lower Kern River gorge is the most profound river channel to exit the western Sierra Nevada Foothills. Geomorphic studies along the western Foothills between 35.5°N and 37°N suggest that lower channel reaches become progressively younger southward from the Kings to Kern drainages, and that the lower Kern gorge is likely as young as ca. 0.5 Ma (Figueroa and Knott, 2010).

Geomorphic and stratigraphic relations along the Kern arch segment of the Foothills ramp are of little use in constraining eastern Sierra crest rock uplift. Pliocene–Quaternary internal faulting of the Kern arch and the southern Sierra south of ~36°N clearly negates the updip projection of bedding surfaces as a constraint for eastern crest rock uplift (Mahéo et al., 2009; Saleeby et al., 2009a). The west tilt of the Kern arch and the updip exhumation of its Tertiary strata appear to be linked to late Cenozoic W-side-up normal faulting along the Greenhorn and Breckenridge faults, and late Quaternary breaks of the Kern Canyon system (Fig. 3; Mahéo et al., 2009; Saleeby et al., 2009a; Amos et al., 2010; Nadin and Saleeby, 2010). The region east of the Kern Valley graben (Fig. 3) is characterized by the relict regional south slope inherited from the Late Cretaceous (Fig. 2), which to the south has been back tilted ~3°N by Neogene extensional faulting (Fig. 3; Mahéo et al., 2009).

The southward progressive youthfulness of lower channel reaches from the Kings to Kern drainages is paralleled by other constraints on geologically recent rock uplift patterns. The comparison of basement and river channel detrital apatite He age arrays from the San Joaquin and Kings River drainages indicates that relief is decreasing in the San Joaquin drainage relative to the Kings drainage (McPhillips and Brandon, 2010). As discussed already, the Kings and Kaweah drainages have slowed considerably in basement incision over the past 1.5 m.y., while the lower Kern channel has undergone accelerated incision through the Quaternary. Geodetic data for the Sierra Nevada indicate a similar pattern for contemporary vertical displacements in Earth's surface (Fay et al., 2008; Bennett et al., 2009; Nadin and Saleeby, 2010; Hammond et al., 2012). Figure 6 shows a synthesis of contemporary vertical displacement data based on global positioning system (GPS) monuments and interferometric synthetic aperture radar (InSAR) data for much of the Sierra Nevada, as well as stratigraphic and level line data for the Kern arch. This synthesis shows that the area shown as the delamination bulge on the Figure 1 inset is undergoing active rock uplift, with the main area of the bulge undergoing ~1 mm/yr, increasing to ~2 mm/yr into the Kern arch area. The rapid vertical displacement pattern of the Kern arch area is truncated to the west by W-side-down normal faulting (Fig. 3). West of the Kern arch, the San Joaquin Basin is in subsidence, although absolute vertical motion is obscured by groundwater removal subsidence (Lofgren and Klausing, 1969; Castle et al., 1983). Figure 6 also shows that the central Foothills swell is actively ascending relative to the northeast edge of Tulare Basin, as well as the ramp to the north of ~38°N. As discussed herein, we interpret this swell as part of the delamination epeirogenic signal as well.

Accelerated Rock Uplift and Active Thermal Transient

The most actively rising region of the southern Sierra Nevada, as delineated here (Fig. 6), also coincides with an active thermal anomaly defined here as the spatial overlap of numerous warm and hot springs and wells with regionally low basement heat flow. Measured heat flow in the Sierra Nevada batholith is amongst the lowest known on continents, particularly along the western Foothills (cf. Saltus and Lachenbruch, 1991). Study of Sierran lower-crustal exposures and mantle xenoliths show that this low-heat-flow signal is inherited from the conductive cooling of the Cretaceous batholith and its mantle wedge from beneath by slab flattening (Ducea and Saleeby, 1996; Lee et al., 2000; Saleeby et al., 2003, 2007; Brady et al., 2006; and modified after Dumitru, 1990). In Figure 7, we plot the locations of warm and hot springs and wells, and "hot oil fields" of the Kern arch (after Laney and Brizzee, 2003; Saleeby and Saleeby, 2009; Cecil et al., 2013). In the Figure 7 inset, we show comparative down-hole temperature data for a sample of hot oil fields on the Kern arch in comparison to values typical of the basin directly west of the arch. These data demonstrate a profound thermal anomaly beneath the Kern arch, which is modeled and discussed in more detail along with down-hole thermochronologic data in Cecil et al. (2013). On Figure 7, we also plot the basement heat-flow data (after Saltus and Lachenbruch, 1991). To this, we overlay a color tone denoting the areas containing younger than 4 Ma volcanic rocks interpreted to have erupted in conjunction with delamination (Ducea and Saleeby, 1998a; Manley et al., 2000; Farmer et al., 2002; Part I). The springs and wells are co-extensive with

Figure 5 (*on following page*). Transverse structure sections across the eastern Tulare Basin and the Kern arch. Locations of sections are given in inset, along with Figure 8 longitudinal structure sections, and Figure 12 western Sierra Foothills topographic profile and eastern Great Valley lithospheric structure section. Wells used for Figure 5 structure sections are given in Supplemental File 1[1]. Stratigraphic picks are also based partly on seismic data in Bloch (1991) and Miller (1999).

[1]Supplemental File 1. Well name and location data for oil wells used in Figure 5 structure sections. If you are viewing the PDF of this paper or reading it offline, please visit http://dx.doi.org/10.1130/GES00816.S1 or the full-text article on www.gsapubs.org to view Supplemental File 1.

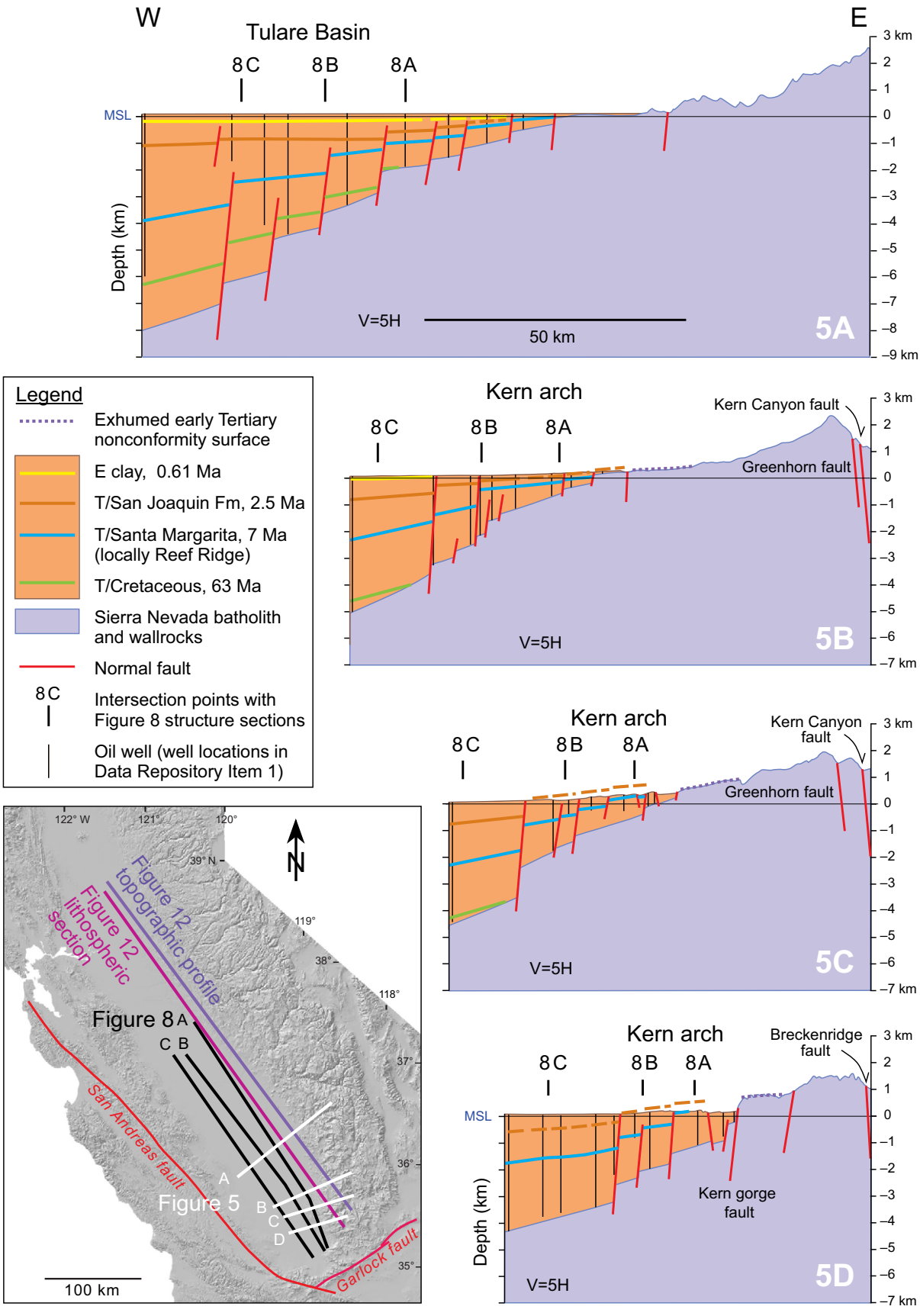
W
E
Tulare Basin
8C
8B
8A
MSL
Depth (km)
V=5H
50 km
5A
3 km
2
1
0
–1
–2
–3
–4
–5
–6
–7
–8
–9 km
Legend
Exhumed early Tertiary nonconformity surface
E clay, 0.61 Ma
T/San Joaquin Fm, 2.5 Ma
T/Santa Margarita, 7 Ma (locally Reef Ridge)
T/Cretaceous, 63 Ma
Sierra Nevada batholith and wallrocks
Normal fault
8C
Intersection points with Figure 8 structure sections
Oil well (well locations in Data Repository Item 1)
Kern arch
Kern Canyon fault
Greenhorn fault
V=5H
5B
–7 km
Kern arch
Kern Canyon fault
Greenhorn fault
V=5H
5C
–7 km
Kern arch
Breckenridge fault
Kern gorge fault
MSL
Depth (km)
V=5H
5D
–7 km
122° W
121°
120°
39° N
119°
38°
118°
37°
36°
35°
N
Figure 12 topographic profile
Figure 12 lithospheric section
Figure 8
A
C B
San Andreas fault
Figure 5
A
B
C
D
Garlock fault
100 km

Figure 5.

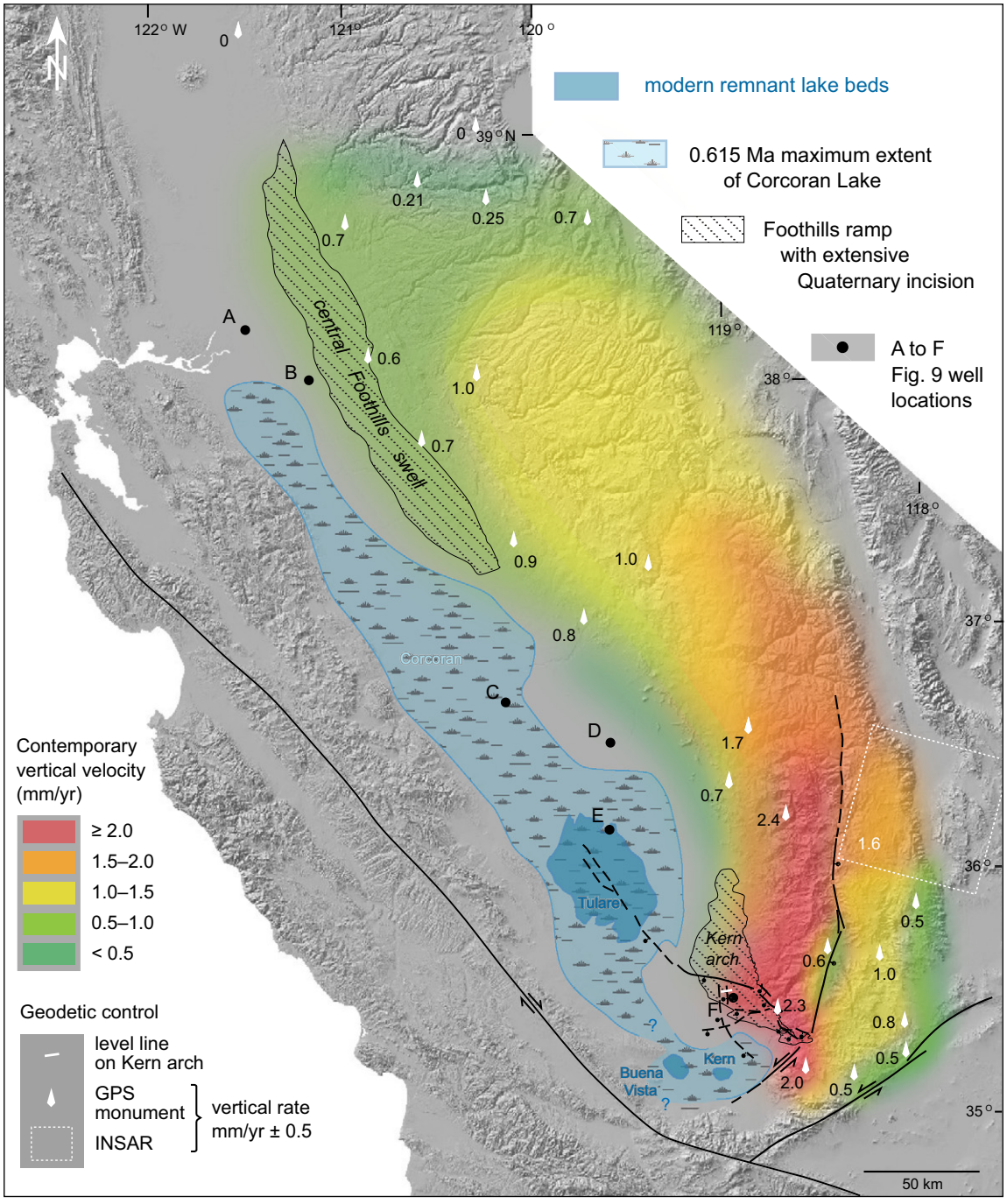

Figure 6. Map showing synthesis of geodetic constraints on the contemporary vertical displacement rates of Sierra Nevada and Kern arch based on global positioning system (GPS) monument, interferometric synthetic aperture radar (InSAR), level line data, and Kern arch stratigraphic constraints. Contouring is interpretive and modified after mechanical contouring of Hammond et al. (2012). Data are synthesized after Castle et al. (1983), Fay et al. (2008), Bennett et al. (2009), Nadin and Saleeby (2010), Hammond et al. (2012), Cecil et al. (2013), and http://www.geol.ucsb.edu/projects/geodesy/ level_lines/X0029_KERN_FRONT.html. Also shown are maximum extent of Corcoran Lake after Frink and Kues (1954), and Figures 5 and 8 structure sections, and locations of wells used for Figure 9 subsidence curves.

the volcanics along the eastern Sierra Nevada region, but they also extend southwestward along the most rapidly rising domain of the delamination bulge (Figs. 6 and 7), which has been nonvolcanic since early Miocene slab window–related volcanism.

We interpret the hydrothermal systems that are delivering the heated waters to springs and wells in the otherwise anomalously cool batholithic host rocks as the "head wave" of an active thermal transient that is being driven by the youngest phases of root delamination. The area of the anomalous thermal transient corresponds to the footwall tilt-block of the Greenhorn–Breckenridge–Kern Canyon normal fault system (Fig. 3), which is the fastest-rising area of the entire Sierra Nevada (Fig. 6). Scattered delamination volcanics and elevated basement heat-flow values to the east of this normal fault system (Fig. 7) represent a more mature thermal state of the crust arising from the late Miocene–Pliocene phases of east-to-west delamination. Accordingly, this eastern, partially equilibrated domain merges northward with the region characterized by more copious delamination volcanism. The western anomalous province overlies prominent mid-crustal and upper-mantle negative conversions in seismic receiver functions that appear to terminate adjacent to the delamination hinge trace (Frassetto et al., 2011; Part I, Figs. 3B and 3C therein). The negative conversions merge northeastward with the negative conversions that lie beneath the area of widespread delamination volcanism. Seismic tomography and refraction data show low-velocity upper mantle extending to the base of the crust beneath the anomalous province as well (Mereu, 1987; Ruppert et al., 1998; Schmandt and Humphreys, 2010; Reeg, 2008; Part I, Figs. 3B and 3C therein). We interpret the shallow, low-velocity mantle as ascended asthenosphere that has replaced the delaminated root, and the negative conversions beneath the anomalous province as domains of partial melt that have yet to render surface eruptions.

The correspondence of the anomalous thermal province with the area of most rapid active rock uplift, their mutual position relative to the delamination hinge trace, and the diminished rock uplift rates in regions to the north are in line with the interpretation that root delamination initiated from east to west in late Miocene–Pliocene time along the southern Sierra, and then transitioned to a south-to-north pattern in Quaternary time in the region of the Kern arch and lower Kern River basement gorge. The resulting delamination hinge trace correspondingly forms an ~90° sector along the southern perimeter of Tulare Basin.

SUBSIDENCE PATTERNS ALONG THE AXIAL TO EASTERN SAN JOAQUIN BASIN

In this section, we pursue anomalous subsidence in Tulare Basin by the analysis of a series of (longitudinal) structure sections drawn parallel to the axis of the southern Great Valley (Fig. 8). We extend this analysis across the Kern arch in pursuit of related subsidence across the arch that has been rendered cryptic due to Quaternary rock uplift and erosion.

Anomalous Subsidence of Tulare Basin

Tulare Basin is recognized as a distinct tectonically controlled late Pliocene–Quaternary accommodation space nested within the San Joaquin Basin (Davis and Green, 1962). It is unique to the entire Great Valley. The current southern limit of the basin corresponds to the actively uplifting Kern arch, but stratigraphic relations discussed here show that the latest Miocene–Pliocene subsidence regime that affected Tulare Basin also extended across the arch, prior to its Quaternary uplift. A high flux of Neogene volcaniclastics shed into northern Tulare Basin from the west flank of the central Sierra Nevada obscures the northern extent of its anomalous subsidence. Constraining the amount of subsidence in Tulare Basin is challenging because it is superposed across late Oligocene to early Pliocene NW-trending facies boundaries that diagonally cross the San Joaquin Basin, such that earlier terrestrial and shoreline environments occupied the principal area of the superposed subbasin, and the current southern margin of the subbasin along the emergent Kern arch was superposed across the Neogene shelf break (Figs. 1 and 2; Klausing and Lohman, 1964; Lofgren and Klausing, 1969; Graham and Williams, 1985; Bloch, 1991; Miller, 1999). Furthermore, the western margin of Tulare Basin coincides with the regional synclinal trough of the Great Valley, as well as the forelimb of the Coast Ranges fold belt. Thus, the initial basin structure over which the Tulare Basin was superposed is geometrically complex, offering little in terms of laterally extensive uniform markers that can be used to track subsidence patterns. Furthermore, much of the younger (Quaternary) strata along the axial to eastern margin of the basin are alluvial-fluvial sands and gravels that offer little in terms of useful stratigraphic or time markers. We approach this problem by deriving subsidence residuals for Tulare Basin relative to regional subsidence patterns along the Great Valley.

Three evenly spaced longitudinal structure sections are presented along the San Joaquin Basin in Figure 8. The section traces are shown on the Figure 5 inset. Well files used to generate the sections are tabulated in Supplemental File 3[3]. Regionally continuous stratigraphic markers along the eastern to axial San Joaquin Basin consist only of the upper Miocene Santa Margarita Formation, an extensive, mainly littoral sand sheet, Upper Cretaceous forearc basin strata, and the basement nonconformity. The range of Santa Margarita deposition is regionally constrained to 12–6.5 Ma (after Bartow and McDougall, 1984; Olson, 1988; Goodman and Malin, 1992; Hosford Scheirer and Magoon, 2003). In our analysis, we generalize the end of deposition as 7 Ma. In the southwestern part of the basin, facies transitions into the

Figure 7 (*on following page*). Map showing locations of warm and hot springs and wells, and hot oil fields of southern Sierra Nevada and Kern arch, and southern Sierra Nevada basement heat-flow sites (after Saltus and Lachenbruch, 1991; U.S. Department of Energy, 2003). Inset shows samples of down-hole temperature determinations for high-thermal-gradient oil fields of Kern arch (Round Mountain and Mount Poso fields) in comparison to determinations in cooler Rosedale field located off the edge of the Kern arch, for which data points lie along a geotherm that is similar to the regional gradients along the western Sierra Nevada and current depositional axis of the San Joaquin Basin (Graham and Williams, 1985; Wilson et al., 1999; Brady et al., 2006; Saleeby and Saleeby, 2009). Down-hole temperature data are given in Supplemental File 2[2]. Also shown are areas affected by early Miocene slab window volcanism, and 0–4 Ma delamination volcanism (Part I).

[2]Supplemental File 2. Down hole temperature data for Mt. Poso and Round Mountain oil fields of Kern Arch, and Rosedale oil field situated off western margin of Kern Arch. Note that all temperature determinations were made prior to steam injection or fire flooding of the respective oil fields. If you are viewing the PDF of this paper or reading it offline, please visit http://dx.doi.org/10.1130/GES00816.S2 or the full-text article on www.gsapubs.org to view Supplemental File 2.

[3]Supplemental File 3. Well name and location data for oil wells used in Figure structure sections. If you are viewing the PDF of this paper or reading it offline, please visit http://dx.doi.org/10.1130/GES00816.S3 or the full-text article on www.gsapubs.org to view Supplemental File 3.

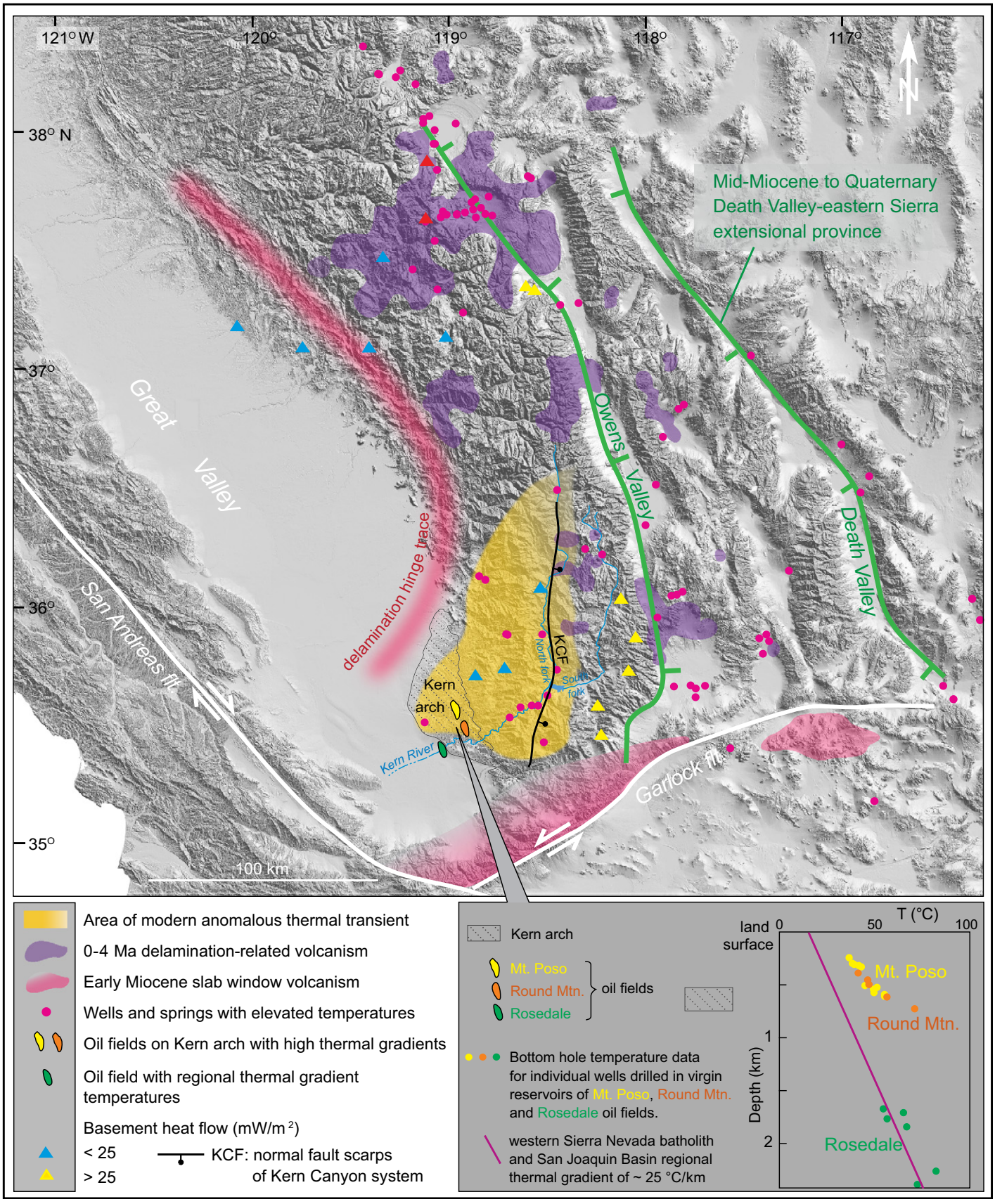
121° W
120°
119°
118°
117°
N
38° N
37°
36°
35°
Mid-Miocene to Quaternary
Death Valley-eastern Sierra
extensional province
Great
Valley
Owens Valley
Death Valley
delamination hinge trace
San Andreas flt.
KCF
North fork
South fork
Kern
arch
Kern River
Garlock flt.
100 km
Area of modern anomalous thermal transient
0-4 Ma delamination-related volcanism
Early Miocene slab window volcanism
Wells and springs with elevated temperatures
Oil fields on Kern arch with high thermal gradients
Oil field with regional thermal gradient temperatures
Basement heat flow (mW/m 2)
< 25
> 25
KCF: normal fault scarps of Kern Canyon system
Kern arch
Mt. Poso
Round Mtn.
Rosedale
oil fields
Bottom hole temperature data for individual wells drilled in virgin reservoirs of Mt. Poso, Round Mtn. and Rosedale oil fields.
western Sierra Nevada batholith and San Joaquin Basin regional thermal gradient of ~ 25 °C/km
T (°C)
land surface
0
50
100
Depth (km)
1
2
Mt. Poso
Round Mtn.
Rosedale

Figure 7.

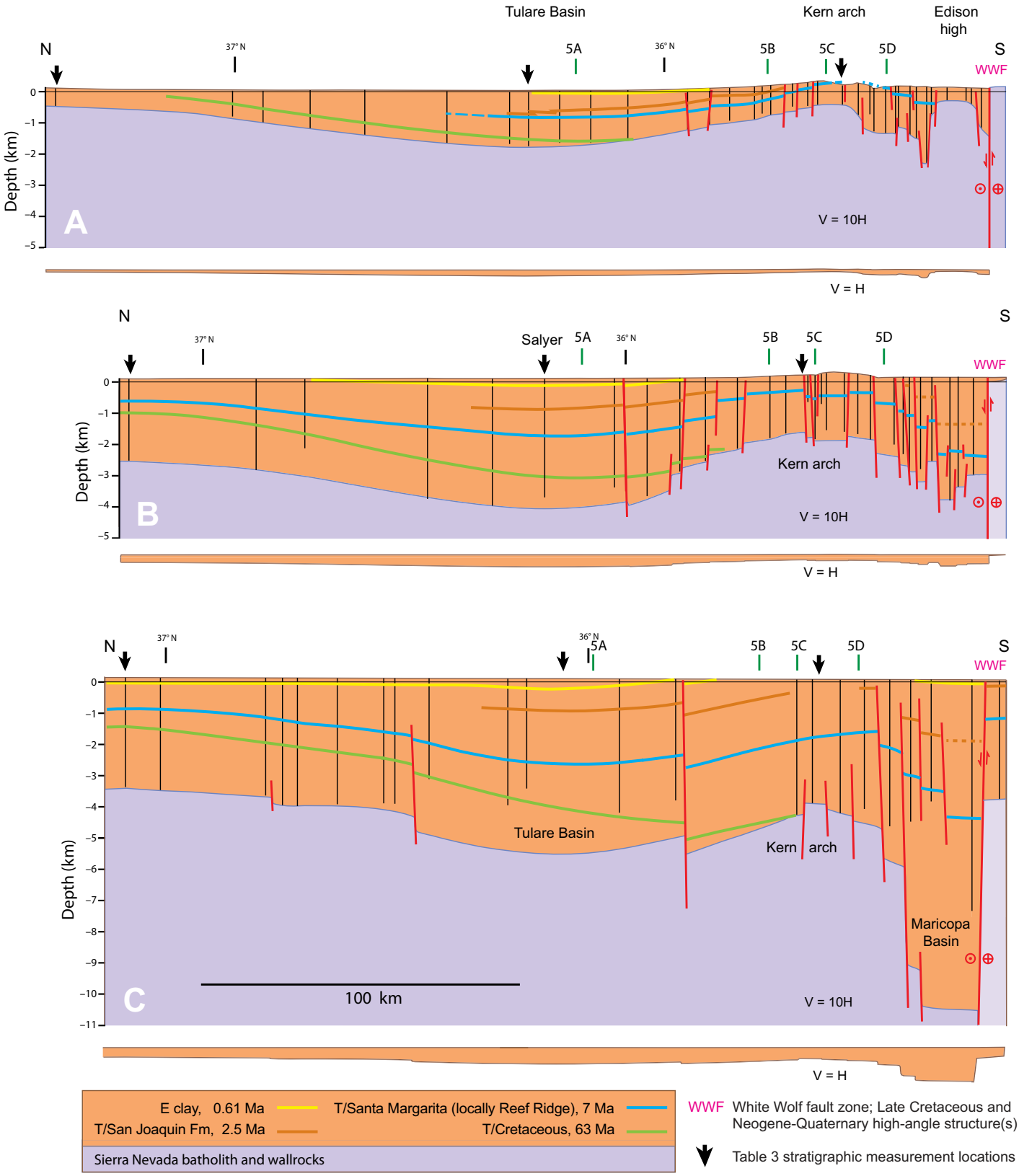

Figure 8. Longitudinal structure sections constructed along axial to eastern San Joaquin Basin. Traces of sections are shown on Figure 5 inset. Names and locations of wells used are given in Supplemental File 3 (see footnote 3). Maricopa Basin normal fault structure is also constrained by proprietary industrial seismic data. Stratigraphic picks are based partly on seismic data in Bloch (1991) and Miller (1999). Basement surface is after May and Hewitt (1948), Wentworth and Zoback (1989), Wentworth et al. (1995), and Saleeby (2007, 2012).

upper Miocene Reef Ridge shale are used in some wells as Santa Margarita age equivalents. Northward along the eastern section (Fig. 8A), Santa Margarita marine sands are swamped out by volcaniclastic debris of the Zilch Formation. Additionally, key Pliocene–Pleistocene stratigraphic horizons are included in Figure 8 above the Santa Margarita unit, as data are available. Shallower levels of the basin typically are not cored or logged, and a predominance of terrestrial deposits inhibits the correlation of what data is available. Local horizons for the top of the Upper Pliocene shallow-marine San Joaquin Formation and its southeastward facies transition into the Kern River Formation (ca. 2.5 Ma) and the Corcoran Clay E-member (ca. 615 ka) are shown, where found. Age constraints for the San Joaquin Formation and E-clay were reviewed in Hosford Scheirer and Magoon (2003).

The Figure 8 structure sections were constructed as a search for the deepest part of Tulare Basin, in longitudinal profile, in order to constrain late Cenozoic subsidence that is anomalous relative to regional subsidence, which is relatively uniform along any given longitudinal trace of the Great Valley. Anomalous subsidence is defined here as the difference in subsidence between the deepest part of Tulare Basin, in longitudinal profile, and subsidence that is expressed at the northwestern ends of each section. For Miocene and younger time, the northern ends of each section are considered typical of regional Great Valley patterns, lacking Tulare-related anomalous subsidence. This analysis also includes determination of structural relief of key stratigraphic horizons between Tulare Basin and the crest area of the Kern arch. The Kern arch constitutes an internally faulted NW-tilted fault block proximal to the western Sierra (Fig. 8A), which diminishes in structural relief progressively westward into the deeper Great Valley basin (Figs. 8B and 8C). In sections 8A and 8B, the Kern arch combined with the Edison basement high form a buried late Cenozoic horst and graben system. Measurement locations for the anomalous subsidence residuals and Tulare Basin–Kern arch structural relief are shown for each section on Figure 8, and the data are compiled in Table 3.

Inspection of Figure 8 leads to designating section 8B as most appropriate for basin center depth relations. This section trace runs ~30 km east of the synclinal axis of the Great Valley, while section 8C is adjacent to the synclinal axis, making a much larger component of its subsidence history related to the regional asymmetry of the Great Valley trough. Section 8A is more proximal to the western Sierra Foothills, which makes the younger critical horizons more susceptible to local facies variations resulting from Pliocene–Quaternary alluvial fans of the western Foothills (cf. Atwater et al., 1986), and the southern reaches of the voluminous Neogene terrestrial volcaniclastic tongue that filled the Sacramento and northern San Joaquin Basins from the northeast (cf. Busby and Putirka, 2009). The Salyer well yields useful data most proximal to the deepest part of section 8B, and unit thicknesses are used from this well for the Table 3 measurements. Log data from the Salyer well, as well as our stratigraphic picks, are presented in Supplemental File 4[4]. From these, we constructed total and tectonic subsidence curves (after Allen and Allen, 1990; Watts, 2001) (Supplemental File 5[5]), and we add these to a synthesis of pertinent published subsidence curves (Moxon, 1987; Moxon and Graham, 1987) for the eastern Great Valley region (Fig. 9; well locations in Fig. 6). Note that on Figure 9, the two wells from the eastern Sacramento Basin (A and B) lack the distinct latest Miocene–Quaternary subsidence phase that is present in the three wells from Tulare basin (C, D, and F). This is in line with our concept of anomalous subsidence in Tulare Basin, and the use of subsidence residuals. Note also that latest Miocene–early Quaternary anomalous subsidence of Tulare Basin continued across the Kern arch (Fig. 9G). This is discussed later herein.

TABLE 3. SELECTED STRATIGRAPHIC DEPTH RELATIONS MEASURED ALONG FIGURE 8 STRUCTURE SECTIONS

Section/horizon	Subsidence residuals (m)	Tulare-Kern arch relief (m)
A. 2.5 Ma	–	–
7 Ma	–	1260
Basement	1325	1350
B. 2.5 Ma	–	–
7 Ma	1150 (625)	1400
Basement	1500	2000
C. 2.5 Ma	–	900
8 Ma	1400	770
Basement	1750	1600

Note: Subsidence residuals are for total subsidence between deepest part of Tulare Basin along respective section traces and northern margin of San Joaquin Basin. Value in parentheses shows tectonic component of total subsidence residual for post–7 Ma (Supplemental File 5 [see text footnote 5]). Structural relief between deepest part of Tulare Basin and Kern arch is measured along section traces between center of basin and crest area of arch. The 2.5 Ma and 7 Ma horizons are for the top of the San Joaquin and Santa Margarita Formations, respectively.

Structural relations along section 8B show that 1150 m of total anomalous subsidence occurred in the central part of Tulare Basin, post–7 Ma (Table 3). This translates into 625 m of anomalous tectonic subsidence (Supplemental File 5 [see footnote 5]). Part I model results for delamination-related tectonic subsidence in Tulare Basin for the 14–22 m.y. interval of model time are ~680 m (Fig. 4B; Table 1). We consider this as good agreement between model results and observation. The Figure 4B displacement curves also make predictions concerning early-stage anomalous subsidence affecting the western Foothills region prior to westward migration of the principal depocenter. Unfortunately, facies relations along the eastern margin of Tulare Basin are such that this cannot be tested by stratigraphic means. Under our paleogeographic synthesis, herein, we present sedimentological data that may record this early-stage subsidence migration pattern.

Structural relief measurements between Tulare Basin center and the crest of the Kern arch for the 7 Ma horizon along sections 8A and B (Table 3) are 1260 and 1400 m, respectively. This is in line with the excess of ~1000 m of strata eroded off the exhumed basement nonconformity along the eastern edge of the Kern arch that was approximated by the projection of bedding relations.

[4]Supplemental File 4. Log record for Salyer well from central Tulare basin. Also shown is our overlay of our stratigraphic picks for the log sequence based on regional patterns in log signatures, and segments of seismic reflection data and cores examined, and on examination of logs from nearby wells not shown. If you are viewing the PDF of this paper or reading it offline, please visit http://dx.doi.org/10.1130/GES00816.S4 or the full-text article on www.gsapubs.org to view Supplemental File 4.

[5]Supplemental File 5. Tabulated data for backstripping and tectonic subsidence calculations for Salyer well of the central Tulare basin area. Bottom data rows are for latest Miocene to Quaternary subsidence residuals measured between Salyer well and the northern margin of the San Joaquin basin along the Figure 8b structure section trace. Backstripping and tectonic subsidence calculations after Allen and Allen (1990) and Watts (2001), and performed on OSXBackstrip by N. Cardozo (http://homepage.mac.com/nfcd/work/programs.html). If you are viewing the PDF of this paper or reading it offline, please visit http://dx.doi.org/10.1130/GES00816.S5 or the full-text article on www.gsapubs.org to view Supplemental File 5.

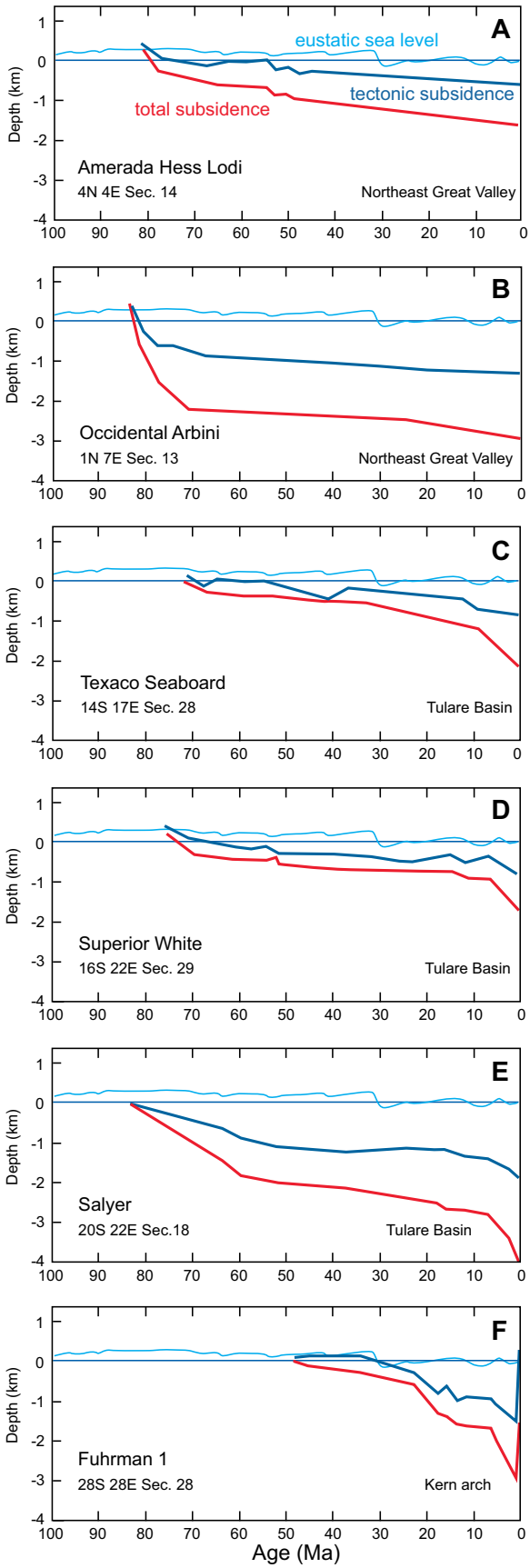

Figure 9. Total and tectonic subsidence curves for oil wells located along eastern Great Valley. Locations are shown in Figure 6. (A–B) Eastern Sacramento Basin, showing very little Pliocene–Quaternary subsidence. (C–E) Tulare Basin, showing anomalous Pliocene–Quaternary subsidence. (F) Medial area of the Kern arch with Pliocene–early Quaternary cryptic subsidence and subsequent late Quaternary rock and surface uplift. Blue line on plots is eustatic sea level from Haq et al. (1987). A–D are after Moxon (1987) and Moxon and Graham (1987); E and F are from data presented here (Supplemental Files 5 and 7 [see footnotes 5 and 7]), and Cecil et al. (2013).

Pliocene–Quaternary Cryptic Subsidence and Rock Uplift of the Kern Arch

Stratigraphic relations along the northwest flank of the Kern arch strongly suggest that the upper Pliocene shallow-marine San Joaquin Formation and its facies transition into the fluvial-deltaic Kern River Formation extended across much, or all of the area of the arch (Figs. 3, 5, and 8). As illustrated in Figures 3, 5C, and 5D, erosion of the crest area of the arch has exhumed the Tertiary section down to lower Miocene levels over a broad area, and thus a substantial thickness of strata may have rested on the area of the arch prior to its Quaternary growth. Assumption of a constant thickness for the upper Neogene strata along sections 8A and 8B across the southern Tulare Basin and the arch suggests that ~1250–1400 m of sediment overburden have been removed from the crest area of the arch (Figs. 5 and 8; Table 3). In order to gain additional constraints on this exhumation, we examined a number of cores from oil fields on the Kern arch. We found a variety of features that constrain the latest Miocene to early Quaternary (ca. 6–1 Ma) depth of burial of the arch, which in conjunction with stratigraphic, geomorphic, and geodetic data summarized herein, further constrain the Quaternary rock uplift and exhumation of the arch. These features include mechanical granulation textures from rapid sediment loading, low-grade metamorphic mineral growth, vitrinite reflectance, (U-Th)/He thermochronometry of detrital apatite grains, and thermal modeling of down-hole temperature determinations (Cecil et al., 2013). Some of the results from this large and diverse data set are summarized in Figure 10.

Figure 10A shows a simplified version of the Figure 8B longitudinal structure section with constraints plotted for post–1 Ma exhumation across the medial area of the Kern arch based on findings from oil fields that are located along the trace of the section (Cecil et al., 2013). Local structural relief on the basement nonconformity has been smoothed across the arch in order to minimize the effect of complex Neogene and possible Late Cretaceous faulting. Significant faults that appear to have been involved in generating the arch uplift are retained. The depth of the ca. 1 Ma depositional surface is approximated across the Tulare and Maricopa Basins, assuming constant subsidence, sedimentation, and compaction rates between 2.5 Ma (top of San Joaquin marker) and the modern surface. In Figure 10B, the ca. 1 Ma depositional surfaces in Tulare and Maricopa Basins, and the ca. 1 Ma surface determined from exhumation across the Kern arch are retrodeformed to a flat profile that is intended to approximate the ca. 1 Ma sedi-

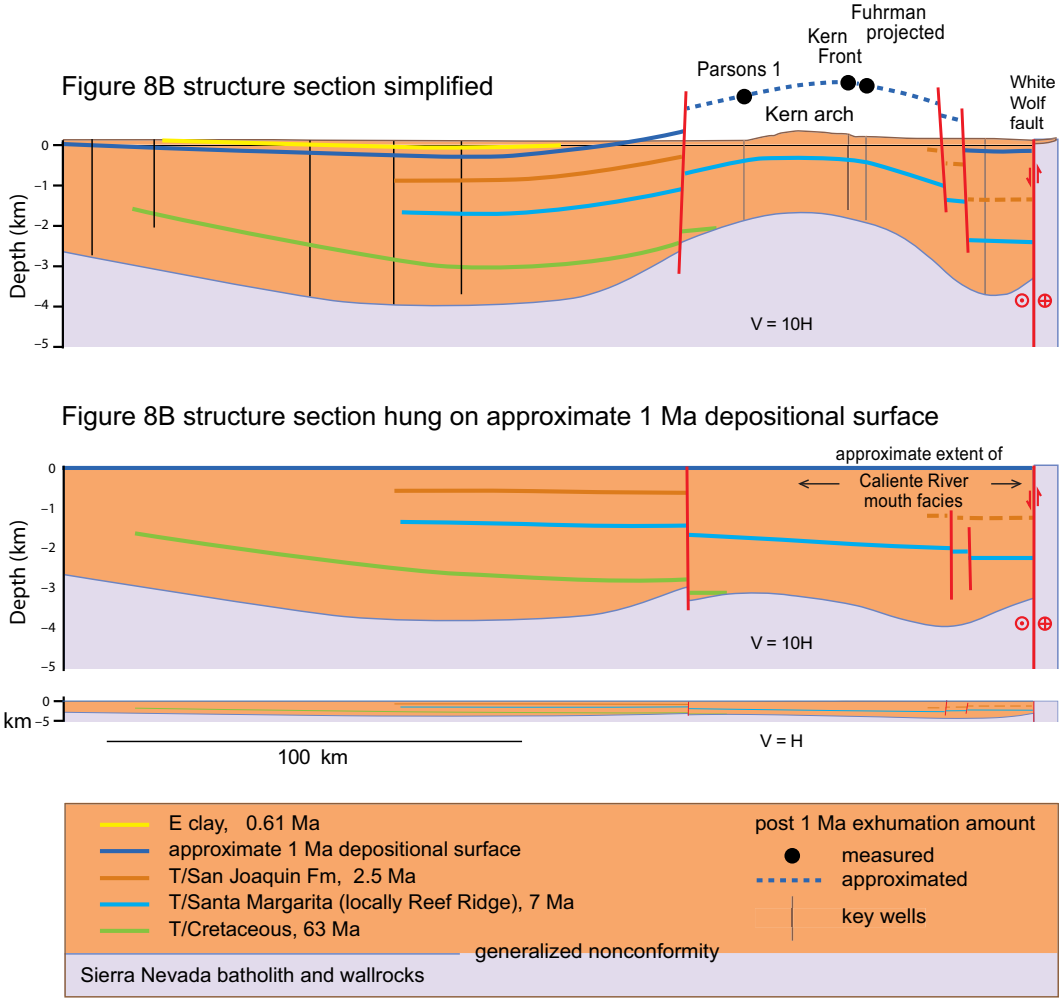

Figure 10. (A) Simplified version of Figure 8B structure section along axial San Joaquin Basin with post–1 Ma exhumation values determined from adjacent oil fields from Cecil et al. (2013) plotted as points, and our interpreted post–1 Ma exhumation profile across the medial area of the Kern arch plotted as dashed line. Fuhrman well exhumation value is projected downdip from ~6 km off section trace based on transverse exhumation gradient across Kern arch determined by Cecil et al. (2013). Parsons 1 well and Kern Front oil field are on section trace. (B) Retrodeformed version of section 10A that brings ca. 1 Ma exhumation depth line into common flat surface with 1 Ma depositional surfaces from Tulare and Maricopa Basins intended to simulate ca. 1 Ma depositional surface. This shows a regionally smooth southerly slope to the axial San Joaquin Basin in Neogene–early Quaternary time, prior to uplift of the Kern arch.

ment surface prior to both the rise of the arch and post–1 Ma subsidence and sedimentation in the adjacent subbasins. Mismatches in the arch-bounding faults are shown, which require either reversals in displacement patterns, or the involvement of additional structures in the uplift of the arch that have yet to be resolved.

The Figure 10B reconstruction shows a regionally continuous southward-facing slope for the eastern San Joaquin Basin at ca. 1 Ma, along the trace of the Figure 8B structure section. This is interpreted to approximate the N-S profile of the axial to eastern San Joaquin Basin prior to the rapid uplift and exhumation of the Kern arch. This is significant because it shows that the area of the arch shared a common Pliocene–early Quaternary anomalous subsidence history with both Tulare Basin and Maricopa Basin, prior to its uplift and exhumation. This reconstruction also shows that latest Miocene to early Quaternary total subsidence increases southward along the basin, due primarily to sediment loading (Fig. 9; also Goodman and Malin, 1992). This loading component increases as the delta and delta front submarine fan system of the Caliente River is approached (Fig. 3). Exhumation and reburial relations along the northern slope of the arch also indicate recent aggradation of Tulare Basin sediments across the previously exhumed margin of the arch. Such aggradation is suggested to be a result of sediment supplied by higher degrees of exhumation across the higher levels of the arch to the east (Cecil et al., 2013), in conjunction with a rise in base level across Tulare Basin by the building out of the Kings River alluvial fan (Atwater et al., 1986).

The Quaternary exhumation of ~1100–1300 m of upper Miocene to lower Quaternary strata off the Kern arch as shown on Figure 10A implies a comparable amount of cryptic subsidence in the region. Fuhrman well offers the widest range of burial indices, including depth-dependent mechanical granulation textures, low-grade metamorphic mineral growth, disturbed (U-Th)/He apatite age arrays, and down-hole temperature constraints (Saleeby and Saleeby, 2009; Cecil et al., 2013). We thus use the Fuhrman well relations here to generalize the cryptic subsidence-superposed rock uplift relations for the medial area of the Kern arch. Oil fields from the eastern part of the arch yield higher post–1 Ma exhumation values of up to ~1800 m (Cecil et al., 2013), but these are more difficult to interpret in terms of cryptic subsidence relations due to the growth of syndepositional grabens along the range front, and also a poorer resolution as to the nature of the exhumed strata (i.e., possible range front proximal alluvial fans). We thus focus on the medial area of the arch and present log data and stratigraphic picks for Fuhrman well in Supplemental File 6[6]. We impose ~1350 m of post–Santa Margarita cryptic subsidence from

[6]Supplemental File 6. Log record Fuhrman#1 well from Ker Arch. Source: California Division of Oil and Gas. Also shown is overlay of our stratigraphic picks for the log sequence based on regional patterns in log signatures, and segments of seismic reflection data and cores examined, and on examination of logs from nearby wells. If you are viewing the PDF of this paper or reading it offline, please visit http://dx.doi.org/10.1130/GES00816.S6 or the full-text article on www.gsapubs.org to view Supplemental File 6.

Cecil et al. (2013) in producing the subsidence plot of Figure 9F (Supplemental File 7[7]). There are no direct constraints on the form of the cryptic subsidence–rock uplift phases of the plot, other than ~1350 m cryptic subsidence, mainly post–2.5 Ma, followed by rock uplift and exhumation in conjunction with the rise of the arch starting at ca. 1 Ma. We designate 1 Ma as the time of maximum sediment loading and subsequent time as the period of rock uplift and exhumation (Fig. 9F). This satisfies Figueroa and Knott's (2010) interpretation for incision of the lower Kern gorge since 0.5 Ma, also considering that before the ~700 m of lower gorge basement incision, ~1–1.4 km of strata were eroded off the basement nonconformity—more than 1 km based on stratigraphic projections (Figs. 5B and 5C; Mahéo et al., 2009) and ~1.4 km from Cecil et al. (2013). The subsidence to uplift transition at ca. 1 Ma is also consistent with seismic-reflection data in Tulare Basin, suggesting that the arch began to rise as a sediment source area at ca. 1 Ma (Miller, 1999), and is consistent with the vertical rate of 2.3 ± 0.5 mm/yr measured on the GPS monument that is located along the southeast margin of the arch (Fig. 6), assuming that this rate became operational at, or shortly after, ca. 1 Ma. A critical feature of the Figure 10 relationships, and of the Figure 9 subsidence curves, shows that "Tulare Basin" anomalous subsidence affected the area of the Kern arch prior to the Quaternary rise of the arch.

LATE CENOZOIC EPEIROGENY AND REGIONAL RELIEF EVOLUTION ALONG THE SIERRA NEVADA MICROPLATE

We now pursue the temporal and spatial relations of epeirogenic deformation across the southern Sierra Nevada region arising from root delamination by an analysis of stratigraphic and geomorphic data along two roughly orthogonal transects: (1) a NE-SW (transverse) transect that crosses the eastern Sierra crest at ~37°N, which is considered applicable to an ~150-km-wide corridor that is centered over the transect; and (2) a NW-SE (longitudinal) transect that synthesizes relations along the eastern San Joaquin Basin–western Foothills transition. The position of the delamination hinge trace is used as a reference for the geodynamic interpretation of the observed epeirogenic displacements, and in this context the results of our Part I modeling are tested against the data synthesis. The uncertainty in correlation of geologic and model time is applied spatially in our analysis. Considering that the San Joaquin drainage appears to be losing relief relative to the Kings drainage (McPhillips and Brandon, 2010), and the Kings drainage has slowed in its recent incision history over the past 1.5 m.y. (Stock et al., 2004, 2005), we correlate modern geologic time for the transverse trace with the 22–23 m.y. interval of model time (Fig. 4B), since modeled eastern crest rock uplift related to root delamination culminates and then ceases over this time interval. Since the Kaweah and Kern drainages are in more youthful stages of geologically recent uplift, we correlate the 20–22 m.y. interval of model time to recent time in these areas. Finally, we add an analysis of the first-order effects of geomorphic forcing and late Cenozoic far-field–induced epeirogeny to the delamination related epeirogenic effects for a more complete analysis of late Cenozoic epeirogeny across the entire microplate.

Transverse Vertical Displacement Profiles

In this section, we discuss Pliocene–Quaternary rock uplift of the southern Sierra Nevada that resulted from the tectonic forcing of root delamination, compounded by the flexural-isostatic response (geomorphic forcing) to accelerated drainage basin erosion in the Sierran uplands and sediment loading in the San Joaquin Basin (i.e., Small and Anderson, 1995; Pelletier, 2007). The geomorphic forcing studies are pertinent to the application of the Part I modeling to eastern Sierra crest rock uplift because such forcing is not accounted for in the modeling. Here, we merge our tectonic forcing results with the geomorphic forcing analyses of Small and Anderson (1995), recognizing that the modeling of Pelletier (2007) suggests that for the magnitude of tectonic forcing that our modeling predicts, a nontrivial component of geomorphic forcing arises. Small and Anderson (1995) used a flexural-isostatic model with distributed erosional unloading across the Sierran uplands, distributed depositional loading across the San Joaquin Basin, and the position of the Foothills tilt axis fixed.

A critical factor to the geomorphic forcing analysis is an approximation for the effective elastic thickness (T_e) of the Sierra Nevada microplate crust. In Small and Anderson (1995), a 10–50 km range of T_e was investigated over mean erosion rates (<ε>) of ≤0.3 mm/yr. A current T_e of ~5–15 km is derived for the Sierra Nevada and its transition into the Great Valley from a combination of geophysical and geomorphic approaches (Lowry et al., 2000; Granger and Stock 2004; Lowry and Perez-Gussinye, 2011). For our first-order analysis, we use a value of 10 ± 5 km. Small and Anderson's model is also dependent on <ε>. Wakabayashi and Sawyer (2001) suggested a Pliocene range-wide value of ~0.15 mm/yr, although this value is shown to be most applicable to main river channel basement incision between the Stanislaus and Kaweah drainages during the late Pliocene (Stock et al., 2004, 2005). The much faster Quaternary <ε> for the lower Kern gorge area and Kern arch, as discussed earlier herein, is not considered pertinent to this analysis and is discussed further later. Long-term <ε> of the Sierra Nevada from end of Cretaceous through at least early Neogene time is ~0.05 mm/yr (Clark et al., 2005; Cecil et al., 2006; Clark and Farley, 2007; Mahéo et al., 2009). Considering these range of rates, and arguments for lower river gradients and erosion rates for the Sierra Nevada through early Cenozoic time (Wakabayashi and Sawyer, 2001; McPhillips and Brandon, 2012; Wakabayashi, 2013), we use <ε> of ~0.1 ± 0.02 mm/yr for Pliocene–Quaternary time. Using these T_e and <ε> values in Small and Anderson's (1995, Fig. 4C) model produces a geomorphic rock uplift response of ~400 ± 100 m since 5 Ma for the southeastern Sierra crest. Added to the ~800 m of delamination-driven uplift (Fig. 4B), we find ~1200 m of rock uplift by compounded delamination and geomorphic forcing.

We posit that topographic relief of the delamination bulge has been superimposed over regional relief patterns of the Sierran uplands, similar to Tulare Basin subsidence being superposed over regional subsidence patterns of the Great Valley. We designate a transect that crosses the medial area of Tulare Basin and the headwaters of the Kings River as a representative profile across the delamination bulge and dynamically linked zone of subsidence. In comparison, we consider a transect centered adjacent to the Mokelumne River drainage (Fig. 1) as being representative of microplate regional physiographic patterns where the effects of root delamination are lacking, or trivial. We base this on: (1) seismic imaging, indicating that the area of this drainage is north of where root delamination is occurring (Reeg, 2008; Schmandt and Humphreys, 2010; Frassetto et al., 2011; Gilbert et al., 2012; C.H. Jones, 2012, written commun.); (2) the pattern of Neogene–Quaternary volcanism (compare Busby and Putirka [2009]

[7]Supplemental File 7. Tabulated data for backstripping and tectonic subsidence calculations for Fuhrman#1 well of the Kern Arch. Note bottom entry is for ~1500 m of cryptic subsidence constrained to latest Miocene-early Quaternary age. Backstripping and tectonic subsidence calculations after Allen and Allen (1990) and Watts (2001), and performed on OSXBackstrip by N. Cardozo (http://homepage.mac.com/nfcd/work/programs.html). If you are viewing the PDF of this paper or reading it offline, please visit http://dx.doi.org/10.1130/GES00816.S7 or the full-text article on www.gsapubs.org to view Supplemental File 7.

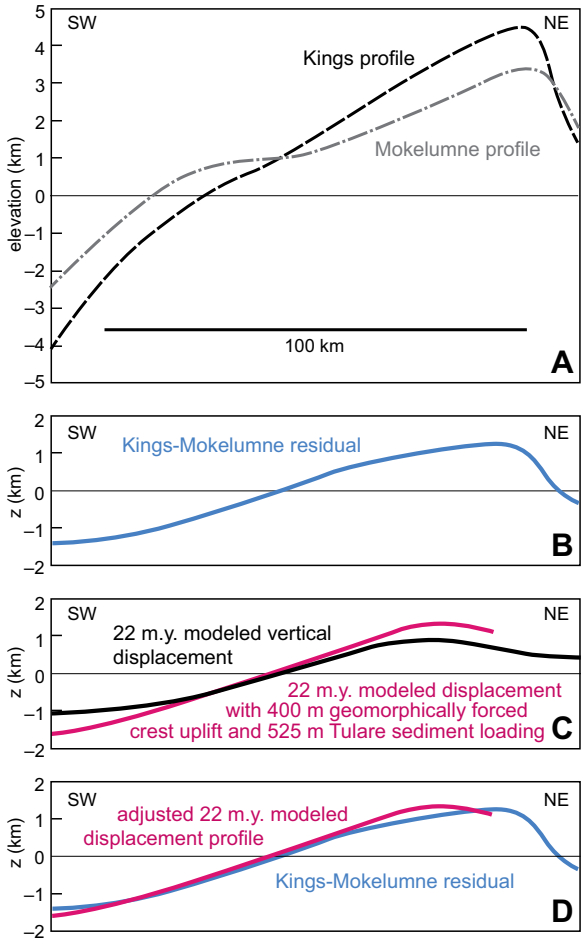

Figure 11. Comparative profiles for Kings River and Mokelumne River transects showing the effects of superposing root delamination-related epeirogenic displacements onto Sierran microplate smoothed topography and Great Valley basement depths. (A) Comparative profiles based on smoothed topography and basement depth structure contours taken from Figure 1 inset. (B) Topographic and basement depth residual plot between the two transects. (C) Plot of 22 m.y. vertical displacement profile from Figure 4B model results, and adjustment of the profile by adding 400 m of eastern Sierra crest rock uplift from geomorphic forcing and 525 m of sediment loading in Tulare Basin (Table 3). (D) Plot showing close correspondence of basement surface residual and adjusted 22 m.y. modeled vertical displacement profile, suggesting that principal difference in Kings and Mokelumne profiles is superposition of delamination bulge across Kings profile.

and Farmer et al. [2002]); and (3) its position to the north of the principal range crest topographic inflection, as well as the area shown by geodetic data to be undergoing resolvable contemporary uplift (Figs. 1 and 6). We interpret the Mokelumne headwater region to be located immediately north of the delamination bulge. In parallel, tectonic subsidence curves for late Cenozoic time along the Great Valley segment of the Mokelumne transect show no sign of Tulare Basin–like anomalous subsidence (Figs. 6 and 9). In Figure 11A, we show comparative smoothed topographic and basement depth profiles for the Kings and Mokelumne transects (Fig. 1 inset), and from these we derive a basement surface profile residual plot (Fig. 11B). If we assume that short-term (<1 m.y.) summit flat erosion rates of 0.012–0.075 mm/yr (Small et al., 1997; Riebe et al., 2000; Stock et al., 2004, 2005) are comparably applicable to the Kings and Mokelumne headwater regions since 5 Ma, the error induced by summit erosion for the crest elevation residual is trivial.

The Figure 11B plot yields an ~1200 m topographic residual for the eastern Sierra crest, and ~1400 m total subsidence residual for the Great Valley basement. The residual profile is to be compared to the 22 m.y. modeled surface displacement profile of Figure 4B. We plot the 22 m.y. profile in Figure 11C, and we adjust it for ~400 m of geomorphically forced rock uplift of the Sierran crest (discussed earlier), and for the ~525 m sediment loading residual determined for the "center" of Tulare Basin (Table 3; Supplemental File 3 [see footnote 3]). The adjusted 22 m.y. model profile is plotted on Figure 11D along with the residual profile, and they are shown to be quite comparable. This is consistent with our hypothesis that the principal differences in regional relief and late Cenozoic subsidence patterns between the northern and southern segments of the microplate result from the superposing of the delamination bulge and its dynamically linked subsidence zone over regional microplate physiographic patterns. The Figure 11D comparison should be considered semiquantitative in that the modeled rock uplift and geomorphic-forced components are both approximations. Nevertheless, the close correspondence of the Figure 11D profiles lends confidence to this analysis considering the regional setting of the Mokelumne profile relative to the region to the south, where numerous features point to ongoing delamination and related surface displacements.

Longitudinal Vertical Displacement Profiles along the Eastern San Joaquin Basin and Western Sierra Nevada Foothills

In Figure 12, we plot a series of vertical displacement profiles constructed along a longitudinal corridor that covers the western Foothills to axial San Joaquin Basin area (Fig. 5 inset). We register the profiles to an underlying lithospheric structure section synthesized from seismic data (Part I, Fig. 3C therein). Vertical displacement profiles based on total thicknesses for the top of the Santa Margarita Formation are constructed from stratigraphic relations of the Figure 8A and 8B structure sections, and from cryptic subsidence data from the Kern arch (Figs. 9F and 10; Saleeby and Saleeby, 2009; Cecil et al., 2013). The top of the Santa Margarita Forma-

Figure 12 (*on following page*). Stacked longitudinal profiles comparing: (A) topography along the western Sierra Nevada Foothills; (B) observed vertical displacement through time for the Upper Miocene Santa Margarita Formation along the Tulare Basin and Kern arch (derived from Figs. 8A and 8B structure sections, Fig. 9 total subsidence curves, and Fig. 10 reconstruction); and (C) lithospheric structure from a synthesis presented in Part I, Figure 3C therein. Profiles are registered to position of delamination hinge trace. Half flexural node spacing based on predicted center of Tulare Basin and peak of Coast Range sympathetic bulge (Fig. 4B) is scaled off on section A to demonstrate similar position of central Foothills swell to sympathetic bulge relative to positions of Tulare Basin anomalous subsidence and the Kern arch expression of the delamination bulge. Note that all well locations used for longitudinal and transverse structure sections are summarized in Supplemental File 8[8]. M—Moho; MSL—mean sea level.

[8]Supplemental File 8. Map summarizing locations of wells used for Figures 5 and 8 structure sections across and along the San Joaquin Basin in relation to traces of structure sections. If you are viewing the PDF of this paper or reading it offline, please visit http://dx.doi.org/10.1130/GES00816.S8 or the full-text article on www.gsapubs.org to view Supplemental File 8.

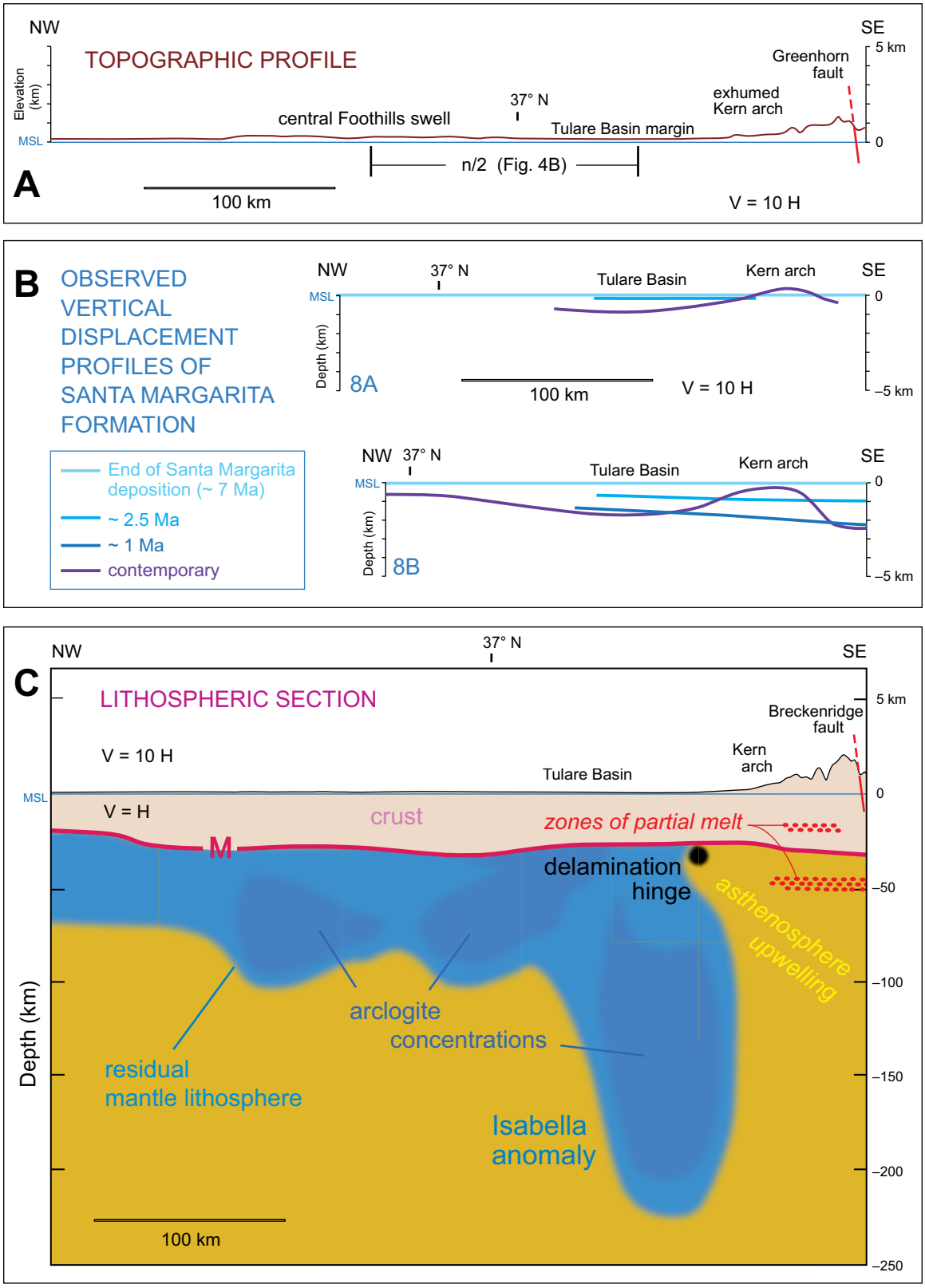
NW
SE
TOPOGRAPHIC PROFILE
Elevation (km)
MSL
5 km
0
Greenhorn fault
exhumed Kern arch
37° N
central Foothills swell
Tulare Basin margin
n/2 (Fig. 4B)
A
100 km
V = 10 H
B
OBSERVED VERTICAL DISPLACEMENT PROFILES OF SANTA MARGARITA FORMATION
End of Santa Margarita deposition (~ 7 Ma)
~ 2.5 Ma
~ 1 Ma
contemporary
NW
37° N
Tulare Basin
Kern arch
SE
MSL
Depth (km)
8A
100 km
V = 10 H
–5 km
8B
C
LITHOSPHERIC SECTION
V = 10 H
V = H
Breckenridge fault
Kern arch
crust
zones of partial melt
M
delamination hinge
asthenosphere upwelling
arclogite concentrations
residual mantle lithosphere
Isabella anomaly
Depth (km)
–50
–100
–150
–200
–250

Figure 12.

tion is defined as sea level at ca. 7 Ma, and depth control for subsequent geologic time is provided by the ca. 2.5 Ma top of the San Joaquin Formation, the ca. 1 Ma maximum burial surface of the Kern arch, and modern depths. Also shown is a topographic profile along the western Foothills that runs parallel to the lithospheric structure section. The profile extends along the eastern margin of Tulare Basin. The topographic profile and lithospheric structure section both cross the upper exhumed levels of the Kern arch along the footwall of the Greenhorn–Breckenridge–Kern Canyon fault system, and the two Santa Margarita displacement profiles run from the center of Tulare Basin across the Kern arch and terminate in Maricopa Basin. Next, we relate the first-order features of the Figure 12 profiles to structural and kinematic relations of the underlying lithospheric structure section.

The Figure 12B profiles show that the axial to eastern San Joaquin Basin, south of ~37°N, went into accelerated subsidence after ca. 7 Ma, and that after ca. 1 Ma, the Kern arch began to emerge, partitioning off the Tulare and Maricopa subbasins. The post–7 Ma accelerated subsidence is interpreted to have been forced by east-to-west–directed root delamination. The initial delamination-related accommodation space formed along the entire eastern to axial San Joaquin Basin in latest Miocene–early Quaternary time, paralleling the initial distribution of the in-place arclogite root (Part I, Fig. 4 therein). Then, as delamination transitioned from east-to-west to south-to-north during Quaternary time, the residual Tulare space continued to subside over the residual root load, while the Kern arch emerged over the area of active delamination. Growth of the arch is dampened westward into the basin (Figs. 8B and 8C), sympathetic with the westward thinning out of the initial arclogite root (Part I, Fig. 4 therein). Eastward from the basin edge, the upper slope of the Kern arch is exhumed of its Tertiary cover strata as it climbs toward the proximal footwall area of the Greenhorn–Breckenridge–Kern Canyon fault system.

Along any given profile running normal to the southern curved segment of the delamination hinge trace (Figs. 1, 3, and 7), the footwall block of the Greenhorn–Breckenridge–Kern Canyon system and the Kern arch form a fault block that is tilted into Tulare Basin (Figs. 8A and 8B), similar to the southern Sierra Nevada west tilt into Tulare Basin in transverse profiles to the north. Our modeling of root delamination predicts crustal extension off the flank of the delaminating root, represented in transverse profile by the eastern Sierra–Death Valley extensional province (Fig. 7). As delamination has transitioned into its south-to-north trajectory, it appears that delamination-driven extension has migrated to the Greenhorn–Breckenridge–Kern Canyon system, and to within Maricopa Basin (Figs. 3 and 8). The Maricopa Basin is commonly referred to as a foredeep to the Tehachapi–San Emigdio fold-and-thrust belt. However, this "foredeep" spatial relationship only developed during the Quaternary rise of the fold-and-thrust belt. Maricopa Basin is clearly controlled by high-angle normal and sinistral faults along the section traces of Figures 8A and 8B, and while the geometry of the White Wolf fault is poorly imaged along the Figure 8C section, where it appears to have inverted to active reverse motion (Bawden et al., 1997), the shallow levels determined for the E-clay proximal to the fault along this section clearly show that the optimal area for active thrust loading of the basin is not under the expected subsidence. Profound sedimentation in Maricopa Basin was controlled by extensional faulting in the early Neogene during slab window opening (Hirst, 1986; Goodman and Malin, 1992; Mahéo et al., 2009), and then in late Pliocene–Quaternary time, interpreted here as the transition into the south-to-north phase of root delamination. These two tectonic forcing regimes provided an accommodation space that underwent profound sediment loading off the delta front of the Caliente River (Figs. 3, 8, 9F, and 10; see also Maricopa Basin subsidence curve presented in Goodman and Malin, 1992).

Rock and surface uplift of the delamination bulge as expressed across the Kern arch and lower Kern gorge area reaches a maximum value of up to ~2000 m (Mahéo et al., 2009; Cecil et al., 2013). This is considerably more than the ~1200 m combined delamination-geomorphic forced uplift deduced previously for the bulge along the eastern Sierra. Our transverse model is not applicable to the acute three-dimensional conditions that characterize the southern curved segment of the delamination hinge (Part I, Figs. 3 and 15 therein; Fig. 13 herein). Focusing of the root load along the curved trace of the hinge, and then its rapid release during the south-to-north phase of delamination could account for a greater tectonic component of subsidence across the arch, followed by proportionally greater epeirogenic uplift. The form of the Santa Margarita displacement profiles on Figure 12 suggests a rapid stationary uplift above the delamination hinge, although the limited resolving power of the profiles could miss a rapid migration pattern to the bulge, as predicted in Figure 4B.

Study of the Figure 12 western Sierra Nevada topographic profile and lithospheric structure section reveals that in addition to the Kern arch sitting in the position of the delamination bulge, the central Foothills swell sits in a position analogous to the sympathetic flexural bulge (Fig. 4B). In the (transverse) model profile, the flexural half-node spacing between the center of Tulare Basin and the peak of the sympathetic bulge is ~135 km. A similar distance is scaled off on Figure 12A northwestward from the center of Tulare Basin. This distance roughly corresponds to the crest area of the central Foothills swell. We posit that as delamination progressed to its Quaternary south-to-north phase, a coupled NE-directed migration of the sympathetic bulge swept beneath the western Foothills and broadly warped the Foothills ramp upwards between 37°N and 38.5°N, forming the central Foothills swell. This broad zone of upward flexure coalesced with the northern shoulder of the principal delamination bulge, rendering the northern wrap pattern of the bulge around northeastern Tulare Basin (Fig. 1 inset; Fig. 6). Propagation of the sympathetic bulge from the Coast Ranges to the central Foothills area during the Quaternary provides a mechanism for the temporary partitioning off of the Great Valley, and the formation of the Corcoran Lake internal basin.

Figure 13 (*on following page*). Conceptual model of the three-dimensional delamination of the arclogite root of the Sierra Nevada batholith modified after Part I, Figure 15 therein. The root is depicted as a tabular mass that was attached to the felsic batholith above at paleo-Moho levels, and underlain by wedge peridotites to ~125 km depth (not shown), after Part I, Figure 4 therein. The delamination pattern shown occurred within the core area of a larger Rayleigh-Taylor (RT) instability that affected the entire mantle lithosphere, as shown on Figure 4A. Surface-level renderings based on smoothed topographic contour patterns are lifted off of each view in order to show principal paleogeographic expressions of delamination. (A) Early stages of regional east-to-west delamination. (B) Hypothetical necking off of a megaboudin, which promoted the ca. 3.5 Ma volcanic pulse. (C) Initiation of south-to-north components of delamination along the southern end of the residual root. (D) Continued south-to-north delamination progressing to the current state of the Isabella anomaly suspended southeastward into the deeper mantle from the area of residual root attachment under Tulare Basin. C and D diagrammatically depict the megaboudin deforming and becoming entrained in the eastern upwelling of the Isabella anomaly RT instability.

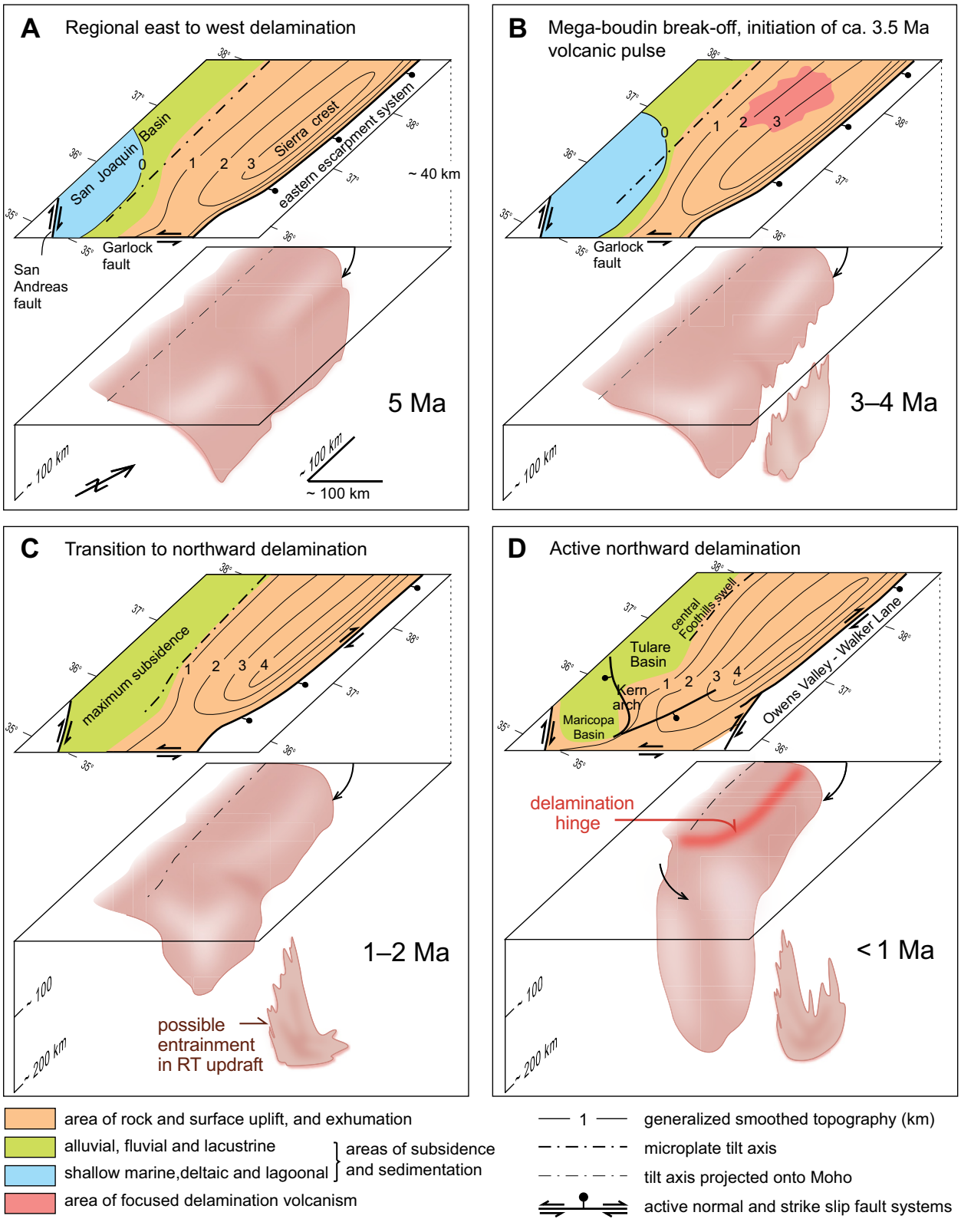
A
Regional east to west delamination
San Joaquin Basin
Sierra crest
eastern escarpment system
~ 40 km
Garlock fault
San Andreas fault
5 Ma
~ 100 km
~ 100 km
B
Mega-boudin break-off, initiation of ca. 3.5 Ma volcanic pulse
Garlock fault
3–4 Ma
~ 100 km
C
Transition to northward delamination
maximum subsidence
possible entrainment in RT updraft
1–2 Ma
~ 100
~ 200 km
D
Active northward delamination
central Foothills swell
Tulare Basin
Kern arch
Maricopa Basin
Owens Valley - Walker Lane
delamination hinge
< 1 Ma
~ 100
~ 200 km
area of rock and surface uplift, and exhumation
alluvial, fluvial and lacustrine
shallow marine,deltaic and lagoonal
areas of subsidence and sedimentation
area of focused delamination volcanism
generalized smoothed topography (km)
microplate tilt axis
tilt axis projected onto Moho
active normal and strike slip fault systems

Figure 13.

The map distribution of Corcoran Lake based on abundant subsurface data from the 710–615 ka Corcoran E-clay (Frink and Kues, 1954; Lettis, 1982, 1988) is shown in Figure 6, and its known subsurface distribution is shown in the structure sections in Figures 5 and 8. The northern limit of the lake parallels the broad culmination of the central Foothills swell, and the age of the lake corresponds in time to constraints presented earlier for growth of the Kern arch. Our hypothesis predicts the contemporaneous rise of the Kern arch and the central Foothills swell, both dynamically linked to the south-to-north phase of delamination. The origin of Corcoran Lake basin has remained enigmatic, with the most widely cited possibilities, i.e., glacial outwash fans or sea-level change controls, encountering problems in timing (Lettis and Unruh, 1991). These authors cite a tectonic control by uplift in the area of the Stockton fault (central Foothills swell) as a little-explored viable possibility, in line with our hypothesis.

Elevation History of the Sierra Nevada

Herein, we have presented an analysis that recognizes regional topographic and bathymetric variation of the Sierra Nevada and Great Valley that dates back to end of Cretaceous time, and to this we have layered on a model for late Miocene to Holocene epeirogenic deformation related to the delamination of the arclogite root of the southern Sierra Nevada batholith. This analysis accounts for many of the first-order physiographic features of the Sierra Nevada microplate, but it is not complete. Supplemental to the Pliocene–Quaternary tilt analysis of the western Foothills ramp, Unruh (1991) suggested that the uplift dynamics of the Sierra Nevada microplate are embedded within a regional epeirogenic field that in general is producing widespread rock uplift distributed across much of the U.S. Cordillera. Such far-field forcing arises from dynamic effects of regional mantle buoyancy structure (Suppe et al., 1975; Lowry et al., 2000). Early Cenozoic plate-margin processes capable of driving regional epeirogeny across the entire microplate include changes in the subduction trajectory of the Farallon plate (Dickinson, 2006; Liu et al., 2010), and the opening and coalescence of multiple slab windows (Atwater and Stock, 1998; Wilson et al., 2005; Humphreys, 2008; Muller et al. 2008). Regional thermomagmatic systems that more profoundly affected the northern Sierra Nevada region include the Yellowstone plume swell, and the ancestral Cascades arc (Suppe et al., 1975; Murphy et al., 1998; Lowry et al., 2000; Pierce et al., 2002; Busby and Putirka, 2009). Deconvolving these potential regional epeirogenic forcing systems, including their decaying phases, is beyond the scope of our analysis, but consideration of their first-order aggregate effect on microplate elevation history is required for our analysis not to be grossly inadequate.

The presence of Upper Cretaceous and Lower Paleogene marine strata in elevated positions at the northern and southern ends of the Sierra Nevada records possible 1000-m-scale rock and surface uplift of at least the southern and northern ends of the microplate over Cenozoic time. These depositional outliers arise as a result of the regional longitudinal paleotopographic gradients that graded to sea level at the two extreme ends of the Sierra Nevada (Fig. 2). The settings of these outliers in relation to stratigraphic relations in adjacent related basins carry implications on such uplift potentially affecting the entire microplate. As much as ~1200 m of Paleocene–Eocene marine fauna–bearing clastic strata sit nonconformably on axial southern Sierra basement with basal elevations spanning ~1400 m to ~1700 m (Fig. 3). There is >1 km of Neogene strata unconformably situated on these strata, much of which has been eroded and transferred into the southeastern San Joaquin Basin (Michael, 1960; Dibblee and Louke, 1970; Wood and Saleeby, 1998; Saleeby and Saleeby, 2010; Table 1 herein). Roughly 1000 m of this uplift can be attributed to early Neogene footwall uplift along the proto–Garlock fault (Fig. 3; and our structural manipulation of Blyth et al. [2010] and Blyth and Longinotti [2013] data). This leaves ~700 m of mid-to-late Cenozoic surface uplift from another mechanism(s). The area of the elevated Eocene marine strata corresponds to the low-lying Late Cretaceous extensional terrane that continued southward into the western Mojave plateau region. Presently, the plateau floor lies at ~800 m elevation. We interpret the plateau to have gained elevation in conjunction with the additional rise of the southern Sierra marine strata. Far-field forcing for this uplift regime may have arisen from shallow low-velocity mantle beneath the region (Reeg, 2008; Schmandt and Humphreys, 2010; C.H. Jones, 2012, written commun.), reflecting upwelling along the southern margin of the Isabella anomaly, and/or the lingering of shallow asthenosphere emplaced into the Pacific-Farallon slab window.

Upper Cretaceous marine strata, typically deltaic facies, are nonconformable across northwestern Sierra Nevada basement, with basal elevations ~100–400 m (Repenning, 1960; Jenkins, 1977; Dickinson et al., 1979; Harwood et al., 1981). Isopach patterns along the northeast Sacramento Basin indicate that the Upper Cretaceous strata were up to ~1000 m thick, indicating 1000-m-scale regional uplift of the entire northern microplate in Cenozoic time. The Upper Cretaceous strata are conformably overlain by relatively thin Paleocene to Upper Eocene terrestrial and marine strata in proximal parts of the basin, above which there is a latest Eocene to middle Miocene hiatus across much of the basin, and which along much of the Foothills ramp completely removed the Upper Cretaceous strata. The position and timing of this hiatus are such that it likely represents an epeirogenic deformation progression forced in sequence by: (1) accretion of the Siletzia large igneous province; (2) opening of the Siletzia/Farallon-Kula slab window; and then (3) initial uplift along the southern margin of the Yellowstone plume swell (Wells et al., 1984; Engebretson et al., 1985; Murphy et al., 1998; Lowry et al., 2000; Pierce et al., 2002; Muller et al., 2008; Humphreys, 2008; McLaughlin et al., 2009). Immediately following this regime, there was an ~13 m.y. period of ancestral Cascade arc volcanism, starting at ca. 16 Ma, with eruptive centers clustered along the eastern Sierra crest as far south as ~38°N (Fig. 2; Busby and Putirka, 2009). The volcanic stratigraphy records multiple pulses of rock uplift and west tilt initiating in middle Miocene time (Busby and Putirka, 2009), indicating that some component of west tilt initiated prior to the more widely recognized Pliocene–Quaternary phase (Unruh, 1991). Thermal expansion of the eastern Sierra region related to ancestral Cascades arc volcanism north of 38°N is another potential source for late Cenozoic transient uplift of the region (Busby and Putirka, 2009). The possibilities for multiple uplift transients having migrated through the northern Sierra Nevada region in Cenozoic time, including their negative decaying phases, and the resulting complexity on regional elevation patterns or river incision imprints are little explored.

A critical factor to this analysis is that evidence for the existence or survival of the arclogite root for the Sierra Nevada batholith is restricted to the region south of ~38°N, as is evidence for its Pliocene–Quaternary removal (Ducea and Saleeby, 1998a, 1998b; Manley et al., 2000; Farmer et al., 2002; Saleeby et al., 2003; Part I, Figs. 3 and 4 therein). In contrast, the Neogene ancestral Cascades arc terminates southward at ~38°N (Fig. 2), underscoring the geodynamic as well as the physiographic contrasts between the northern and southern Sierra Nevada. This suggests that the southern Sierra Nevada arclogite root and its substrate of wedge peridotite, which together had been quenched to a lithospheric geotherm in the Late Cretaceous (Ducea and Saleeby, 1996; Saleeby et al., 2003), inhibited the southwest sweep of the Neogene arc from Nevada into the eastern Sierra Nevada

region south of 38°N (after Dickinson, 2006; Busby and Putirka, 2009). Compounded on this longitudinal contrast along the microplate, there are the effects of the ≥16 Ma initiation of the Yellowstone plume in a position proximal enough to the northern Sierra Nevada to place much of the region within the 1000 m plume swell isopleth (Lowry et al., 2000; Pierce et al., 2002). The ca. 16 Ma Lovejoy (plume) basalt erupted in the northern Sierra Nevada region further indicates proximity to the plume head (Garrison et al., 2008). Subsequent migration of the plume in theory has resulted in ~300 m of subsidence of the northern Sierra Nevada region off the southwest margin of the plume swell.

The survey of far-field forcing mechanisms presented here suggests two principal components: (1) a SW Cordilleran-wide system that operated on the entire microplate arising from Farallon slab subduction dynamics, and the opening and coalescence of multiple slab windows; and (2) thermal-magmatic forcing of the Yellowstone plume swell and ancestral Cascades arc, which was focused in the northern Sierra Nevada region. It seems likely that epeirogenic forcing in the Sierra Nevada region by the southward opening of the Siletzia/Farallon-Kula slab window had decayed to zero by Neogene time (Humphreys, 2008). This suggests that the principal drivers of late Cenozoic far-field epeirogeny across the Sierra Nevada microplate were the Yellowstone plume swell in the north and the Pacific-Farallon slab window in the south, with the coalescence and overlap of these two systems initiating at ca. 10 Ma at ~38°N, and progressing northward to the modern Mendocino triple junction (Atwater and Stock, 1998; Pierce et al., 2002; Wilson et al., 2005). These two systems together are suggested to have raised the entire axial to eastern Sierra Nevada region at 500–1000 m scale and the western Foothills region at 100–200 m scale. Focused uplift arising from the ancestral Cascades arc is likely to have been additive to the plume swell uplift, and then to have thermally decayed as the arc progressively shut off northward with the migration of the triple junction, just as the plume swell effect was decaying as the plume migrated eastward (Lowry et al., 2000; Pierce et al., 2002; Busby and Putirka, 2009).

A more subtle but potentially profound effect that the ancestral Cascades arc had on Sierra Nevada physiographic evolution was to blanket the northern Sierra Nevada with Neogene volcanic strata, and raise the Neogene base level of the Sacramento Basin by the building out of a terrestrial volcaniclastic apron (Busby and Putirka, 2009). This preserved early Cenozoic paleolandscape features in the northern Sierra Nevada, accentuating physiographic contrasts with the southern Sierra Nevada, where early Cenozoic landscape features lay bare through the Neogene, rendering them susceptible to continued erosional modification. In Figure 2, local paleorelief that dates back to end of Cretaceous time is color coded across the Sierra Nevada. These could represent minimum values, particularly in the northern Sierra Nevada. River canyons north of the Stanislaus drainage that incise into basement below Neogene reference surfaces (Wakabayashi and Sawyer, 2001; Wakabayashi, 2013) are not well constrained on the timing(s) of such basement incision, and thus some nontrivial component of the observed basement incision could also date back to the paleorelief regime that is coded on Figure 2. Deep basement channels inherited from either the margin of the Nevadaplano from end of Cretaceous time and/or forced by the early Cenozoic opening of the Siletzia/Farallon-Kula slab window could have laid buried beneath the ancestral Cascades volcaniclastic apron, to be reincised into and likely deepened sometime following the ca. 5 Ma disruption of the volcanic source by westward encroachment of the eastern escarpment system, and northward migration of the Mendocino triple junction. In this context, the Neogene reference surfaces used to document basement incision could be remnants of volcanic strata perched on ancient strath terraces cut into basement. That is to say, the topographically lowest preserved Neogene, and locally Oligocene, volcaniclastic rocks may not mark the deepest point in observed paleochannels, but rather higher levels of the paleochannel fills as well as interchannel cover. In this scenario, the deepest parts of the canyon fills were completely stripped of their Neogene deposits in late Pliocene–Pleistocene time. This underscores the fact that there are currently no direct constraints on the age of basement incision north of the Stanislaus River.

The analysis presented here recognizes the importance of the physiographic contrasts between the northern and southern Sierra Nevada. It also points out the likelihood of fundamental lithospheric structural contrasts between the two regions that date back to end of Cretaceous time, and which strongly controlled the Neogene–Quaternary physiographic development of the two regions. Nevertheless, the entire microplate appears to have responded comparably in terms of regional uplift to the integrated far-field forcing mechanisms recognized. Layered on top of this regional epeirogeny, the ancestral Cascades arc has rendered a strong contrast in the preservation state of paleolandscape features, and the delamination of the southern Sierra Nevada batholith arclogite root has driven profound focused epeirogeny across the southern microplate. These two regimes underscore fundamental ancient lithospheric contrasts between the northern and southern Sierra Nevada (Part I, Fig. 4 therein) and account for distinct physiographic differences between the two regions that were pointed out by early investigators (Matthes, 1965; Christensen, 1966).

PALEOGEOGRAPHIC EXPRESSIONS OF MANTLE LITHOSPHERE REMOVAL

The late Cenozoic paleogeography of the Sierra Nevada microplate is accented by a number of features that appear to be direct expressions of the progression of underlying mantle lithosphere removal. These are summarized here. Special attention is placed on the tectonics and paleogeography that preceded and influenced root delamination and its surface expressions, as well as our kinematic model for three-dimensional delamination in the southern Sierra region since ca. 5 Ma (Fig. 13).

Early and middle Miocene extensional tectonism, deepening of the San Joaquin Basin, and formation of the Walker graben occurred in crust that had undergone extension and tectonic erosion of its underlying mantle lithosphere during the Late Cretaceous, above the lateral ramp in the Rand subduction megathrust (Figs. 1, 2, and 3; Part I, Fig. 4 therein). The Miocene phase of extension was forced by the northward opening of the Pacific-Farallon slab window (Atwater and Stock, 1998; Wilson et al., 2005), which, according to our model, also instigated mantle lithosphere mobilization beneath the southern Sierra Nevada region. The intensity of Miocene extension dropped significantly northward across the ~35.5°N limit of Late Cretaceous large-magnitude extension (Figs. 2 and 3), mimicking lithospheric structure that had been established in the Late Cretaceous. Pliocene (?)–Quaternary extension affected the same area as the Miocene extension, but it also extended northward through the area of the northern Kern arch and Tulare Basin, as recoded by numerous high-angle normal faults (Nugent, 1942; Croft and Gordon, 1968; Saleeby and Foster, 2004, their Data Repository Map; Figs. 3, 5, and 8). The lateral ramp in the Rand subduction megathrust left the arclogite root of the Sierra Nevada batholith truncated and liable for delamination. As discussed in Part I, the added gravitational potential of the high-standing Nevadaplano foreland to the Sierra Nevada batholith, as opposed to the lower potential of the southern Sierra–Mojave extended terrane (Part I, Fig. 4 therein), favored the east-to-west over south-to-north initial pattern in delamination, once the slab win-

dow perturbation was regionally imposed. As discussed in Part I, and herein, this required special circumstances to promote the current south-to-north delamination regime.

The 10 ± 2 Ma (late Miocene) mantle lithosphere separation, and derivative inception of the Sierra Nevada microplate (Fig. 4A), is expressed by stratigraphic relations along much of the Great Valley, as well as across the southern end of the microplate. This event is interpreted to mark the initiation of regional west tilt to the microplate, which accelerated in Pliocene time (Unruh, 1991). Sediment provenance, dispersal, and strandline relations changed abruptly across the entire San Joaquin Basin and into the southern Sacramento Basin at the time of microplate inception, with a marine incursion northward along the western margin of the microplate, and the deposition of the extensive "Santa Margarita" sand sheet(s) (Fig. 2). The granitic provenance of the Santa Margarita detritus signals the rejuvenation of major Sierra Nevada drainages in progression to the widely recognized Pliocene phase of river incision. In the southernmost Sierra Nevada, rise of the eastern crest region is recorded by the south and eastward delivery of copious Sierran detritus into the El Paso Basin (Fig. 3; and Loomis and Burbank, 1988), and the westward redistribution of the Walker graben fill into the southern San Joaquin Basin by the Caliente River (Fig. 3; Saleeby and Saleeby, 2010; Saleeby et al., 2013). Voluminous sediment loading from the redistributed Walker graben fill drove profound latest Miocene to early Quaternary subsidence in the Maricopa Basin, and the adjacent area that became the Kern arch, in conjunction with N-side-down normal displacement on the White Wolf fault (Figs. 8B and 8C). The Caliente River delta front issued submarine fans into the San Joaquin Basin, which served as important petroleum traps (MacPherson, 1978; Harrison and Graham, 1999). The results of our thermomechanical modeling (Fig. 4B; Part I, Figs. 11 and 13 therein) further indicate that during the structural progression to lithosphere separation, the load of the arclogite root drove ~300 m of subsidence along the eastern Sierra Nevada–Basin and Range transition. This provided accommodation space for the development of late Miocene–Pliocene lake formation along the transition zone (Bachman, 1978; Bacon et al., 1982), which was subsequently disrupted by extensional faulting and eastern Sierra crest uplift as root delamination accelerated through Pliocene time.

Figure 13 diagrammatically shows renderings of our model of arclogite root delamination in three dimensions since ca. 5 Ma, in relation to regional paleogeographic patterns. The top of the root is viewed along Moho levels from the southeast. Surface-level views are lifted off the Moho view in order to render delamination-related physiographic changes through time. In Figures 13A to 13C (5 Ma to 2 Ma), delamination is shown to have driven Pliocene rock uplift of the southern Sierra Nevada, as is clearly expressed by accelerated river incision and west tilting (Huber, 1981; Unruh, 1991; Wakabayashi and Sawyer, 2001; Stock et al., 2004, 2005), and by the exhumation of the Walker graben fill (Fig. 3). Accelerated uplift of the Sierra Nevada over this time period is paralleled by accelerated or anomalous subsidence in the San Joaquin Basin.

The results of our thermomechanical modeling suggest that a total of ~500 m of anomalous subsidence was first focused along the western Sierra Foothills, and then subsidence migrated westward to the center of the basin as the delamination bulge grew and expanded into the Foothills region (Fig. 4B). The model predicts a rapid reversal from subsidence to rock uplift within the model time period that we correlate to the late Pliocene (~17–20 m.y.). The apparent ease with which kilometer-scale exhumation of the Pliocene–lower Quaternary sediments of the Kern arch has occurred since 1 Ma (Fig. 10) suggests a low preservation potential of correlative sediments that may have aggraded across the Foothills during the initial subsidence phase. The position of the top of the upper Pliocene San Joaquin Formation, relative to the position of the exhumed nonconformity/basement pediment surface to the east (Fig. 4), indicates that the shallow-marine conditions represented by the formation could have easily spread eastward across the entire low-relief surface as a result of the (modeled) early phase of subsidence of the Foothills. This is in line with the unique sedimentology and geomorphic setting of the eastern reaches of the San Joaquin Formation. Upper Miocene–lower Pliocene strata of the eastern San Joaquin Basin are dominantly sand rich, representing shallow-marine and deltaic facies. During late Pliocene time, this changed dramatically to fine-grained green siltstones and mudstones of the San Joaquin Formation, signaling sediment starvation. This sedimentological change to relatively low-energy conditions immediately adjacent to the western Sierra occurred precisely when nearby documented river incision rates were greatest (Stock et al., 2004, 2005). The forms of the 14–20 m.y. modeled displacement curves (Fig. 4B) are such that river gradients could have increased along the axial to eastern Sierra, accelerating main channel incision, while the Foothills region was under subsidence and very likely marine conditions. Our petrographic studies show that the eastern San Joaquin Formation is characterized by tonalitic gruss layers within a green siltstone matrix. A simple explanation for this distinct detrital association is that marine conditions with limited sediment transport capability spread across the mainly tonalitic basement pediment that lies along the east margin of the basin. The larger sediment dispersal events of this unique ephemeral environment correspond to the spreading of proximal basement-derived gruss into the shallow basin. We posit that the temporary low-energy conditions that developed so proximal to the uplands resulted from the initial subsidence signal suppressing western Sierra river gradients as subsidence temporarily embayed into the uplands. This may have resulted in a brief period of profound aggradation, the record of which was erosionally erased as the delamination bulge subsequently expanded into the western Sierra region. Alternatively, the predicted subsidence-uplift transient for the Foothills area may have been dampened by the necking off of an adjacent root fragment at ca. 3.5 Ma, as discussed next.

In Figure 13, it is further hypothesized that the necking off and foundering of the northeast portion of the actively delaminating root profoundly affected subsequent kinematic patterns of delamination, as well as its surface expressions. The physical conditions that favored the initial east-to-west phases of delamination, as opposed to south to north, and the physical rationale and evidence for hypothesizing the necking off and foundering of a fragment of the root are covered in Part I. Possibly the clearest surface expression of the foundering of this fragment is the overlying pulse of ca. 3.5 Ma delamination volcanism that uniquely affected the corresponding area of the Sierra Nevada (Fig. 13B; Manley et al., 2000; Farmer et al., 2002). Following the detachment of the foundered root fragment, the residual root was configured in such a way as to transition into the south-to-north delamination of its southern end. The prior history of east-to-west delamination had, according to our model tests (Part I, Fig. 10 therein), established the lower-crustal channel across the entire arclogite root–felsic batholith interface, whereupon the release of the partially delaminated limb, which also inhibited south-to-north delamination, and the resulting concentration of the root load to the south instigated the south-to-north delamination phase. This transition caused W-side-up normal faulting of the eastern escarpment system to step over to the Greenhorn–Breckenridge–Kern Canyon system, which followed the Late Cretaceous basement damage zone of the Kern Canyon fault (Mahéo et al., 2009; Saleeby et al., 2009a; Amos et al., 2010; Nadin and Saleeby, 2010). This stepover in W-side-up normal faulting

developed in conjunction with the west tilt and uplift pattern of the Kern arch (Figs. 3 and 13D).

The Quaternary rise of the Kern arch profoundly affected depositional and geographic patterns of the eastern San Joaquin Basin (Fig. 13D). The Tulare and Maricopa subbasins were partitioned off from the principal San Joaquin Basin depocenter at this time. The distribution of the Corcoran E-clay in the subsurface (Figs. 6 and 8) suggests that growth of the Kern arch pushed the southeastern shore of Corcoran Lake westward, leaving the southern part of Corcoran Lake embayed eastward in Tulare Basin. The analysis presented here for Figure 12 longitudinal relationships posits that similar dynamics were at work driving late Quaternary crustal deformation along the eastern San Joaquin Basin–western Foothills transition as a result of south-to-north delamination as those that operated during east-to-west delamination. Specifically, the Kern arch corresponds to the delamination bulge, and the central foothills swell corresponds to its sympathetic bulge (Fig. 4B). It follows that a late Quaternary axis of maximum delamination-driven subsidence should follow a transverse trend through Tulare Basin. The area of this axis could correspond to the maximum depth of the Corcoran E-clay on the Figure 8 structure sections, as well as the veneer of Quaternary fluvial sediments that have aggraded across the exhumed ancient pediment surface and up into the lower Kaweah drainage (Figs. 3 and 5A; Saleeby et al., 2013). Rise of the central Foothills swell is hypothesized to have temporarily partitioned off the southern Great Valley as the internal Corcoran Lake basin (Fig. 6), and ultimately promoted the current broadened zone of incision of Pliocene and Quaternary strata along the central segment of the Foothills ramp. Growth of the Kern arch and the building out of the Kings River alluvial fan (Atwater et al., 1986) have left the residual Corcoran Lake basin as the partitioned Tulare and Buena Vista and Kern lakebeds (Fig. 6).

Uplift of the southern Coast Ranges is also suggested to be in part a result of mantle lithosphere removal dynamics. The central segment of the San Andreas fault, in the southern Coast Ranges, is shown to lie on the relative plate-motion trajectory between the Pacific and North American plates (Argus and Gordon, 2001), calling into question the common interpretation that recent phases of the Coast Range uplift result from plate-margin–driven transpression. The results of our modeling indicate that up to ~500 m of total rock uplift of the southern Coast Ranges results from regional flexure that is sympathetic to the Sierran delamination bulge (Fig. 4B). Furthermore, excess gravitational potential created by the Sierran uplift as well as extension along the eastern Sierra–Death Valley province are sufficient to drive crustal shortening across the western margin of the microplate (Jones et al., 1996, 2004; Lowry et al., 2000), expressed as blind thrusts rooted westward beneath the Coast Ranges (Fig. 1).

SUMMARY AND CONCLUSIONS

The historical debate as to whether the high elevations of the Sierra Nevada are an ancient feature inherited from the Late Cretaceous or result from geologically recent uplift has continued into the current research era (cf. House et al., 1998, 2001; Poage and Chamberlain, 2002; Wakabayashi and Sawyer, 2001; Jones et al., 2004; Mulch et al., 2006; Busby and Putirka, 2009; Cassel et al., 2009, 2012; Molnar, 2010; Wakabayashi, 2013). Rarely is the question of transient vertical displacements considered in this debate. This is not surprising in that such transients by nature include potentially significant cryptic signals. Furthermore, a dynamic framework in which to consider such transients has not been widely recognized. We have attempted to leverage a diversity of constraints on this problem, including stratigraphy and geomorphology across the Sierra Nevada microplate, geophysical imaging of the underlying upper mantle, and dynamic modeling of the partial removal of its mantle lithosphere, in order to better resolve the principal components of Sierra Nevada elevation history. We find considerable evidence for significant regional and local paleorelief throughout the microplate dating back to end of Cretaceous time, with such paleorelief still strongly expressed in microplate physiography and basin structure. We also find evidence for far-field tectonic forcing that elevated the entire microplate at kilometer scale in the Cenozoic and contributed to its regional west tilt. The far-field forcing of the Yellowstone plume head and multiple slab window encounters, as well as the thermal swell of the ephemeral ancestral Cascades arc, probably carried both positive and negative vertical displacement transients, confounding their elevation change and river incision imprints on the Sierra Nevada. Furthermore, numerical modeling of low-temperature thermochronometric and depth of basement exhumation data suggests kilometer-scale east-central Sierra Nevada region elevation decay during early to mid-Cenozoic time, followed by similar-scale late Cenozoic rock and surface uplift that we derive from combined delamination, geomorphic, and far-field forcing mechanisms (McPhillips and Brandon, 2012). These profound model predictions are not at odds with our integrated physiographic-geodynamic model, nor are they at odds with the primary observations cited for the contemporary dominance of paleorelief versus the dominance of geologically recently generated relief.

Resolution of the far-field–forced and paleorelief components of Sierra Nevada microplate physiography facilitates the resolution of more local epeirogenic transients related to mantle lithosphere removal. Our procedure for the resolution of these local components is driven by iterations in thermomechanical modeling and comparison of model predictions for surface responses with stratigraphic and geomorphic data. Model iterations encompassing lithospheric structure and composition and geologic history have led to the bundling of model constraints and predictions into consistency with the principal surface-level observations. Our preferred model in terms of lithospheric structure and compositional constraints predicts ~800 m of Pliocene–Quaternary eastern Sierra rock uplift, driven by the delamination of the arclogite root that formed beneath the southern Sierra Nevada batholith, and ~680 m of contemporaneous tectonic subsidence in the Great Valley where the mantle lithosphere root remains attached to the crust. The predicted tectonic subsidence compares well with the ~625 m of anomalous tectonic subsidence resolved stratigraphically in the Tulare Basin of the Great Valley. Comparisons between model predictions and observations for eastern Sierra crest rock uplift are more complex due to exhumation during uplift. We derive a geomorphically forced rock uplift component of ~400 m (after Small and Anderson, 1995; Pelletier, 2007), stimulated by delamination forcing, summing to ~1200 m of southeastern crest uplift. This alone is short of the estimated 2000 ± 500 m of Pliocene–Quaternary rock uplift of the eastern crest based on stratigraphic-geomorphic geometric constructions (Huber, 1981; Unruh, 1991; Wakabayashi and Sawyer, 2001), although adding in kilometer-scale, far-field–forced regional uplift brings these into agreement, assuming some component of west tilt accompanied the regional uplift pattern. In addition to these reasonably favorable quantitative comparisons between model predictions and stratigraphic-geomorphic data, we find that distinct variations in the regional morphology of the Sierra Nevada–Great Valley basement surface are favorably predicted by our modeling as well. This lends further support to our conceptual model that the principal physiographic differences between the northern and southern Sierra Nevada microplate arise from the superposing of delamination-related epeirogeny primarily across the southern reaches of the microplate. These results, backed by close attention to geologic structure and history in the formulation of

our thermomechanical models, lend confidence that this modeling is reasonably approximating the underlying dynamics for the southern Sierra Nevada case of mantle lithosphere removal.

ACKNOWLEDGMENTS

This research was supported by National Science Foundation grants EAR-0230383 and EAR-0606903, a grant from the George and Betty Moore Foundation, and Faculty Research Funds from the Université Pierre et Marie Curie, France. This is Caltech Tectonics Observatory Contribution 142. Conversations and field excursions with C.J. Busby, J. Gillespe, S.A. Graham, J.S. Lewis, D.D. Miller, K. Putirka, A.G. Sylvester, and J. Wakabayashi helped enrich this work. We also acknowledge the editorial efforts of J.R. Unruh, C.H. Jones, and D.L. Harry in greatly improving the clarity of this publication.

REFERENCES CITED

Addicott, W.O., 1965, Miocene Macrofossils of the Southeastern San Joaquin Valley, California: U.S. Geological Survey Professional Paper 525-C, p. 101–109.

Addicott, W.O., 1970, Miocene Gastropods and Biostratigraphy of the Kern River Area, California: U.S. Geological Survey Professional Paper 642, 174 p., 21 pl.

Allen, P.A., and Allen, J.R., 1990, Basin Analysis, Principles and Applications: Oxford, UK, Blackwell Scientific Publications, 560 p.

Amos, C.B., Kelson, K.I., Rood, D.H., Simpson, D.T., and Rose, R.S., 2010, Late Quaternary slip rate on the Kern Canyon fault at Soda Spring, Tulare County, California: Lithosphere, v. 2, p. 411–417, doi:10.1130/L100.1.

Anderson, D.L., 2005, Large igneous provinces, delamination, and fertile mantle, *in* Saunders, A.D., ed., Large Igneous Provinces: Origin and Environmental Consequences: Elements, v. 1, p. 271–275.

Argus, D.F., and Gordon, R.G., 1991, Current Sierra Nevada–North America motion from very long baseline interferometry: Implications for the kinematics of the Western United States: Geology, v. 19, p. 1085–1088, doi:10.1130/0091-7613(1991)019<1085:CSNNAM>2.3.CO;2.

Argus, D.F., and Gordon, R.G., 2001, Present tectonic motion across the Coast Ranges and San Andreas fault system in central California: Geological Society of America Bulletin, v. 113, no. 12, p. 1580–1592, doi:10.1130/0016-7606(2001)113<1580:PTMATC>2.0.CO;2.

Atwater, B.F., Adam, D.P., Bradbury, J.P., Forester, R.M., Mark, R.K., Lettis, W.R., Fisher, G.R., Gobalet, K.W., and Robinson, S.W., 1986, A fan dam for Tulare Lake, California, and implications for the Wisconsin glacial history of the Sierra Nevada: Geological Society of America Bulletin, v. 97, p. 97–109, doi:10.1130/0016-7606(1986)97<97:AFDFTL>2.0.CO;2.

Atwater, T., and Stock, J., 1998, Pacific–North American plate tectonics of the Neogene southwestern United States: An update: International Geology Review, v. 40, p. 375–402, doi:10.1080/00206819809465216.

Bachman, S.B., 1978, Pliocene–Pleistocene break-up of the Sierra Nevada–White-Inyo Mountains block and formation of Owens Valley: Geology, v. 6, p. 461–463, doi:10.1130/0091-7613(1978)6<461:PBOTSN>2.0.CO;2.

Bacon, C.R., Giovannetti, D.M., Duffield, W.A., Dalrymple, G.B., and Drake, R.T., 1982, Age of the Coso Formation, Inyo County, California: U.S. Geological Survey Bulletin 1527, 37 p.

Bandy, O.L., and Arnal, R.E., 1969, Middle Tertiary basin development, San Joaquin Valley, California: Geological Society of America Bulletin, v. 80, p. 783–820.

Bartley, J.M., Glazner, A.F., Coleman, D.S., Kylander-Clark, A.R.C., and Friedrich, A.M., 2007, Large Laramide dextral offset across Owens Valley, California, and its possible relation to tectonic unroofing of the southern Sierra Nevada, *in* Till, A.B., Roeske, S.M., Foster, D.A., and Sample, J.C., eds., Exhumation Processes along Major Continental Strike-Slip Fault Systems: Geological Society of America Special Paper 434, p. 129–148.

Bartow, J.A., 1984, Geologic Map and Cross Sections of the Southern Margin of the San Joaquin Valley, California: U.S. Geological Survey Miscellaneous Investigation Series Map I-1497, scale 1: 125,000, 2 sheets.

Bartow, J.A., and McDougall, K., 1984, Tertiary Stratigraphy of the Southeastern San Joaquin Valley, California: U.S. Geological Survey Bulletin 1529J, 41 p.

Batt, G.E., Harper, G.D., Helzler, M., and Roden-Tice, M., 2010, Cretaceous sedimentary blanketing and tectonic rejuvenation in the western Klamath Mountains: Insights from thermochronology: Central European Journal of Geosciences, v. 2, p. 138–151, doi:10.2478/v10085-009-0041-4.

Bawden, G.W., Donnellan, A., Kellogg, L.H., Danan, D., and Rundle, J.B., 1997, Geodetic measurements of horizontal strain near the White Wolf fault, Kern County, California, 1926–1993: Journal of Geophysical Research, v. 102, p. 4957–4967, doi:10.1029/96JB03554.

Bennett, R.A., Fay, N.P., Hreinsdottir, S., Chase, C., and Zandt, G., 2009, Increasing long-wavelength relief across the southeastern flank of the Sierra Nevada, California: Earth and Planetary Science Letters, v. 287, p. 255–264, doi:10.1016/j.epsl.2009.08.011.

Bloch, R.B., 1991, San Andreas Fault to Sierra Nevada Range (Sheet 3 of 3), *in* Bloch, R.B., and Graham, S.A., coordinators, West Coast Regional Cross Section: Tulsa, Oklahoma, American Association of Petroleum Geologists, West Coast Regional Cross Section Series, scale 1:125,000.

Blyth, A.E., and Longinotti, N., 2013, Exhumation of the southern Sierra Nevada/eastern Tehachapi Mountains constrained by low-temperature thermochronology: Implications for the initiation of the Garlock fault: Lithosphere (in press).

Blyth, A.E., Longinotti, N., and Khalsa, S., 2010, Post–20 Ma exhumation of the southern Sierra Nevada–Tehachapi Mountains, from fission-track and (U-Th)/He analyses: Geological Society of America Abstract With Programs, v. 42, no. 4, paper 20–7.

Brady, R.J., Ducea, M.N., Kidder, S., and Saleeby, J., 2006, The distribution of radiogenic heat production as a function of depth in the Sierra Nevada batholith, California: A new approach to an old problem: Lithos, v. 86, p. 229–244, doi:10.1016/j.lithos.2005.06.003.

Busby, C.J., and Putirka, K., 2009, Miocene evolution of the western edge of the Nevada Plano in the central and northern Sierra Nevada: Paleocanyons, magmatism and structure: International Geology Review, v. 51, p. 670–701, doi:10.1080/00206810902978265.

Buwalda, J.P., 1954, Geology of the Tehachapi Mountains, California, *in* Jahns, R.H., ed., Geology of Southern California: California Division of Mines Bulletin 170, p. 131–142.

Cassel, E.J., Graham, S.A., and Chamberlain, C.P., 2009, Cenozoic tectonic and topographic evolution of the northern Sierra Nevada, California, through stable isotope paleoaltimetry in volcanic glass: Geology, v. 37, p. 547–550, doi:10.1130/G25572A.1.

Cassel, E.J., Graham, S.A., Chamberlain, C.P., and Henry, C.D., 2012, Early Cenozoic topography, morphology, and tectonics of the northern Sierra Nevada and western Basin and Range: Geosphere, v. 8, p. 229–249, doi:10.1130/GES00671.1.

Castle, R.O., Church, J.P., Yerkes, R.F., and Manning, J.C., 1983, Historical Surface Deformation near Oildale, California: U.S. Geological Survey Professional Paper 1245, 42 p, 1 pl.

Cecil, M.R., Ducea, M.N., Reiners, P.W., and Chase, G.C., 2006, Cenozoic exhumation of the northern Sierra Nevada, California, from (U-Th)/He thermochronology: Geological Society of America Bulletin, v. 118, p. 1481–1488, doi:10.1130/B25876.1.

Cecil, M.R., Saleeby, Z., Le Pourhiet, L., Saleeby, J., and Farley, K.A., 2013, Pliocene–Quaternary subsidence and exhumation of the eastern San Joaquin Basin, California, in response to mantle lithosphere removal: Geosphere (in review).

Chapman, A.D., and Saleeby, J., 2012, Geologic Map of the San Emigdio Mountains, Southern California: Geological Society of America Map and Chart Series MCH101, scale: 1:40,000.

Chapman, A.D., Kidder, S., Saleeby, J.B., and Ducea, M.N., 2010, Role of extrusion of the Rand and Sierra de Salinas schists in Late Cretaceous extension and rotation of the southern Sierra Nevada and vicinity: Tectonics, v. 29, no. 5, doi:10.1029/2009TC002597.

Chapman, A.D., Saleeby, J., Wood, D.J., Piasecki, A., and Farley, K.A., 2012, Regional displacement analysis and palinspastic restoration of dispersed crustal fragments in the southern Sierra Nevada, California: Geosphere, v. 8, no. 2, p. 314–341, doi:10.1130/GES00740.1.

Cheadle, M.J., Czuchra, B.L., Byrne, T., Ando, C.J., Oliver, J.E., Brown, L.D., Kaufman, S., Malin, P.E., and Phinney, R.A., 1986, The deep crustal structure of the Mojave Desert, California, from COCORP seismic-reflection data: Tectonics, v. 5, p. 293–320, doi:10.1029/TC005i002p00293.

Christensen, M.N., 1966, Late crustal movements in the Sierra Nevada of California: Geological Society of America Bulletin, v. 77, p. 163–182, doi:10.1130/0016-7606(1966)77[163:LCCMIT]2.0.CO;2.

Clark, M.K., and Farley, K.A., 2007, Sierra Nevada river incision from apatite $^{4}He/^{3}He$ thermochronometry [abs.]: EOS (Transactions, American Geophysical Union), v. 88, no. 52, p. F2186.

Clark, M.K., Maheo, G., Saleeby, J., and Farley, K.A., 2005, The non-equilibrium (transient) landscape of the Sierra Nevada, California: GSA Today, v. 15, no. 9, p. 4–10, doi:10.1130/1052-5173(2005)015[4:TNLOTS]2.0.CO;2.

Clinton, J.F., Hauksson, E., and Solanki, K., 2006, An evaluation of the SCSN moment tensor solutions: Robustness of the Mw magnitude scale, style of faulting and automation method: Bulletin of the Seismological Society of America, v. 96, p. 1689–1705, doi:10.1785/0120050241.

Coles, S., Prothero, D.R., Quinn, J.P., and Swisher, C.C., III, 1997, Magnetic stratigraphy of the middle Miocene Bopesta Formation, southern Sierra Nevada, California, *in* Girty, G.H., Hanson, R.E., and Cooper, J.D., eds., Geology of the Western Cordilleran: Perspectives from Undergraduate Research: Los Angeles, California, Pacific Section, Society of Economic Paleontologists and Mineralogists, v. 82, p. 21–34.

Cox, B.F., 1987, Stratigraphy, depositional environments, and paleotectonics of the Paleocene and Eocene Golar Formation, El Paso Mountains, California—Geologic summary and roadlog, *in* Cox, B.F., ed., Basin Analysis and Paleontology of the Paleocene and Eocene Golar Formation, El Paso Mountains, California: Los Angeles, California, Pacific Section, Society of Economic Paleontologists and Mineralogists, Guidebook 57, p. 1–29.

Croft, M.G., and Gordon, G.V., 1968, Geology, Hydrology, and Quality of Water in Hanford-Visalia Area, San Joaquin Valley, California: U.S. Geological Survey Open File Report 68–67, 63 p., 10 plates.

Cundall, P.A., and Board, M., 1988, A microcomputer program for modeling large-strain plasticity problems, *in* Swoboda, G., ed., Numerical Methods in Geomechanics: Innsbruck, Austria, Taylor & Francis, p. 2101–2108.

Davis, G.A., and Burchfiel, B.C., 1973, Garlock fault: An intra-continental transform structure, southern California: Geological Society of America Bulletin, v. 84, p. 1407–1422, doi:10.1130/0016-7606(1973)84<1407:GFAITS>2.0.CO;2.

Davis, G.H., and Green, J.H., 1962, Structural Control of Interior Drainage, Southern San Joaquin Valley, California: U.S. Geological Survey Professional Paper 450D, p. D89–D91.

Davis, T.L., and Lagoe, M.B., 1988, A structural interpretation of major tectonic events affecting the western and southern margins of the San Joaquin Valley, California, *in* Graham, S.A., ed., Studies of the Geology of the San Joaquin Basin: Los Angeles, California, Pacific Section: Society of Economic Paleontologists and Mineralogists, Field Trip Guidebook 60, p. 65–87.

DeCelles, P.G., 2004, Late Jurassic to Eocene evolution of the Cordilleran thrust belt and foreland basin system, western U.S.: American Journal of Science, v. 304, p. 105–168, doi:10.2475/ajs.304.2.105.

Dibblee, T.W., Jr., and Louke, G.P., 1970, Geologic map of the Tehachapi quadrangle, Kern County, California: U.S. Geological Survey, Miscellaneous Geologic Investigations Map I-607, scale 1:62,500.

Dibblee, T.W., Jr., and Warne, A.H., 1986, Inferred relation of the Oligocene to Miocene Bealville fanglomerate to the Edison fault, Caliente Canyon area, Kern County, California, *in* Studies of the Geology of the San Joaquin Basin: Upland, California, Society of Economic Paleontologists and Mineralogists, Pacific Section, p. 223–232.

Dibblee, T.W., Jr., Bruer, W.G., Hackel, O., and Warne, A.H., 1965, Geologic map of the southeastern San Joaquin Valley (Kern River to Grapevine Canyon) Kern County, California, *in* Hackel, O., ed., Geology of Southeastern San Joaquin Valley, California: Bakersfield, California, Pacific Section, American Association of Petroleum Geologists, 40 p.

Dickinson, W.R., 2006, Geotectonic evolution of the Great Basin: Geosphere, v. 2, no. 7, p. 353–368, doi:10.1130/GES00054.1.

Dickinson, W.R., Ingersol, R.V., and Graham, S.A., 1979, Paleogene sediment dispersal and paleotectonics in northern California: Geological Society of America Bulletin, v. 90, Part II, no. 10, p. 1458–1528.

Ducea, M., 2001, The California Arc: Thick granitic batholiths, eclogitic residues, lithospheric-scale thrusting, and magmatic flare-ups: GSA Today, v. 11, no. 11, p. 4–10, doi:10.1130/1052-5173(2001)011<0004:TCATGB>2.0.CO;2.

Ducea, M.N., and Saleeby, J.B., 1996, Buoyancy sources for a large, unrooted mountain range, the Sierra Nevada, California; evidence from xenolith thermobarometry: Journal of Geophysical Research, v. 101, p. 8229–8244, doi:10.1029/95JB03452.

Ducea, M.N., and Saleeby, J.B., 1998a, A case for delamination of the deep batholithic crust beneath the Sierra Nevada, California: International Geology Review, v. 40, p. 78–93, doi:10.1080/00206819809465199.

Ducea, M.N., and Saleeby, J.B., 1998b, The age and origin of a thick mafic-ultramafic keel from beneath the Sierra Nevada batholith: Contributions to Mineralogy and Petrology, v. 133, p. 169–185, doi:10.1007/s004100050445.

Ducea, M.N., Kidder, S., Chesley, J.T., and Saleeby, J., 2009, Tectonic underplating of trench sediments beneath magmatic arcs: The central California example: International Geology Review, v. 51, no. 1, p. 1–26, doi:10.1080/00206810802602767.

Dumitru, T.A., 1990, Subnormal Cenozoic geothermal gradients in the extinct Sierra Nevada arc: Consequences of Laramide and post-Laramide shallow-angle subduction: Journal of Geophysical Research, v. 95, p. 4925–4941, doi:10.1029/JB095iB04p04925.

Engebretson, D.C., Cox, A., and Gordon, R.G., 1985, Relative Motions between Oceanic and Continental Plates in the Pacific Basin: Geological Society of America Special Paper 206, 59 p.

Farmer G.L., Glazner, A.F., and Manley, C.R., 2002, Did lithospheric delamination trigger late Cenozoic potassic volcanism is the southern Sierra Nevada, California?: Geological Society of America Bulletin, v. 114, no. 6, p. 754–768.

Fay, N.P., and Humphreys, E.D., 2008, Forces acting on the Sierra Nevada block and implications for the strength of the San Andreas fault system and the dynamics of continental deformation in the western United States: Journal of Geophysical Research, v. 113, p. B12415, doi:10.1029/2008JB005809.

Fay, N.P., Bennett, R.A., and Hreinsdottir, S., 2008, Contemporary vertical velocity of the central Basin and Range and uplift of the Sierra Nevada: Geophysical Research Letters, v. 35, p. L20309, doi:10.1029/2008GL034949.

Figueroa, A.M., and Knott, J.R., 2010, Tectonic geomorphology of the Sierra Nevada Mountains (California): Evidence for uplift and basin formation: Geomorphology, v. 123, p. 34–45, doi:10.1016/j.geomorph.2010.06.009.

Frassetto, A.M., Zandt, G., Gilgert, H., Owens, T.J., and Jones, C.H., 2011, Lithospheric structure of the Sierra Nevada from receiver functions and implications for lithospheric foundering: Geosphere, v. 7, p. 898–921, doi:10.1130/GES00570.1.

Frink, J.W., and Kues, H.A., 1954, Corcoran clay-A Pleistocene lacustrine deposit in San Joaquin Valley, California: American Association of Petroleum Geologists Bulletin, v. 38, no. 11, p. 2357–2371.

Galewsky, J., 2009a, Rain shadow development during the growth of mountain ranges: An atmospheric dynamics perspective: Journal of Geophysical Research, v. 114, p. F01018, doi:10.1029/2008JF001085.

Galewsky, J., 2009b, Orographic precipitation isotopic ratios in stratified atmospheric flows: Implications for paleo-elevation studies: Geology, v. 37, p. 791–794, doi:10.1130/G30008A.1.

Garrison, N., Busby, C.J., Gans, P.B., Putirka, K., and Wagner, D.L., 2008, A mantle plume beneath California? The mid-Miocene Lovejoy flood basalt, northern California, *in* Wright, J., and Shervais, J., eds., Ophiolites, Arcs and Batholiths: Geological Society of America Special Paper 438, p. 551–572.

Gilbert, H., Yingjie, Y., Jones, C.H., Owens, T.J., Zandt, G., and Stachnik, J., 2012, Imaging lithospheric foundering in the structure of the Sierra Nevada: Geosphere, v. 8, p. 1310–1330, doi:10.1130/GES00790.1.

Goodman, E.D., and Malin, P.E., 1992, Evolution of the southern San Joaquin Basin and mid-Tertiary transitional tectonics, central California: Tectonics, v. 11, p. 478–498, doi:10.1029/91TC02871.

Graham, S.A., and Williams, L.A., 1985, Tectonic, depositional, and diagenetic history of Monterey Formation (Miocene, central San Joaquin Basin, California): American Association of Petroleum Geologists Bulletin, v. 69, p. 385–411.

Granger, D.E., and Stock, G.M., 2004, Using cave deposits as geologic tiltmeters: Application to postglacial rebound of the Sierra Nevada, California: Geophysical Research Letters, v. 31, p. L22501, doi:10.1029/2004GL021403.

Grove, K., 1993, Latest Cretaceous basin formation within the Salinian terrane of west-central California: Geological Society of America Bulletin, v. 105, p. 447–463, doi:10.1130/0016-7606(1993)105<0447:LCBFWT>2.3.CO;2.

Guacci, G., and Purcell, C.W., 1978, Evidence for middle Pleistocene and possible Holocene faulting on the Pond–Poso Creek fault, southern San Joaquin Valley, California: Geological Society of America Abstracts with Programs, v. 10, no. 3, p. 108.

Hammond, W.C., Blewitt, G., Li, Z., Plag, H.P., and Kreemer, C., 2012, Contemporary uplift of the Sierra Nevada, western U.S., from GPS and InSAR measurements: Geology, v. 40, no. 7, p. 667–670, doi:10.1130/G32968.1.

Haq, B.U., Hardenbol, J., and Vai, P.R., 1987, Chronology of fluctuating sea levels since the Triassic: Science, v. 235, p. 1156–1167, doi:10.1126/science.235.4793.1156.

Harrison, C.P., and Graham, S.A., 1999, Upper Miocene Stevens sandstone, San Joaquin Basin, California: Reinterpretation of petroliferous, sand-rich, deep-sea depositional system: American Association of Petroleum Geologists Bulletin, v. 83, no. 6, p. 898–923.

Harwood, D.S., and Helley, E.J., 1987, Late Cenozoic Tectonism of the Sacramento Valley, California: U.S. Geological Survey Professional Paper 1359, 46 p.

Harwood, D.S., Helley, E.J., and Doukas, M.P., 1981, Geologic Map of the Chico Monocline and Northeastern Part of the Sacramento Valley, California: U.S. Geological Survey Miscellaneous Investigations Map I-1238, scale 1:62,500.

Henry, C.D., 2012, Eocene–early Miocene paleotopography of the Sierra Nevada–Great Basin–Nevadaplano based on widespread ash-flow tuffs and paleovalleys: Geosphere, v. 8, p. 1–27, doi:10.1130/GES00727.1.

Henry, C.D., and Perkins, M.E., 2001, Sierra Nevada–Basin and Range transition near Reno, Nevada: Two-stage development at 12 and 3 Ma: Geology, v. 29, p. 719–722, doi:10.1130/0091-7613(2001)029<0719:SNBART>2.0.CO;2.

Hirst, B., 1986, Tectonic development of the Tejon and adjacent areas, Kern County, California, *in* Bell, P., ed., Structure and Stratigraphy of the East Side San Joaquin Valley: Bakersfield, California, Pacific Section, American Association of Petroleum Geologists, p. 2–8.

Hosford Scheirer, A., and Magoon, L.B., 2003, Age, distribution, and stratigraphic relationship of rock units in the San Joaquin Basin province, California, *in* U.S. Geological Survey San Joaquin Basin Assessment Team, eds., Petroleum Systems and Geologic Assessment of Oil and Gas in the San Joaquin Basin Province, California: U.S. Geological Survey Professional Paper 1713, chap. 5, p. 1–107.

House, M.A., Wernicke, B.P., and Farley, K.A., 1998, Dating topography of the Sierra Nevada, California, using apatite (U-Th)/He ages: Nature, v. 396, p. 66–69, doi:10.1038/23926.

House, M.A., Wernicke, B.P., and Farley, K.A., 2001, Paleogeomorphology of the Sierra Nevada, California, from (U-Th)/He ages in apatite: American Journal of Science, v. 301, p. 77–102, doi:10.2475/ajs.301.2.77.

Huber, N.K., 1981, Amount and Timing of Late Cenozoic Uplift and Tilt of the Central Sierra Nevada, California—Evidence from the Upper San Joaquin River Basin: U.S. Geological Survey Professional Paper 1197, 28 p.

Huffman, O.F., 1972, Lateral displacement of Upper Miocene rocks and the Neogene history of offset along the San Andreas fault in central California: Geological Society of America Bulletin, v. 83, p. 2913–2946, doi:10.1130/0016-7606(1972)83[2913:LDOUMR]2.0.CO;2.

Humphreys, E.D., 2008, Cenozoic slab windows beneath the western United States: Arizona Geological Society Digest, v. 22, p. 389–396.

Imperato, D.P., 1995, Studies of the Stratigraphy and Structure of the Great Valley of California and Implications for Plate Tectonics [Ph.D. dissertation]: Santa Barbara, California, University of California, 271 p.

Jacobson, C.E., Dawson, M.R., and Postlethwaite, C.E., 1988, Structure, metamorphism, and tectonic significance of the Pelona, Orocopia, and Rand Schists, Southern California, *in* Ernst, W.G., ed., Metamorphism and Crustal Evolution of the Western United States: Rubey Volume: Englewood Cliffs, New Jersey, Prentice-Hall, p. 976–997.

Jenkins, O.P., 1977, Geologic Map of California, Sacramento and San Jose Sheets: Sacramento, California, California Division of Mines and Geology, scale 1:250,000.

Jones, C.H., Hanimori, K., and Roecker, S.W., 1994, Missing roots and mantle "drips": Regional P_n and teleseismic arrival times in the southern Sierra Nevada and vicinity, California: Journal of Geophysical Research, v. 99, no. B3, p. 4567–4601, doi:10.1029/93JB01232.

Jones, C.H., Unruh, J.R., and Sonder, L.J., 1996, The role of gravitational potential energy in active deformation in the southwestern United States: Nature, v. 381, p. 37–41, doi:10.1038/381037a0.

Jones, C.H., Farmer, G.L., and Unruh, J., 2004, Tectonics of Pliocene removal of lithosphere of the Sierra Nevada, California: Geological Society of America Bulletin, v. 116, p. 1408–1422, doi:10.1130/B25397.1.

Klausing, R.L., and Lohman, K.E., 1964, Upper Pliocene Marine Strata on the East Side of the San Joaquin Valley, California: U.S. Geological Survey Professional Paper 475-D, p. 14–17.

Laney, P., and Brizzee, J., 2003, California Geothermal Resources: U.S. Department of Energy, Geothermal Technologies Program Publication Number INEEL/MISC-03–01044 Rev. 1, 1 p.

Lee, C.T., Yin, Q., Rudnick, R.L., Chesley, J.T., and Jacobsen, S.B., 2000, Re-Os isotopic evidence for pre-Miocene delamination of lithospheric mantle beneath the Sierra Nevada, California: Science, v. 289, p. 1912–1916, doi:10.1126/science.289.5486.1912.

Le Pourhiet, L., Burov, E., and Moretti, I., 2004, Rifting through a stack of inhomogeneous thrusts (the dipping pie concept): Tectonics, v. 23, no. 4, doi:10.1029/2003TC001584.

Le Pourhiet, L., Gurnis, M., and Saleeby, J., 2006, Mantle instability beneath the Sierra Nevada Mountains in California and Death Valley extension: Earth and Planetary Science Letters, v. 251, no. 1–2, p. 104–119, doi:10.1016/j.epsl.2006.08.028.

Lettis, W.R., 1982, Late Cenozoic Stratigraphy and Structure of the Western Margin of the Central San Joaquin Valley, California: U.S. Geological Survey Open File Report 82–525, 203 p.

Lettis, W.R., 1988, Quaternary geology of the northern San Joaquin Valley, *in* Graham, S.A., ed., Studies of the

Geology of the San Joaquin Basin: Los Angeles, California, Pacific Section, Society of Economic Paleontologists and Mineralogists, v. 60, p. 333–351.

Lettis, W.R., and Unruh, J.R., 1991, Quaternary geology of the Great Valley, California, *in* Dupre, W.R., et al., eds., Quaternary Nonglacial Geology: Conterminous U.S.: Boulder, Colorado, Geological Society of America, The Geology of North America, v. K-2, p. 164–176.

Li, Y.G., Henyey, T.L., and Silver, L.T., 1992, Aspects of the crustal structure of the western Mojave Desert, California, from seismic-reflection and gravity-data: Journal of Geophysical Research, v. 97, p. 8805–8816, doi:10.1029/91JB02119.

Liu, L., Gurnis, M., Seton, M., Saleeby, J., Muller, D., and Jackson, J., 2010, The role of oceanic plateau subduction in the Laramide orogeny: Nature Geoscience, doi:10.1038/ngeo829.

Lofgren, B.E., and Klausing, R.L., 1969, Land Subsidence due to Ground-Water Withdrawal, Tulare-Wasco Area, California: U.S. Geological Survey Professional Paper 437-B, 103 p.

Lofgren, D.L., Honey, J.G., McKenna, M.C., Zondervan, R.L., and Smith, E.E., 2008, Paleocene primate from the Goler Formation of the Mojave Desert in California, *in* Wang, X., and Barnes, L.G., eds., Geology and Vertebrate Paleontology of Western and Southern North America, Contributions in Honor of David P. Whistler: National History Museum of Los Angeles County Science Series Volume 41, p. 11–28.

Loomis, D.P., and Burbank, D.W., 1988, The stratigraphic evolution of the El Paso basin, southern California: Implications for the Miocene development of the Garlock fault and uplift of the Sierra Nevada: Geological Society of America Bulletin, v. 100, p. 12–28, doi:10.1130/0016-7606(1988)100<0012:TSEOTE>2.3.CO;2.

Lowry, A.R., and Perez-Gussinye, M., 2011, The role of crustal quartz in controlling Cordilleran deformation: Nature, v. 471, p. 353–357, doi:10.1038/nature09912.

Lowry, A.R., Ribe, N.M., and Smith, R.B., 2000, Dynamic elevation of the Cordillera, western United States: Journal of Geophysical Research, v. 105, no. B10, p. 23,371–23,390, doi:10.1029/2000JB900182.

Lucas, S.G., and Reynolds, R.E., 1991, Late Cretaceous (?) plesiosaurs from Cajon Pass, California: San Bernardino County Museum Association Quarterly, v. 38, p. 53–54.

Luffi, P., Saleeby, J., Lee, C.T.A., and Ducea, M., 2009, Lithospheric mantle duplex beneath the central Mojave Desert revealed by xenoliths from Dish Hill, California: Journal of Geophysical Research, v. 114, no. B3, B03202, doi:10.1029/2008JB005906.

MacPherson, B.A., 1978, Sedimentation and trapping mechanism in Upper Miocene Stevens and older turbidite fans of southeastern San Joaquin Valley, California: American Association of Petroleum Geologists Bulletin, v. 62, p. 2243–2274.

Mahéo, G., Farley, K.A., Clark, M.K., and Shuster, D., 2004, Cooling and exhumation of the Sierra Nevada batholith in the Mount Whitney area (California) based on (U-Th)/He thermochronometry: Washington, D.C., American Geophysical Union, Fall Meeting 2004, abstract T41D–1252.

Mahéo, G., Saleeby, J., Saleeby, Z., and Farley, K.A., 2009, Tectonic control on southern Sierra Nevada topography, California: Tectonics, v. 28, TC6006, doi:10.1029/2008TC002340.

Malin, P.E., Goodman, E.D., Henyey, T.L., Li, Y.-G., Okaya, D.A., and Saleeby, J.B., 1995, Significance of seismic reflections beneath a tilted exposure of deep continental crust, Tehachapi Mountains, California: Journal of Geophysical Research, v. 100, p. 2069–2087, doi:10.1029/94JB02127.

Manley, C.R., Glazner, A.F., and Farmer, G.L., 2000, Timing of volcanism in the Sierra Nevada of California: Evidence for Pliocene delamination of the batholithic root: Geology, v. 28, p. 811–814, doi:10.1130/0091-7613(2000)28<811:TOVITS>2.0.CO;2.

Matthes, F.E., 1965, Glacial Reconnaissance of Sequoia National Park, California: U.S. Geological Survey Professional Paper 504-A, 58 p.

May, J.C., and Hewitt, R.L., 1948, The basement complex in well samples from Sacramento and San Joaquin Valleys, California: California Division of Mines and Geology Journal, v. 44, p. 129–158.

McLaughlin, R.J., Blake, M.C., Sliter, W.V., Wentworth, C.M., and Graymer, R.W., 2009, The Wheatfork terrane: A remnant of Siletzia (?) in Franciscan coastal belt of northern California: Geological Society of America Abstracts with Programs, v. 41, no. 7, p. 519.

McPhillips, D., and Brandon, M.T., 2010, Using tracer thermochronology to measure modern relief change in the Sierra Nevada, California: Earth and Planetary Science Letters, v. 296, p. 373–383, doi:10.1016/j.epsl.2010.05.022.

McPhillips, D., and Brandon, M.T., 2012, Topographic evolution of the Sierra Nevada measured directly by inversion of low-temperature thermochronology: American Journal of Science, v. 312, p. 90–116, doi:10.2475/02.2012.02.

Mereu, R.F., 1987, An interpretation of the seismic-refraction data recorded along profile SJ6: Morro Bay–Sierra Nevada, California, USA, *in* Walter, A.W., and Mooney, W.D., eds., Interpretations of the SJ-6 Seismic Reflection/Refraction Profile, South-Central California, USA: U.S. Geological Survey Open-File Report 87–73, p. 20–24.

Michael, E.D., 1960, The Geology of the Cache Creek Area, Kern County, California [M.S. thesis]: Los Angeles, California, University of California, 145 p., 5 pl.

Miller, D.D., 1999, Sequence Stratigraphy and Controls on Deposition of the Upper Cenozoic Tulare Formation, San Joaquin Valley, California [Ph. D. Dissertation]: Stanford, California, Stanford University, 179 p.

Miller, D.M., Wells, M.L., Dewitt, E., Walker, J.D., and Nakata, J., 1996, Late Cretaceous extensional fault system across the northeastern Mojave Desert: San Bernardino County Museum Association Quarterly, v. 43, no. 1, p. 77–84.

Molnar, P., 2010, Deuterium and oxygen isotopes, paleoelevations of the Sierra Nevada, and Cenozoic climate: Geological Society of America Bulletin, v. 122, p. 1106–1115, doi:10.1130/B30001.1.

Monastero, F.C., Walker, J.D., Katzenstein, A.M., and Sabin, A.E., 2002, Neogene evolution of the Indian Wells Valley, east-central California, *in* Glazner, A.F., Walker, J.D., and Bartley, J.M., eds., Geologic Evolution of the Mojave Desert and Southwestern Basin and Range: Geological Society of America Memoir 195, p. 199–228.

Mount, V.S., and Suppe, J., 1987, State of stress near the San Andreas fault: Implications for wrench tectonics: Geology, v. 15, p. 1143–1146, doi:10.1130/0091-7613(1987)15<1143:SOSNTS>2.0.CO;2.

Moxon, I.W., 1987, History and Controls of Subsidence in the Great Valley Forearc Basin, California [Ph.D. dissertation]: Stanford, California, Stanford University, 272 p.

Moxon, I.W., and Graham, S.T., 1987, History and controls of subsidence in the Late Cretaceous–Tertiary Great Valley forearc basin, California: Geology, v. 15, p. 626–629, doi:10.1130/0091-7613(1987)15<626:HACOSI>2.0.CO;2.

Mulch, A., Graham, S.A., and Chamberlain, C.P., 2006, Hydrogen isotopes in Eocene river gravels and paleoelevation of the Sierra Nevada: Science, v. 313, p. 87–89, doi:10.1126/science.1125986.

Müller, R.D., Sdrolias, M., Carmen, G., and Roest, W.R., 2008, Age, spreading rates, and spreading asymmetry of the world's oceanic crust: Geochemistry Geophysics Geosystems, v. 9, p. Q04006, doi:10.1029/2007GC001743.

Murphy, J.B., Oppliger, G.L., and Brimhall, G.H., 1998, Plume modified orogeny: An example from the western United States: Geology, v. 26, p. 731–734.

Nadin, E.S., and Saleeby, J., 2010, Quaternary reactivation of the Kern Canyon fault system, southern Sierra Nevada, California: Geological Society of America Bulletin, v. 122, p. 1671–1685, doi:10.1130/B30009.1.

Nilsen, T.H., 1984, Stratigraphy, sedimentology, and tectonic framework of the Upper Cretaceous Hornbrook Formation, Oregon and California, *in* Nilsen, T.H., ed., Geology of the Upper Cretaceous Hornbrook Formation, Oregon and California: Los Angeles, California, Pacific Section, Society of Economic Paleontologists and Mineralogists, v. 42, p. 51–88.

Nugent, L.E., Jr., 1942, The genesis of subordinate conjugate faulting in the Kern River salient, California: The Journal of Geology, v. 50, p. 900–913, doi:10.1086/625090.

Olson, H.C., 1988, Middle Tertiary Stratigraphy, Depositional Environments, Paleoecology, and Tectonic History of the Southeastern San Joaquin Basin, California [Ph.D. dissertation]: Stanford, California, Stanford University, 353 p.

Pelletier, J.D., 2007, Numerical modeling of the Cenozoic geomorphic evolution of the Sierra Nevada, California: Earth and Planetary Science Letters, v. 259, p. 85–96, doi:10.1016/j.epsl.2007.04.030.

Phillips, F.M., McIntosh, W.C., and Dunbar, N.W., 2011, Chronology of late Cenozoic volcanic eruptions onto relict surfaces in the south-central Sierra Nevada, California: Geological Society of America Bulletin, v. 123, no. 5–6, p. 890–910, doi:10.1130/B30000.1.

Pierce, K.L., Morgan, L.A., and Saltus, R.W., 2002, Yellowstone plume head: Postulated tectonic relations to the Vancouver slab, continental boundaries and climate, *in* Bonnichsen, B., White, C.M., and McCurry, M., eds., Tectonic and Magmatic Evolution of the Snake River Plain Volcanic Province: Idaho Geological Survey Bulletin 30, p. 5–33.

Poage, M.A., and Chamberlain, C.P., 2002, Stable isotopic evidence for pre–middle Miocene rain shadow in the western Basin and Range: Implications for the paleotopography of the Sierra Nevada: Tectonics, v. 21, p. 1–9, doi:10.1029/2001TC001303.

Poliakov, A., Cundall, P.A., Podladchikov, Y.Y., and Lyakhovsky, V., 1993, An explicit inertial method for the simulation of visco-elastic flow: An evaluation of elastic effect in two and three layer models, *in* Stone, D.B., and Runcorn, S.K., eds., Flow and Creep in the Solar System: Observation, Modeling and Theory: Dordrecht, Netherlands, Kluwer Academic Publishers, p. 175–195.

Pysklywec, R.N., and Cruden, A.R., 2004, Coupled crust mantle dynamics and intraplate tectonics: Two dimensional numerical and three-dimensional analogue modeling: Geochemistry Geophysics Geosystems, v. 5, no. 10, p. Q10003, doi:10.1029/2004GC000748.

Reeg, H., 2008, Seismic Structure of the Crust and Upper Mantle of the Sierra Nevada, California [M.S. thesis]: Boulder, Colorado, University of Colorado, 139 p., http://gateway.proquest.com/openurl?url_ver=Z39.88-2004&rft_val_fmt=info:ofi/fmt:kev:mtx:dissertation&res_dat=xri:pqdiss&rft_dat=xri:pqdiss:1460872.

Reid, S.A., 1988, Late Cretaceous and Paleogene sedimentation along the east side of the San Joaquin Basin, *in* Graham, S.A., ed., Studies of the Geology of the San Joaquin Basin: Los Angeles, California, Pacific Section, Society of Economic Paleontologists and Mineralogists, v. 60, p. 157–171.

Repenning, C.A., 1960, Geologic Summary of the Central Valley of California with Reference to the Disposal of Liquid Radioactive Waste: U.S. Geological Survey Trace Elements Investigations Report 769, 69 p.

Riebe, C.S., Kirchner, J.W., Granger, D.E., and Finkel, R.C., 2000, Erosional equilibrium and disequilibrium in the Sierra Nevada, inferred from cosmogenic ^{26}Al and ^{10}Be in alluvial sediment: Geology, v. 28, p. 803–806, doi:10.1130/0091-7613(2000)28<803:EEADIT>2.0.CO;2.

Ruppert, S., Fliedner, M.M., and Zandt, G., 1998, Thin crust and active upper mantle beneath the southern Sierra Nevada in the western United States: Tectonophysics, v. 286, p. 237–252, doi:10.1016/S0040-1951(97)00268-0.

Saleeby, J., 2003, Segmentation of the Laramide slab—Evidence from the southern Sierra Nevada region: Geological Society of America Bulletin, v. 115, p. 655–668, doi:10.1130/0016-7606(2003)115<0655:SOTLSF>2.0.CO;2.

Saleeby, J., 2007, Western extent of the Sierra Nevada batholith in the Great Valley basement: Eos (Transactions, American Geophysical Union), v. 88, no. 52, p. F2186.

Saleeby, J., 2012, Late Cretaceous structure and tectonics of the California Great Valley forearc, and relationships with the southern Sierra-Salinia supra-subduction core complex: Geological Society of America Abstracts with Programs, v. 44, no. 7, p. 490.

Saleeby, J., and Foster, Z., 2004, Topographic response to mantle lithosphere removal, southern Sierra Nevada region, California: Geology, v. 32, p. 245–248, doi: 10.1130/G19958.1.

Saleeby, Z., and Saleeby, J., 2009, Pliocene cryptic subsidence followed by rapid Quaternary uplift in relation to mantle lithosphere removal, Kern arch, eastern San Joaquin Basin, California: Geological Society of America Abstracts with Programs, v. 41, no. 7, p. 180.

Saleeby, Z., and Saleeby, J., 2010, Erosional stripping of the southeastern San Joaquin Basin margin off the southern Sierra Nevada basement uplift: Geological Society of America Abstracts with Programs, v. 42, no. 4, p. 68.

Saleeby, J., Ducea, M., and Clemens-Knott, D., 2003, Production and loss of high-density batholithic root, southern Sierra Nevada region: Tectonics, v. 22, no. 6, p. 1–24, doi:10.1029/2002TC001374.

Saleeby, J., Farley, K., Kistler, R.W., and Fleck, R., 2007, Thermal evolution and exhumation of deep level batholithic exposures, southernmost Sierra Nevada, California, *in* Cloos, M., Carlson, W.D., Gilbert, M.C., Liou, J.G., and Sorensen, S.S., eds., Convergent Margin Terranes and Associated Regions, a Tribute to W.G. Ernst: Geological Society of America Special Paper 419, p. 39–66.

Saleeby, J., Saleeby, Z., Nadin, E., and Maheo, G., 2009a, Step over in the structure controlling the regional west tilt of the Sierra Nevada microplate: Eastern escarpment to Kern Canyon system, *in* Ernst, W.G., ed., Special Volume on the Nevada Plano: International Geology Review, v. 51, no. 7–8, p. 634–669.

Saleeby, J.B., Saleeby, Z., Chapman, A.D., and Nadin, E., 2009b, Origin and evolution of the White Wolf fault and the Maricopa Basin, southernmost California Great Valley: Geological Society of America Abstracts with Programs, v. 41, no.7, p. 180.

Saleeby, J., Le Pourhiet, L., Saleeby, Z., and Gurnis, M., 2012, Epeirogenic transients related to mantle lithosphere removal in the southern Sierra Nevada region, California: Part I. Implications of thermal-mechanical modeling: Geosphere, v. 8, p. 1286-1309, doi:10.1130/GES00746.1.

Saleeby, J., Saleeby, Z., and Sousa, F., 2013, From deep to modern time along the western Sierra Nevada Foothills of California, San Joaquin to Kern River drainages, *in* Putirka, K., ed., Geologic Excursions from Fresno, California, and the Central Valley: A Tour of California's Iconic Geology: Geological Society of America Fieldguide 32, p. 1–26, doi:10.1130/2013.0032(03).

Saltus, R.W., and Lachenbruch, A.H., 1991, Thermal evolution of the Sierra Nevada: Tectonic implications of new heat flow data: Tectonics, v. 10, p. 325–344, doi:10.1029/90TC02681.

Schmandt, B., and Humphreys, E., 2010, Seismic heterogeneity and small-scale convection in the southern California upper mantle: Geochemistry Geophysics Geosystems, v. 11, no. 5, doi:10.1029/2010GC003042.

Small, E.E., and Anderson, R.S., 1995, Geomorphically driven late Cenozoic rock uplift in the Sierra Nevada, California: Science, v. 270, p. 277–281, doi:10.1126/science.270.5234.277.

Small, E.E., Anderson, R.S., Repka, J.L., and Finkel, R., 1997, Erosion rates of alpine bedrock summit surfaces deduced from in situ ^{10}Be and ^{26}Al: Earth and Planetary Science Letters, v. 150, p. 413–425, doi:10.1016/S0012-821X(97)00092-7.

Sousa, F., Saleeby, J., Farley, K., and Unruh, J., 2013, The southern Sierra Nevada Foothills bedrock pediment: Geological Society of America Abstracts with Programs, v. 44, no. 3 (in press).

Stock, G.M., Anderson, R.S., and Finkel, R.C., 2004, Pace of landscape evolution in the Sierra Nevada, California, revealed by cosmogenic dating of cave sediments: Geology, v. 32, no. 3, p. 193–196, doi:10.1130/G20197.1.

Stock, G.M., Anderson, R.S., and Finkel, R.C., 2005, Rates of erosion and topographic evolution of the Sierra Nevada, California, inferred from cosmogenic ^{26}Al and ^{10}Be concentrations: Earth Surface Processes and Landforms, v. 30, p. 985–1006, doi:10.1002/esp.1258.

Suppe, J., Powell, C., and Berry, R., 1975, Regional topography, seismicity, volcanism, and the present-day tectonics of the western United States: American Journal of Science, v. 275-A, p. 397–436.

Surpless, B.E., Stockli, D.F., Dumitru, T.A., and Miller, E.L., 2002, Two-phase westward encroachment of Basin and Range extension into the northern Sierra Nevada: Tectonics, v. 21, no. 1, p. 2-1–2-10, doi:10.1029/2000TC001257.

United States Department of Energy, 2003, California Geothermal Resources Map: http://geothermal.inel.gov/maps/ca.pdf.

Unruh, J.R., 1991, The uplift of the Sierra Nevada and implications for late Cenozoic epeirogeny in the western Cordillera: Geological Society of America Bulletin, v. 103, p. 1395–1404, doi:10.1130/0016-7606(1991)103<1395:TUOTSN>2.3.CO;2.

Unruh, J.R., Humphrey, J., and Barron, A., 2003, Transtensional model for the Sierra Nevada frontal fault system, eastern California: Geology, v. 31, p. 327–330, doi:10.1130/0091-7613(2003)031<0327:TMFTSN>2.0.CO;2.

Wakabayashi, J., 2013, Paleochannels, stream incision, erosion, topographic evolution, and alternative explanations of paleoaltimetry, Sierra Nevada, California: Geosphere, v. 9, doi:10.1130/GES00814.1.

Wakabayashi, J., and Sawyer, T.L., 2001, Stream incision, tectonics, uplift, and evolution of topography of the Sierra Nevada, California: The Journal of Geology, v. 109, p. 539–562, doi:10.1086/321962.

Watts, A.B., 2001, Isostasy and Flexure of the Lithosphere: Cambridge UK, Cambridge University Press, 480 p.

Wells, R.E., Engebretsen, D.C., Snavely, P.D., Jr., and Coe, R.S., 1984, Cenozoic plate motions and the volcanotectonic evolution of western Oregon and Washington: Tectonics, v. 3, no. 2, p. 275–294, doi:10.1029/TC003i002p00275.

Wentworth, C.M., and Zoback, M.D., 1989, The style of late Cenozoic deformation at the eastern front of the California Coast Ranges: Tectonics, v. 8, no. 2, p. 237–246, doi:10.1029/TC008i002p00237.

Wentworth, C.M., Fisher, G.R., Levine, P., and Jachens, R.C., 1995, The Surface of Crystalline Basement, Great Valley and Sierra Nevada, California: A Digital Map Database: U.S. Geological Survey Open-File Report 95–96, 18 p.

Williams, T.A., 1997, Basin-Fill Architecture and Forearc Tectonics, Cretaceous Great Valley Group, Sacramento Basin, Northern California [Ph.D. Dissertation]: Stanford, California, Stanford University, 412 p.

Wilson, A.M., Garven, G., and Boles, J.R., 1999, Paleohydrology of the San Joaquin Basin, California: Geological Society of America Bulletin, v. 111, no. 3, p. 432–439, doi:10.1130/0016-7606(1999)111<0432:POTSJB>2.3.CO;2.

Wilson, D.S., McCrory, P.A., and Stanley, R.G., 2005, Implications of volcanism in coastal California for Neogene deformation history of western North America: Tectonics, v. 24, TC3008, doi:10.1029/2003TC001621.

Wood, D.J., and Saleeby, J.B., 1998, Late Cretaceous–Paleocene extensional collapse and disaggregation of the southernmost Sierra Nevada batholith: International Geology Review, v. 39, p. 289–325.

Yan, Z.M., Clayton, R.W., and Saleeby, J., 2005, Seismic refraction evidence for steep faults cutting highly attenuated continental basement in the central Transverse Ranges, California: Geophysical Journal International, v. 160, p. 651–666, doi:10.1111/j.1365-246X.2005.02506.x.

Zandt, G., Gilbert, H., Owens, T., Ducea, M., Saleeby, J., and Jones, C., 2004, Active foundering of a continental arc root beneath the southern Sierra Nevada, California: Nature, v. 431, p. 41–46, doi:10.1038/nature02847.

Zoback, M.D., Zoback, M.L., Mount, V.S., Suppe, J., Eaton, J.P., Healy, J.H., Oppenheimer, D., Reasenberg, P., Jones, L., Raleigh, C.B., Wong, I.G., Scotti, O., and Wentworth, C., 1987, New evidence on the state of stress on the San Andreas fault system: Science, v. 238, p. 1105–1111, doi:10.1126/science.238.4830.1105.

Zoback, M.L., Anderson, R.E., and Thompson, G.A., 1981, Cenozoic evolution of state of stress and style of tectonism in the Basin and Range Province of western united States: Philosophical Transactions of the Royal Society of London, v. 300, p. 407–434.